

Use Authorization

In presenting this thesis in partial fulfillment of the requirements for an advanced degree at Idaho State University, I agree that the Library shall make it freely available for inspection. I further state that permission to download and/or print my thesis for scholarly purposes may be granted by the Dean of the Graduate School, Dean of my academic division, or by the University Librarian. It is understood that any copying or publication of this thesis for financial gain shall not be allowed without my written permission.

Signature _____

Date _____

**LOW-CYCLE FATIGUE BEHAVIOR OF REINFORCING STEEL IN IDAHO BRIDGE
COLUMNS DURING EARTHQUAKES**

by

Supreme Maskey

A thesis

submitted in partial fulfillment

of the requirements for the degree of

Master of Science in the Department of Civil and Environmental Engineering

Idaho State University

Fall 2017

Committee Approval

To the Graduate Faculty:

The members of the committee appointed to examine the thesis of SUPREME MASKEY find it satisfactory and recommend that it be accepted.

Major Advisor

Dr. Arya Ebrahimpour

Committee Member

Dr. James Mahar

Graduate Faculty Representative

Dr. Marco Schoen

TABLE OF CONTENTS

LIST OF FIGURES	v
LIST OF TABLES	vii
ABSTRACT	viii
CHAPTER 1 - INTRODUCTION.....	1
1.1. Background and Description.....	1
1.2. Objectives	4
1.3. Thesis Overview	5
CHAPTER 2 - LITERATURE REVIEW.....	6
2.1. Fatigue Life and Low-cycle Fatigue	6
2.2. Low-cycle Fatigue in Reinforcing Steel Bars	15
2.3. Comparison of ASTM A615 and ASTM A706 reinforcing steel bars	25
2.4. Summary	29
CHAPTER 3 - METHODOLOGY.....	30
3.1. Methods and Assumptions in Modeling the Three Idaho Bridges	30
3.2. Material Properties in Nonlinear Columns	31
3.3. Method of Seismic Analysis	32
3.4. Bridge on SH-36 over Bear River at Preston.....	33
3.5. Bridge on US-95 over US-20/26 and UPRR at Parma	35
3.6. Bridge on SH-22 over I-15 at Dubois	37
CHAPTER 4 - RESULTS.....	40
4.1. Results for Computer Analyses	40
4.2. Comparison of Results with AASHTO Guide Specifications	44
4.3. Low-cycle fatigue results	47
CHAPTER 5 - SUMMARY AND CONCLUSIONS.....	53
REFERENCES	57
APPENDIX A - Procedures for Estimating Integral Abutment Stiffness Values	60
APPENDIX B - Bridge Computer Models and Output Data	68

LIST OF FIGURES

Figure 1.1 Maximum Elastic and Inelastic Displacements (Marsh, et al., 2014)).....	2
Figure 1.2 Chain Analogy for Capacity-Protected Design (Paulay and Priestly, 1992).....	3
Figure 2.1 Typical hysteresis loops for $R = -2$ (Koh & Stephens, 1991)	8
Figure 2.2 Typical hysteresis loops for $R = 0.5$ (Koh & Stephens, 1991)	9
Figure 2.3 Monotonic and cyclic stress-strain behavior for all strain ratios. (Koh & Stephens, 1991)	10
Figure 2.4 Low cycle fatigue behavior for $R = -1$. (Koh & Stephens, 1991)	11
Figure 2.5 Log-log strain amplitude vs reversals to failure for each strain ratio. (Koh & Stephens, 1991)	13
Figure 2.6 Low cycle fatigue behavior for all strain ratios. (Koh & Stephens, 1991).....	14
Figure 2.7 Correlation of Morrow’s model for mean stress. (Morrow, 1968).....	14
Figure 2.8 Physical modeling of reinforcing steel behavior: (a) in-situ conditions of reinforcing bar; and (b) specimen fabrication procedure. (Mander et al., 1994).....	16
Figure 2.9 Typical Fatigue-life Curve for an Engineering Alloy (Brown and Kunnath, 2000) ...	18
Figure 2.10 Strain vs Number of Half Cycles to Failure for A615 steel (Brown and Kunnath, 2000)	20
Figure 2.11 Strain vs Number of Half Cycles to Failure for A706 steel (Zhou, 2008)	21
Figure 2.12 Strain vs Number of Half Cycles to Failure for A615 steel (Hawileh et al., 2009) ..	23
Figure 2.13 Strain vs Number of Half Cycles to Failure for A706 steel (Hawileh et al., 2009) ..	24
Figure 2.14 Strain vs Number of Half Cycles to Failure for A615 and A706 steels (Brown and Kunnath, 2000) (Zhou, 2008) (Hawileh et al., 2009)	25
Figure 3.1 Plan View of SH-36 over Bear River Bridge at Preston (NTS)	34
Figure 3.2 Elevation View of SH-36 over Bear River Bridge at Preston (NTS).....	34
Figure 3.3 Preston Bridge Column Section	35
Figure 3.4 Plan View of SH-36 over US-20/26 and UPRR at Parma (NTS)	36
Figure 3.5 Elevation View of SH-36 over US-20/26 and UPRR at Parma (NTS)	36
Figure 3.6 Parma Bridge Column Section	37
Figure 3.7 Plan View of SH-22 over I-15 Bridge at Dubois (NTS)	38
Figure 3.8 Elevation View of SH-22 over I-15 Bridge at Dubois (NTS)	38
Figure 3.9 Dubois Bridge Column Section.....	38
Figure 4.1 Preston Bridge Column Displacements/Drifts under Longitudinal Load	42
Figure 4.2 Preston Bridge Column Displacements/Drifts under Transverse Load	42
Figure 4.3 Preston Bridge Stress-strain Values in the Most Stressed Steel Bar in the CIP Column	43
Figure 4.4 Combined Strain vs Number of Half Cycles to Failure plot for ASTM A706 steel from Zhou (2008) and Hawileh et al. (2009).....	47
Figure 4.5 Combined Strain vs Number of Half Cycles to Failure plot for ASTM A615 steel from Brown and Kunnath (2000) and Hawileh et al. (2009).....	48
Figure 4.6 Combined Strain vs Number of Half Cycles to Failure plot for ASTM A615 and ASTM A706 steel (Brown and Kunnath, 2000) (Zhou, 2008) (Hawileh et al., 2009)	49
Figure A.1 Abutment Backfill Reaction Force versus Displacement.....	61
Figure A.2 Top of the Pile Lateral Force versus Displacement, Bending about the Strong Axis	62
Figure A.3 Top of the Pile Lateral Force versus Displacement, Bending about the Weak Axis .	65
Figure B.1 Preston Bridge Lateral Deflection vs. Depth of a pipe pile (Northeast Abutment)....	70
Figure B.2 Preston Bridge Lateral Deflection vs. Depth of a pipe pile (Southwest Abutment)...	71

Figure B.3 Preston Bridge Reinforced Column Detail 77
Figure B.4 Preston Bridge Column Elastic Stiffness Ratio (Koh & Stephens, 1991) 79
Figure B.5 Preston Bridge Linear Elastic Model with Node Numbers. 81
Figure B.6 Preston Bridge Linear Elastic Model with Element Numbers..... 82
Figure B.7 USGS Design Maps Summary Report..... 83
Figure B.8 Preston Bridge Nonlinear Cast-in-place Model with Node Numbers 97
Figure B.9 Preston Bridge Nonlinear Cast-in-place Model with Element Numbers 98
Figure B.10 Preston Bridge Moment vs Rotation..... 102

LIST OF TABLES

Table 2.1 #6 Specimens: Low-cycle Fatigue Results for A615 steel (Brown and Kunnath, 2000)	19
Table 2.2 #7 Specimens: Low-cycle Fatigue Results for A615 steel (Brown and Kunnath, 2000)	19
Table 2.3 #8 Specimens: Low-cycle Fatigue Results for A615 steel (Brown and Kunnath, 2000)	19
Table 2.4 #8 Specimens: Low-cycle Fatigue Results for A706 steel (Zhou, 2008)	21
Table 2.5 #6 Specimens: Low-cycle Fatigue Results for A615 steel (Hawileh et al., 2009)	22
Table 2.6 #6 Specimens: Low-cycle Fatigue Results for A706 steel (Hawileh et al., 2009)	24
Table 2.7 Stress properties of ASTM A706 Grade 60 and ASTM A615 Grade 60 reinforcing steel bars (AASHTO Seismic Guide, 2015).	26
Table 2.8 Comparison of minimum percent elongation in ASTM A706 and A615 rebars (Gustafson, 2007)	27
Table 2.9 Cost comparison for ASTM A706 and ASTM A615 rebars at 60 ft. (American Construction Supply, Inc., 2017)	28
Table 4.1 Preston Bridge Displacements, Drifts, and Column Base Reactions	41
Table 4.2 Displacement and Drift Capacity versus Demand for Bridge Columns	46
Table 4.3 Stress and Strain in Steel Bar and Number of Half Cycles for Steel Bar Fatigue Failure for a Preston Bridge Column.	50
Table 4.4 Stress and Strain in Steel Bar and Number of Half Cycles for Steel Bar Fatigue Failure for a Parma Bridge Column.	51
Table 4.5 Stress and Strain in Steel Bar and Number of Half Cycles for Steel Bar Fatigue Failure for a Dubois Bridge Column.	52
Table B.1 Preston Bridge Weight of Structure to Nodes from Deck, Pier Cap, and Top Half of Columns	79
Table B.2 Preston Bridge Calculation of Seismic Loads in the Longitudinal Direction.	85
Table B.3 Preston Bridge Calculation of Seismic Loads in the Transverse Direction.	86
Table B.4 Preston Bridge Final Abutment Stiffness Calculation for Longitudinal Direction	93
Table B.5 Preston Bridge Final Abutment Stiffness Calculation for Transverse Direction	94
Table B.6 Preston Bridge Comparison of Updated and Original Transverse Design Loads	95
Table B.7 Preston Bridge Linear Elastic Displacements and Column Base Reactions for Seismic Loads in the Longitudinal Direction	95
Table B.8 Preston Bridge Linear Elastic Displacements and Column Base Reactions for Seismic Loads in the Transverse Direction	96
Table B.9 Preston Bridge Linear Elastic Calculated Drift for Top of the Columns	96
Table B.10 Preston Bridge Nonlinear CIP Displacements and Column Base Reactions for Seismic Loads in the Longitudinal Direction	110
Table B.11 Preston Bridge Nonlinear CIP Displacements and Column Base Reactions for Seismic Loads in the Transverse Direction	111
Table B.12 Preston Bridge Nonlinear CIP Calculated Drift for Top of the Columns	111

ABSTRACT

Idaho is listed as the sixth most seismically active state in the United States. Seismic design of bridges is based on ductile behavior of bridge components when subjected to large ground motions. Bridges are typically designed such that the columns act as the ductile link between the deck and the foundation. The reinforcing steel bars in concrete bridge columns are prone to low cycle fatigue damage. During an earthquake, the reinforcing steel can undergo large inelastic strains of up to six percent (0.06) and fail due to plastic deformation. In this project, three bridges in Idaho are analyzed for seismic conditions of the city of Montpelier, which is the most seismically active location in Idaho. Computer models are created for these bridges with reinforced concrete deck and columns in OpenSees. These bridges are subjected to lateral seismic forces in the longitudinal and transverse directions and their corresponding column drifts are calculated. The Idaho Transportation Department is using ASTM A615 Grade 60 steel in the bridge columns. AASHTO recommends the use of both ASTM A615 and A706 reinforcing steel. In this study, the fatigue models from different researchers are considered for ASTM A615 and ASTM A706 reinforcing steel bars. The number of cycles to failure at different strain levels is estimated for both ASTM A615 and ASTM A706 reinforcing steel bars in the bridge columns based on the material properties. Comparison between the ASTM A615 and ASTM A706 rebars is made based on their low-cycle fatigue behavior in bridge columns. ASTM A706 reinforcing bars performed better than ASTM A615 bars.

CHAPTER 1 - INTRODUCTION

1.1. Background and Description

During an earthquake, the components of a structure will be exposed to inconsistent strains which will have varying tension and compression values. This kind of repeated loading weakens the material and is known as fatigue. A material subjected to cyclic loading may fail at stress levels much lower than the material yield or ultimate strength. Fatigue failure is a cumulative process of crack formation, spreading and fracture. Fatigue life of a material is estimated as number of cycles to failure, N_f (Stephens & Fuchs, 2001). Failure is defined as the fracture of the material (cracks propagate to complete fracture) when it is repeatedly loaded in tensile or compressive stress (Koh & Stephens, 1991). Majority of the mechanical engineering applications deal with high-cycle fatigue ($10^3 - 10^7$ cycles). For this type of testing, the strain amplitudes rarely exceed 0.01 (Mander, Panthaki, & Kasalanati, 1994). However, the strain reversals during an earthquake can have high stress levels and yet low number of cycles. For materials that have elastic-plastic properties, such as reinforcing steel, the fatigue-life curve can be broken up into two distinct regions. The first describes low-cycle fatigue behavior (less than 1000 cycles to failure) and is controlled by plastic deformations (Brown & Kunnath, 2000). The second describes high-cycle fatigue behavior and is controlled primarily by elastic deformation. The structural components of bridges can undergo large inelastic strains up to 0.06 and fail due to plastic deformation. This type of failure is known as low-cycle fatigue (LCF) failure.

When a component is subject to low cycle fatigue, it is repeatedly plastically deformed. For example, if a part were to be loaded in tension until it is permanently deformed (plastically deformed), that would be considered one-half cycle of low cycle fatigue. In order to complete a

full-cycle, the part would need to be deformed back into its original shape. The number of LCF cycles that a part can withstand before failing is much lower than that of regular fatigue (DeLuca, 2001). The response of reinforced-concrete structures to seismic forces can be predicted using a moment-curvature analysis by estimating the cyclic stress-strain behavior of the reinforcing steel in the critical region of the member (Dodd & Restrepo-Posada, 1995).

Seismic design of bridges is based on the ductile behavior of the bridge components under large earthquake loads. These ductile damage modes generally involve yielding of various structural members and the corresponding plastic deformation in these members. The maximum displacements in a bridge can be predicted using conventional elastic analysis techniques. This is based on various time-history analyses of yielding structures. This means, in many bridges, the displacements assuming elastic behavior are about the same as for a yielding bridge ($\Delta_{Inelastic\ max} = \Delta_{Elastic\ max}$) in Figure 1.1 (Marsh, Buckle, & Kavazanjian Jr, 2014).

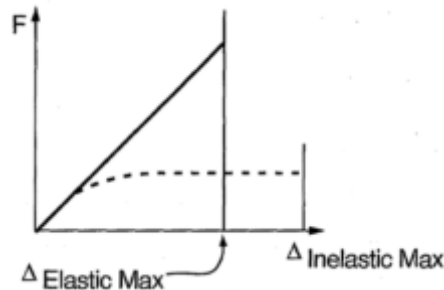


Figure 1.1 Maximum Elastic and Inelastic Displacements (Marsh, et al., 2014))

The capacity design concept developed by (Paulay & Priestley, 1992) can be illustrated using a chain analogy shown in Figure 1.2. If one link of the chain is ductile and the tensile strength of that link is less than the strength of the other links, which may even be brittle, the chain will exhibit ductile behavior based on the behavior of the one ductile link. However, if any

of the brittle links have strengths lower than that of the ductile link, then the chain will exhibit brittle behavior. In the case of a bridge, the entire lateral load path is analogous to the chain, and individual elements, such as columns, foundations, abutments, and superstructure comprise the links in the chain. This pertains to the columns acting as the link between the deck and the foundation in a bridge. Any deformation during an earthquake should likely occur in the columns rather than the deck or the foundation.

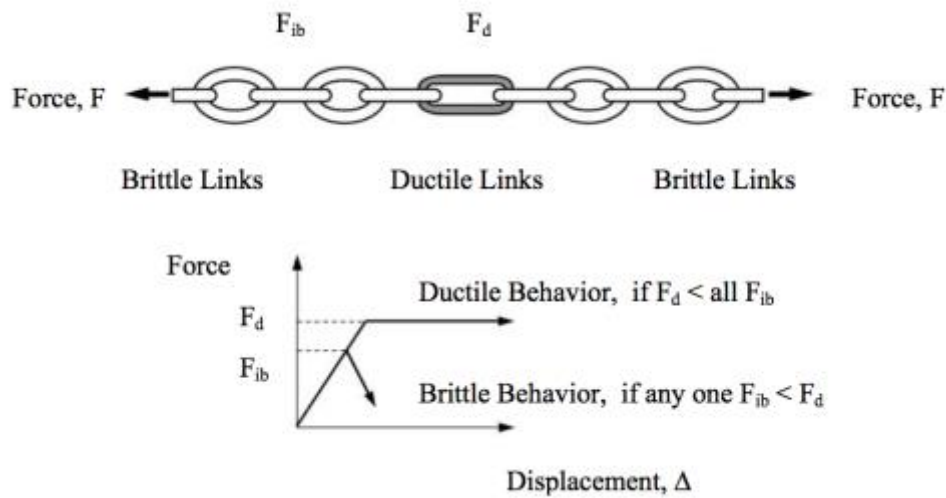


Figure 1.2 Chain Analogy for Capacity-Protected Design (Paulay and Priestly, 1992)

One notable incident in which the failure was due to low-cycle fatigue was the 1994 Northridge earthquake. Many buildings and bridges collapsed, and as a result over 9,000 people were injured (Taylor, 2016). Researchers at the University of Southern California analyzed the main areas of a ten-story building that were subjected to low-cycle fatigue. Unfortunately, there was limited experimental data available to directly construct a S-N curve for low-cycle fatigue, so most of the analysis consisted of plotting the high-cycle fatigue behavior on a S-N curve and extending the line for that graph to create the portion of the low-cycle fatigue curve using the Palmgren-Miner method. Ultimately, this data was used to more accurately predict and analyze

similar types of damage that the ten-story steel building in Northridge faced (Nastar, Anderson, Brandow, & Nigbor, 2010).

AASHTO permits the use of ASTM A615 Grade 60 and ASTM A706 Grade 60 steel bars in regions that fall into Seismic Design Categories (SDC) B and C. It also states, for SDC D, ASTM A706 shall be used in members where plastic hinging is expected (American Association of State Highway and Transportation Officials, 2015). ASTM A706 bars were initially produced to only Grade 60 with a minimum yield strength $f_y = 60,000 \text{ psi}$ (420 MPa), while ASTM A615 bars can have different grades ranging from Grade 40 to 80. However, ASTM A706 bars are currently produced in Grades 60 and 80. In broad terms, ASTM A706 steel is more demanding and includes requirements for controlled tensile properties and restrictions on chemical composition, while ASTM A615 steel does not include comparable requirements. Idaho Transportation Department (ITD) has been using ASTM A615 Grade 60 bars in many of the bridges in Idaho.

1.2. Objectives

Idaho is listed as the 6th most seismically active state in the United States. Around the world, low-cycle fatigue is not a new topic for research, yet it is still very new in terms of the amount of data that can be found for reinforcing bars. The objective of this research is to analyze the low-cycle fatigue behavior of the reinforcing bars in bridge columns in Idaho. Bridges from Preston, Parma, and Dubois were modeled in OpenSees and subjected to lateral seismic forces in the longitudinal and transverse directions. The corresponding displacements and drifts were calculated for the top of the columns. These bridges were analyzed for seismic conditions of the

city of Montpelier, that happens to be in the most seismically active region in Idaho. The number of cycles to failure for different levels of strains are estimated based on available data for both ASTM A615 Grade 60 and ASTM A706 Grade 60 reinforcing bars. This is based on the possibility of using ASTM A706 bars in Idaho bridges, replacing ASTM A615 bars.

1.3. Thesis Overview

This thesis document consists of five chapters in total. Chapter 1 provides the roadmap and brief introduction for the research. Chapter 2 provides a detailed literature review of relevant research associated with this thesis. The literature review chapter consists of study on fatigue life and low-cycle fatigue. It also comprises of studies made by different researchers on low-cycle fatigue behavior for ASTM A615 and ASTM A706 reinforcing steels and their corresponding fatigue models. The methodology for the seismic analyses of the three Idaho bridges is provided in Chapter 3. This chapter includes the assumptions for the procedure and computer modeling of these bridges in OpenSees (University of California, Berkeley, 2016). The three bridges considered were subjected to the seismic conditions for Montpelier, Idaho. Chapter 4 contains all the results associated with the bridge analyses. This comprises of the drift values for the top of the bridge columns. Drift is defined as the ratio of the displacement to the height of the structure. The results chapter also includes the low-cycle fatigue results at different strain levels using both ASTM A615 and ASTM A706 reinforcing steels for all three bridges. The low-cycle fatigue behaviors of these steels were compared. Chapter 5 summarizes the thesis and the results with appropriate conclusions and recommendations.

CHAPTER 2 - LITERATURE REVIEW

This chapter provides a literature review relevant to the study of low cycle fatigue behavior of reinforcing steel. Fatigue has always been one of the most important mechanisms of failure in reinforcing steel. During a seismic event, structural members can experience large strain reversals. This kind of strain reversals during an earthquake can have high levels of stress, but still low number of cycles. This can lead to failure of the structural components, which can be termed as low cycle fatigue failure.

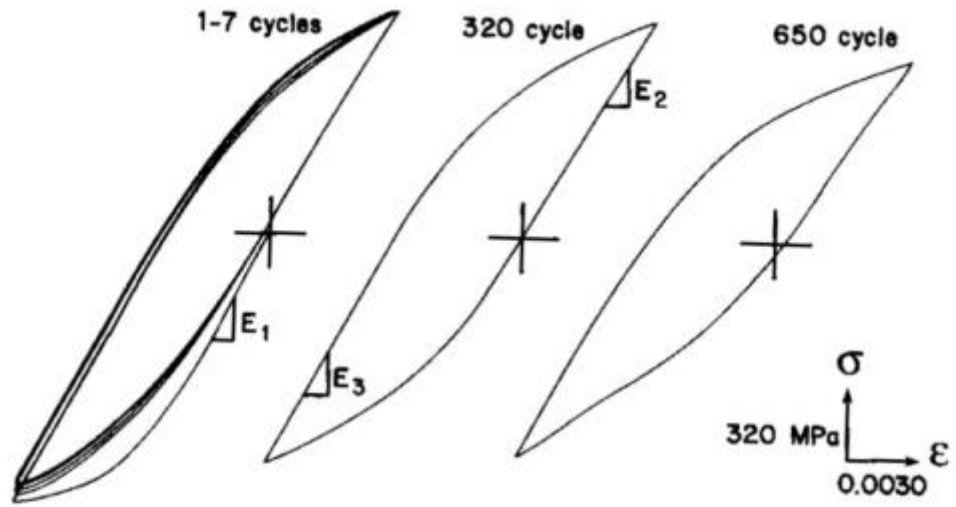
AASHTO permits the use of ASTM A615 Grade 60 and ASTM A706 Grade 60 rebars in regions that fall into Seismic Design Categories (SDC) B and C. AASHTO also states that for SDC D, ASTM A706 Grade 60 rebar shall be used in members where plastic hinging is expected (American Association of State Highway and Transportation Officials, 2015). Idaho Transportation Department (ITD) has been mostly using ASTM A615 Grade 60 in their bridge columns. One of the objectives of this thesis is to compare the low cycle fatigue behavior and cost differences of ASTM A615 Grade 60 and ASTM A706 Grade 60 rebars.

2.1. Fatigue Life and Low-cycle Fatigue

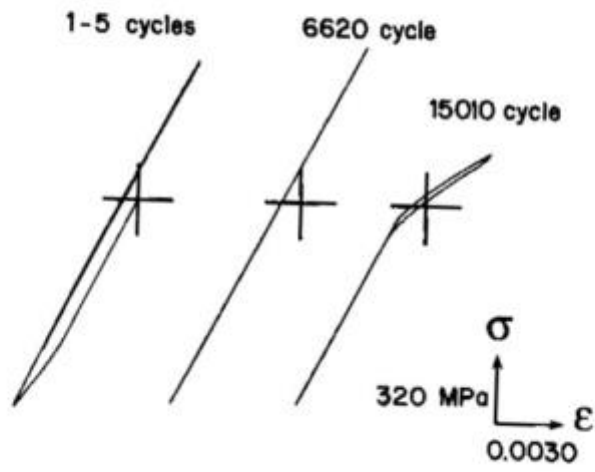
Fatigue life analysis using low cycle fatigue behavior has been used in research and design for many years. The low cycle fatigue is affected by the residual and mean stresses and has been presented in various ways over the years. Fatemi & Stephens studied the mean stress relaxation and the influence of mean strain/stress on the cyclic stress-strain relationship for a material (Fatemi & Stephens, 1987). The mean strain doesn't have any positive or negative effect on the fatigue life unless it produces a mean stress (Koh & Stephens, 1991). The study by Koh &

Stephens performed comprehensive investigation into the influence of mean strain-stress under strain-controlled low-cycle fatigue conditions with both positive and negative mean strains using high strength thick-walled pressure vessel steel. In this research, strain ratios of $R = -2, -1, 0, 0.5, 0.75$ were used to investigate the mean strain and mean stress effects on the low cycle fatigue behavior. R is defined as the ratio of minimum strain to maximum strain, $\frac{\epsilon_{min}}{\epsilon_{max}}$.

Representative hysteresis loops for strain ratios under both large and small strain-controlled amplitudes are shown in Figures 2.1 and 2.2. For a negative mean strain test with $R = -2$ and a relatively large strain amplitude of 0.008, Figure 2.1(a), shows continuous increase of minimum compressive stress resulting in significant relaxation of negative mean stress. However, for a negative mean strain test with a relatively small strain amplitude of 0.004, as shown in Figure 2.1(b), the cyclic stress and strain response is essentially elastic, and no significant compressive mean stress relaxation is seen. Very similar mean stress behavior was observed in the tensile mean strain tests. For example, Figure 2.2(a) for the larger strain amplitude with $R = 0.5$ shows typical tensile mean stress relaxation during the initial cycles throughout the fatigue life. The tests of high mean tensile strain, but with a relatively small strain amplitude in Figure 2.2 (b) shows the same mean stress relaxation at the very beginning of the test, but followed by stabilized behavior. Under $R = -1$ test conditions mean stresses were essentially zero until just before fracture.



(a) $\Delta\epsilon/2 = 0.008$



(b) $\Delta\epsilon/2 = 0.004$

Figure 2.1 Typical hysteresis loops for $R = -2$ (Koh & Stephens, 1991)

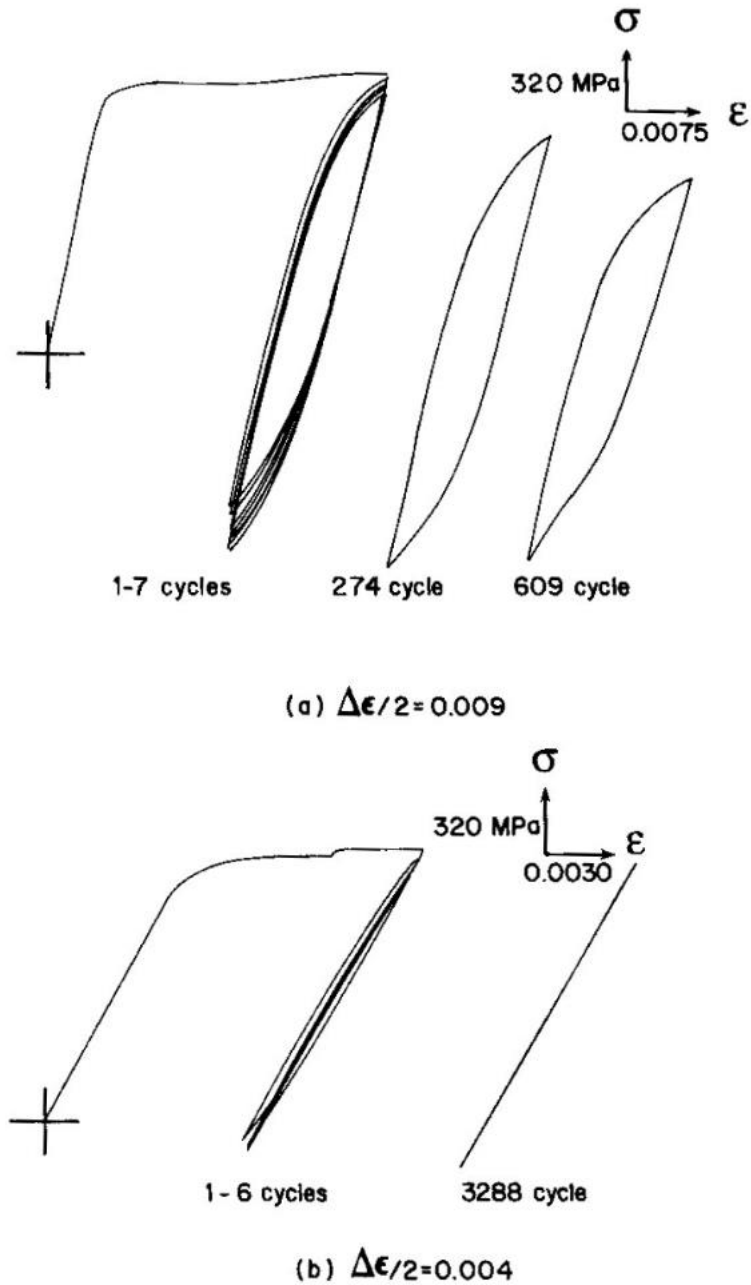


Figure 2.2 Typical hysteresis loops for $R = 0.5$ (Koh & Stephens, 1991)

The hysteresis loops of strain amplitudes below 0.005 were elastic during testing with all R ratios. At 0.005, a small plastic strain appeared. This confirms that the mean or residual stress is relaxed by plastic deformation. The mean stresses in higher strain amplitude tests dropped quickly to a steady-state low value of mean stress.

The cyclic stress-strain curve which represents the cyclic properties of a material was obtained using the companion specimen method that connects the maximum stress of the stabilized half-life hysteresis loops of the $R = -1$, low cycle fatigue tests.

The cyclic stress-strain curve is represented by

$$\frac{\Delta\varepsilon}{2} = \frac{\Delta\varepsilon_e}{2} + \frac{\Delta\varepsilon_p}{2} \quad (2.1)$$

where, $\varepsilon_e = \text{elastic strain}$, $\varepsilon_p = \text{plastic strain}$

The $R = -1$ cyclic stress-strain curve, and all data points from the mean strain tests are shown in Figure 2.3.

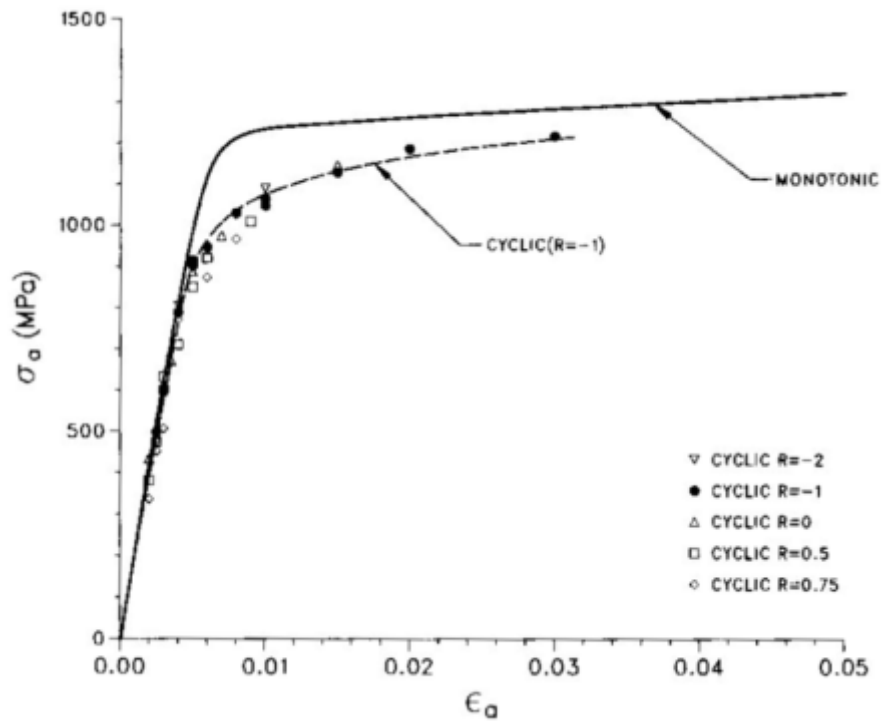


Figure 2.3 Monotonic and cyclic stress-strain behavior for all strain ratios. (Koh & Stephens, 1991)

The usual low cycle fatigue curve for $R = -1$ is shown in Figure 2.4.

A log-log scale total strain-life model used by Stephens and Koh for A356-T6 cast aluminum alloy was used to improve the conventional $R = -1$ strain-life model given by

$$\frac{\Delta\varepsilon}{2} = M(2N_f)^m \quad (2.2)$$

where,

$\frac{\Delta\varepsilon}{2}$ = strain amplitude

N_f = number of cycles to failure

M, m = constants

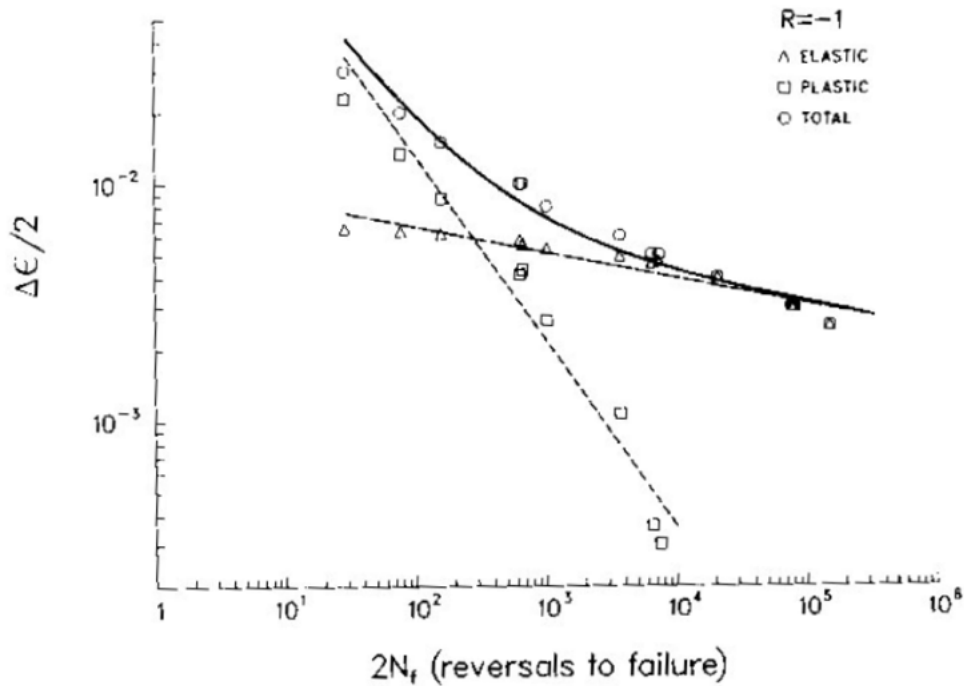


Figure 2.4 Low cycle fatigue behavior for $R = -1$. (Koh & Stephens, 1991)

Total strain-life curves of the low cycle fatigue tests for each strain ratio are shown in Figure 2.5. Figure 2.6 shows the superposition of data from all strain ratios. The difference in fatigue life for the same strain amplitude can be attributed to the mean stress. The larger the

magnitude of mean stress, the greater the difference in the fatigue life at the same strain amplitude (see Figure 2.6). This means, the mean strain with zero mean stress does not significantly affect the fatigue life, while means strain with considerable mean stress does affect the fatigue life significantly. Therefore, the mean stress can be considered as a major factor in low cycle fatigue. Tensile mean stress is detrimental to the fatigue life, while the compressive mean stress is beneficial.

To account for the mean stress in low cycle fatigue, Morrow (Morrow, 1968) modified the equation as:

$$\frac{\Delta\varepsilon}{2} = \frac{\sigma'_f - \sigma_m}{E} (2N_f)^b + \varepsilon'_f (2N_f)^c \quad (2.3)$$

Coffin (1954) and Manson (1953) were among the first to propose an equation relating strain amplitude to the number of cycles to failure (Coffin, 1954) (Manson, 1953):

$$\varepsilon_p = \varepsilon_f (2N_f)^c \quad (2.4)$$

where; ε_p = *plastic strain amplitude*

ε'_f = *a material constant to be determined by fatigue testing*

c = *fatigue exponent*

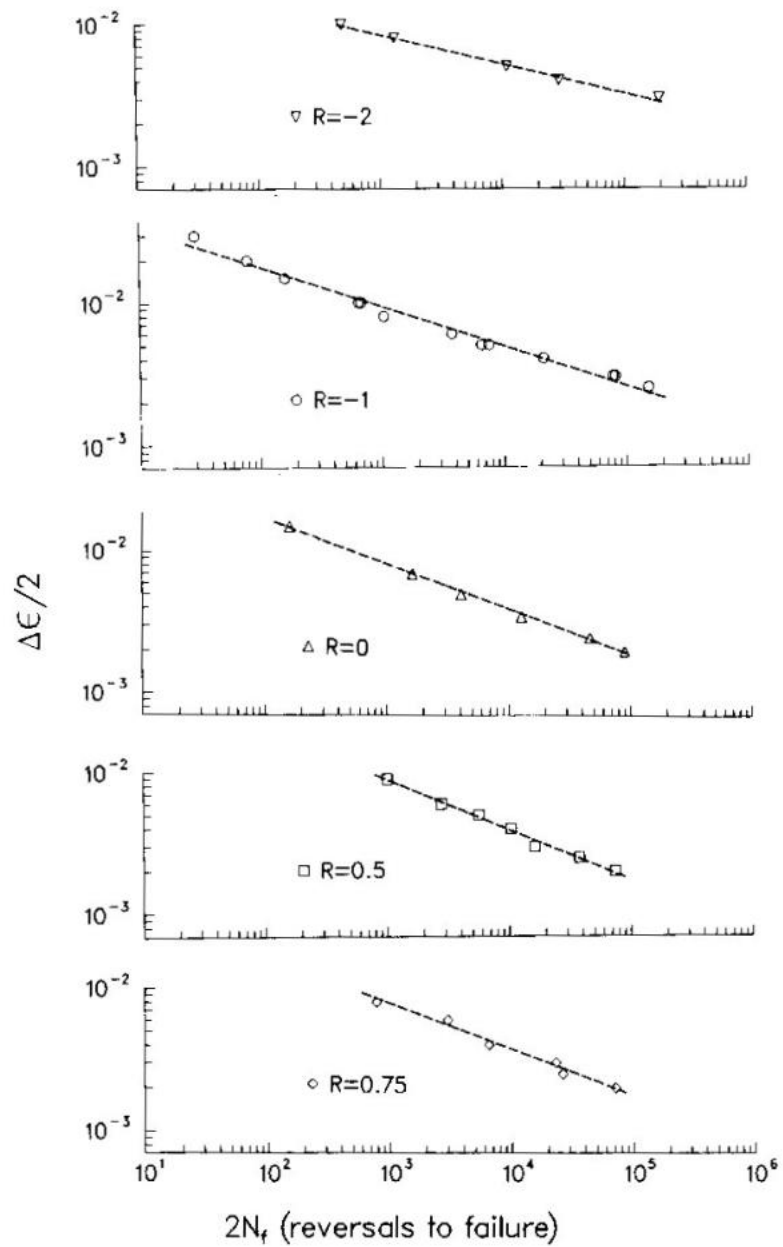


Figure 2.5 Log-log strain amplitude vs reversals to failure for each strain ratio. (Koh & Stephens, 1991)

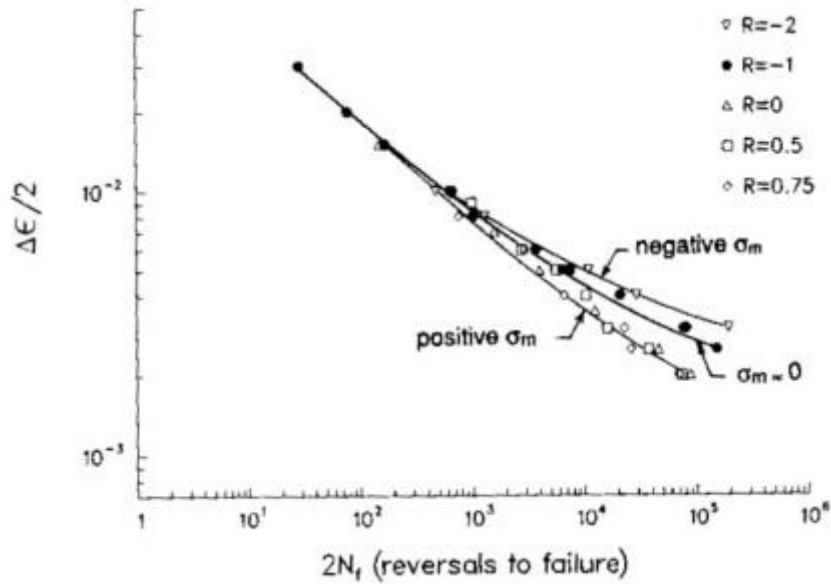


Figure 2.6 Low cycle fatigue behavior for all strain ratios. (Koh & Stephens, 1991)

Comparison of fatigue lives using Morrow's equation with experimental fatigue lives is shown in Figure 2.7.

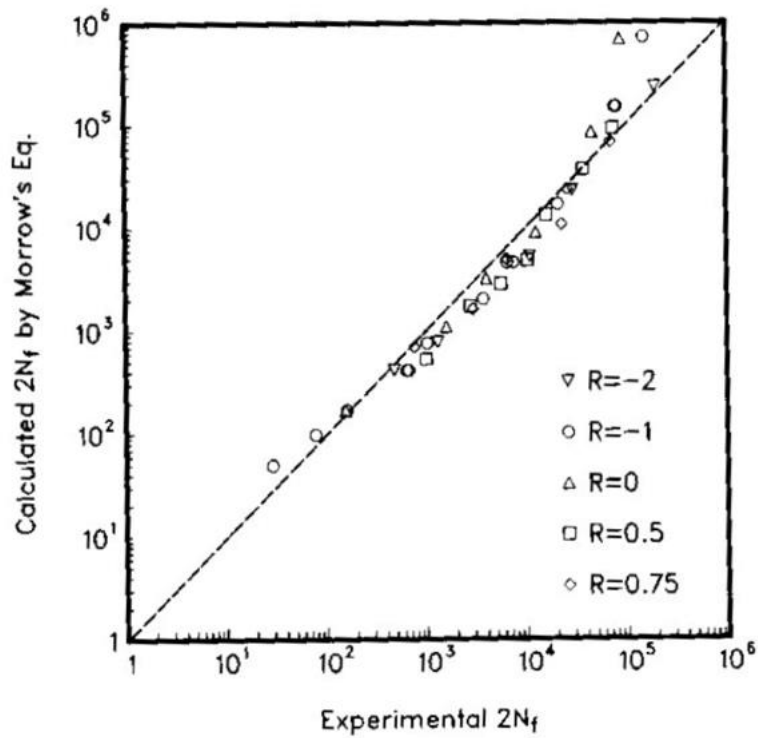


Figure 2.7 Correlation of Morrow's model for mean stress. (Morrow, 1968)

Smith et al, proposed another popular model as (Smith, Topper, & Watson, 1970):

$$\sqrt{\sigma_{max}\varepsilon_a E} = f(2N_f) \quad (2.9)$$

and

$$\sigma_{max}\varepsilon_a = \frac{(\sigma'_f)^2}{E} (2N_f)^{2b} + \sigma'_f \varepsilon'_f (2N_f)^{b+c} \quad (2.10)$$

$$= A(N_f)^\alpha + B(N_f)^\beta \quad (2.11)$$

The study by Koh & Stephens (1991) concluded that the cyclic stress-strain response based upon half-life hysteresis loop peaks were very similar for all strain R values. Only a slight amount of additional cyclic softening occurred with strain R ratios not equal to -1. Additionally, Mean strains did not affect low cycle fatigue life unless they were accompanied by half-life mean stress. Tensile mean stress was detrimental to low cycle fatigue life while compressive mean stress did not have much effect. All these equations derived from various studies are used for estimating the fatigue life of reinforcing steel under different strain level.

2.2. Low-cycle Fatigue in Reinforcing Steel Bars

One of the earliest and most common practices of low-cycle fatigue testing of reinforcing steel comprises of the test specimens usually machined to form a smooth reduced section. However, the reinforcing steel used for concrete structures have deformations for better bond to concrete formed as a part of the steel rolling process. Thus, to reflect the actual behavior of the bar, it is important to leave the original cross section of the deformed reinforcing bar unaltered during testing. This is to directly capture the inelastic bucking that occurs in the compression region of a structural concrete element (Mander, Panthaki, & Kasalanati, 1994). The study by

Mander et al. (1994) is one of the most significant in terms of low-cycle behavior of reinforcing steel and this paper is being referenced in many of the sections in this thesis. The physical modeling of the reinforcing steel behavior for Mander et al. (1994) is shown in Figure 2.8.

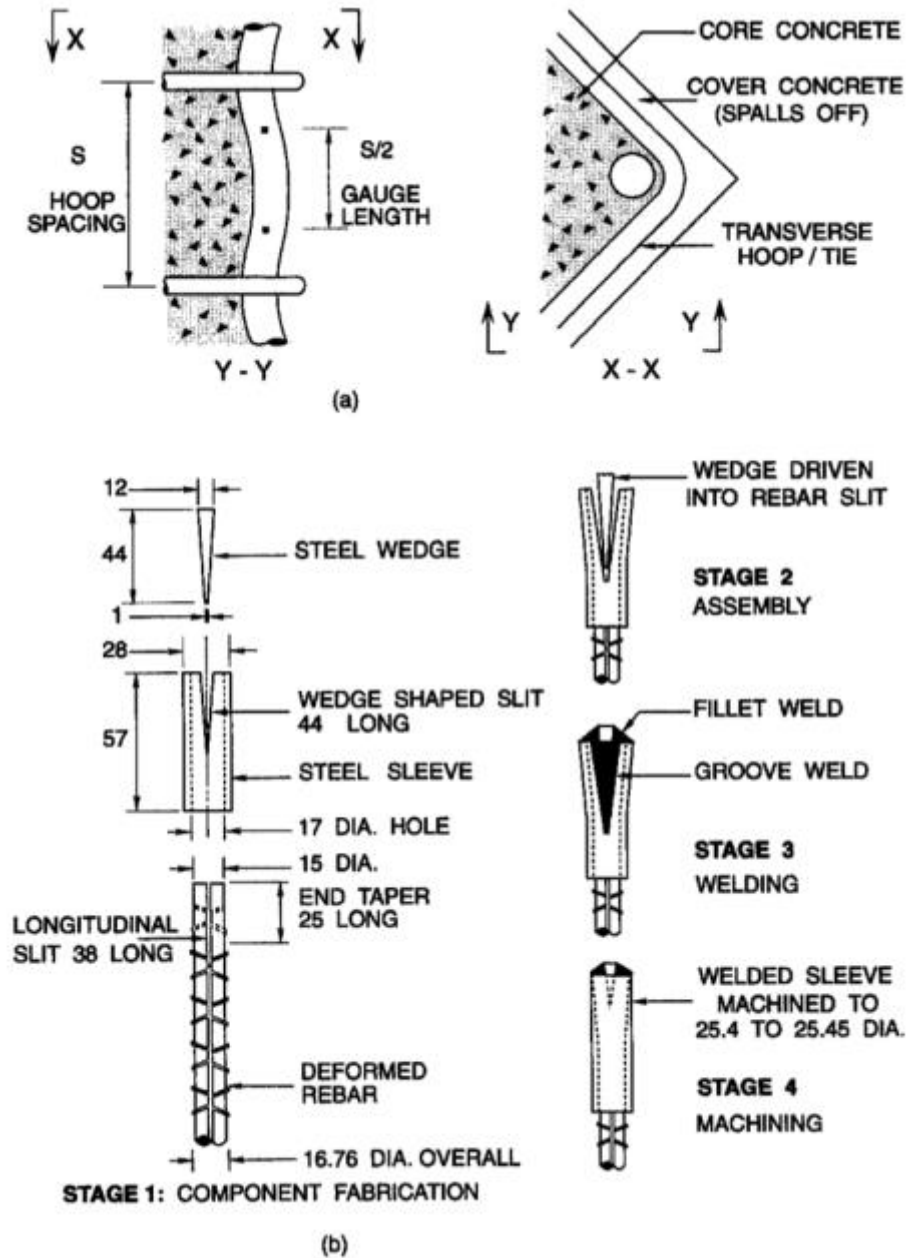


Figure 2.8 Physical modeling of reinforcing steel behavior: (a) in-situ conditions of reinforcing bar; and (b) specimen fabrication procedure. (Mander et al., 1994)

Mander (1994) tested two different types of steel with various specimens in each type. ASTM A722 type II hot-rolled and proof-stressed alloy-steel bar having a specified minimum ultimate tensile strength of 1083 MPa, represented by P was the first type of material that was used. Whereas, the second type of material used, represented by R was ASTM A615 Grade 40 deformed billet-steel reinforcing bar having a minimum specified yield strength of 276 MPa.

Mean stress effects come into play for longer fatigue lives that have a predominantly elastic strain component. For cases that have low strain amplitudes (< 0.005), the fatigue life may increase or decrease depending on the sign of the mean stress being compressive or tensile (Koh & Stephens, 1991). As shown earlier in Figure 2.6, at higher strain amplitudes, where plastic strains are significant, mean stress relaxation occurs, which tends to reduce any mechanically or thermally induced mean stresses toward zero or a very small value such that it has no perceptible effect on the fatigue life. Thus, for the range of strain amplitudes used for the study of low-cycle fatigue (1 – 6 %), mean stress effects are negligible.

Mander's study found that for high-strength bars under cyclic-strain reversals, the peak cycle stress drops quickly in the first few cycle, i.e., softening occurs. Whereas, for reinforcing bars, cycling causes hardening over the first few cycle, after which the peak cycle stress decreases very gradually to almost constant value over many cycle until incipient failure occurs at the onset of a fatigue crack. Cycling can continue, but the crack propagates quickly with the peak stress dropping rapidly until fracture occurs. For low-cycle fatigue tests on ordinary deformed reinforcing steel bar or high-strength prestressing-steel thread bar with large strain amplitudes (1 – 5 %) typical of segments from longitudinal reinforcement histories under strong seismic excitations, mean stress and mean strain have negligible effect on low-cycle fatigue life.

For seismic design, conventional wisdom requires ductile detailing that maximizes the displacement/curvature ductility in the structural elements. In Mander's study, the displacement ductility of the high-strength steel threaded bar is only 17% of the deformed mild-steel bar. It is therefore not surprising that seismic codes limit the yield strength of the reinforcing steel to grade 60 ($f_y = 414 \text{ MPa}$).

Low-cycle fatigue of the longitudinal reinforcing steel is one of the most important failure modes of seismic damage in reinforced concrete bridge columns. Brown and Kunnath (2000) performed low-cycle fatigue tests on ASTM A615 Grade 60 steel to develop a fatigue-life relationship for typical longitudinal reinforcement that aid the development of cumulative damage models. (Brown & Kunnath, 2000). A typical fatigue-life curve for a material is shown in Figure 2.9.

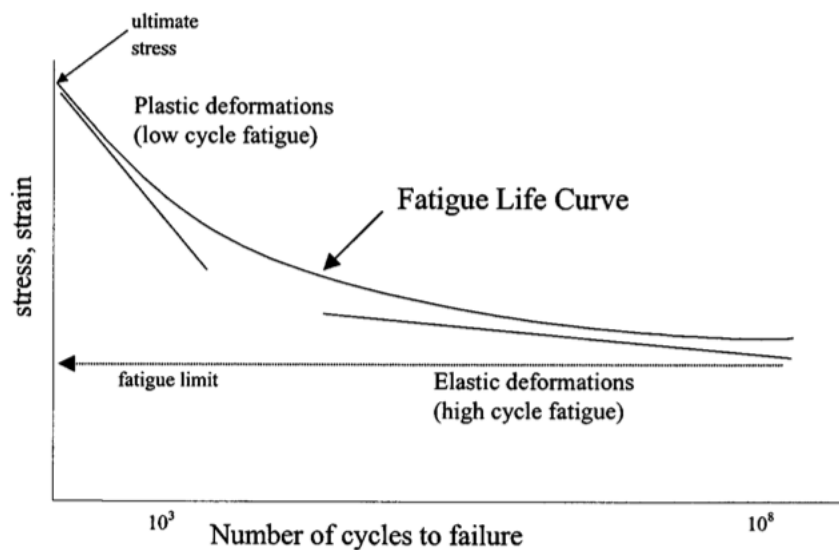


Figure 2.9 Typical Fatigue-life Curve for an Engineering Alloy (Brown and Kunnath, 2000)

Brown and Kunnath (2000) tested reinforcing bars (#6, #7, and #8) for a strain range of +/-0.015 and +/-0.030. The results for the low-cycle fatigue tests for these reinforcing bars are shown in Tables 2.1, 2.2, and 2.3 and a visual representation is shown in Figure 2.10.

Table 2.1 #6 Specimens: Low-cycle Fatigue Results for A615 steel (Brown and Kunnath, 2000)

Strain, ϵ	Number of half cycles to failure, $2N_f$
0.0150	174
0.0175	122
0.0200	98
0.0225	88
0.0250	60
0.0300	44

Table 2.2 #7 Specimens: Low-cycle Fatigue Results for A615 steel (Brown and Kunnath, 2000)

Strain, ϵ	Number of half cycles to failure, $2N_f$
0.0125	308
0.0150	184
0.0175	122
0.0175	190
0.0200	92
0.0225	84
0.0250	76
0.0250	76
0.0275	44
0.0300	48

Table 2.3 #8 Specimens: Low-cycle Fatigue Results for A615 steel (Brown and Kunnath, 2000)

Strain, ϵ	Number of half cycles to failure, $2N_f$
0.0150	222
0.0175	156
0.0200	122
0.0225	88
0.0250	56

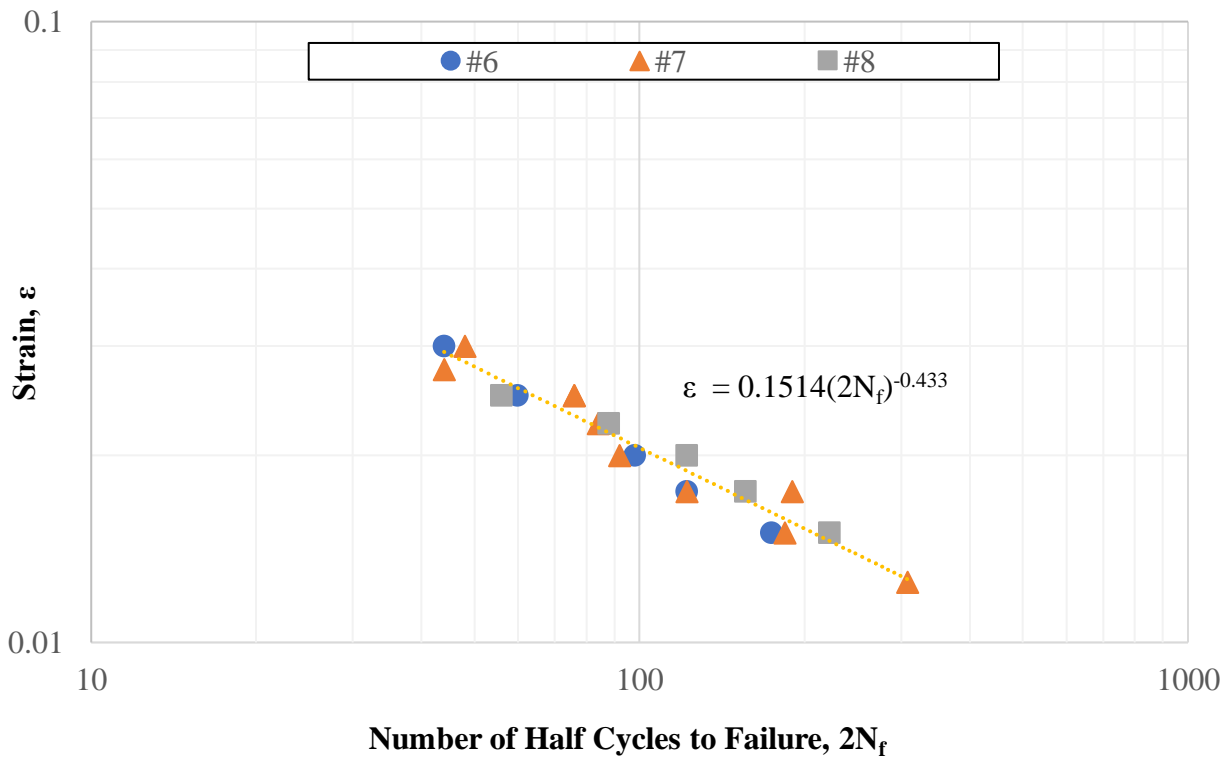


Figure 2.10 Strain vs Number of Half Cycles to Failure for A615 steel (Brown and Kunnath, 2000)

Another experimental study on low-cycle fatigue behavior for steel reinforcing bars was conducted by Zhou (2008) using five different kinds of #8 size steel bars (Zhou, 2008). One of these five different steel types was ASTM A706 Grade 60 steel. The results for the low-cycle fatigue tests for A706 steel are shown in Table 2.4 and in Figure 2.11.

Table 2.4 #8 Specimens: Low-cycle Fatigue Results for A706 steel (Zhou, 2008)

Strain, ϵ	Number of half cycles to failure $2N_f$
0.02614	136
0.02437	158
0.02074	218
0.01393	368
0.01407	475
0.01461	529
0.0139	485
0.01022	944
0.00744	1600
0.00673	2372

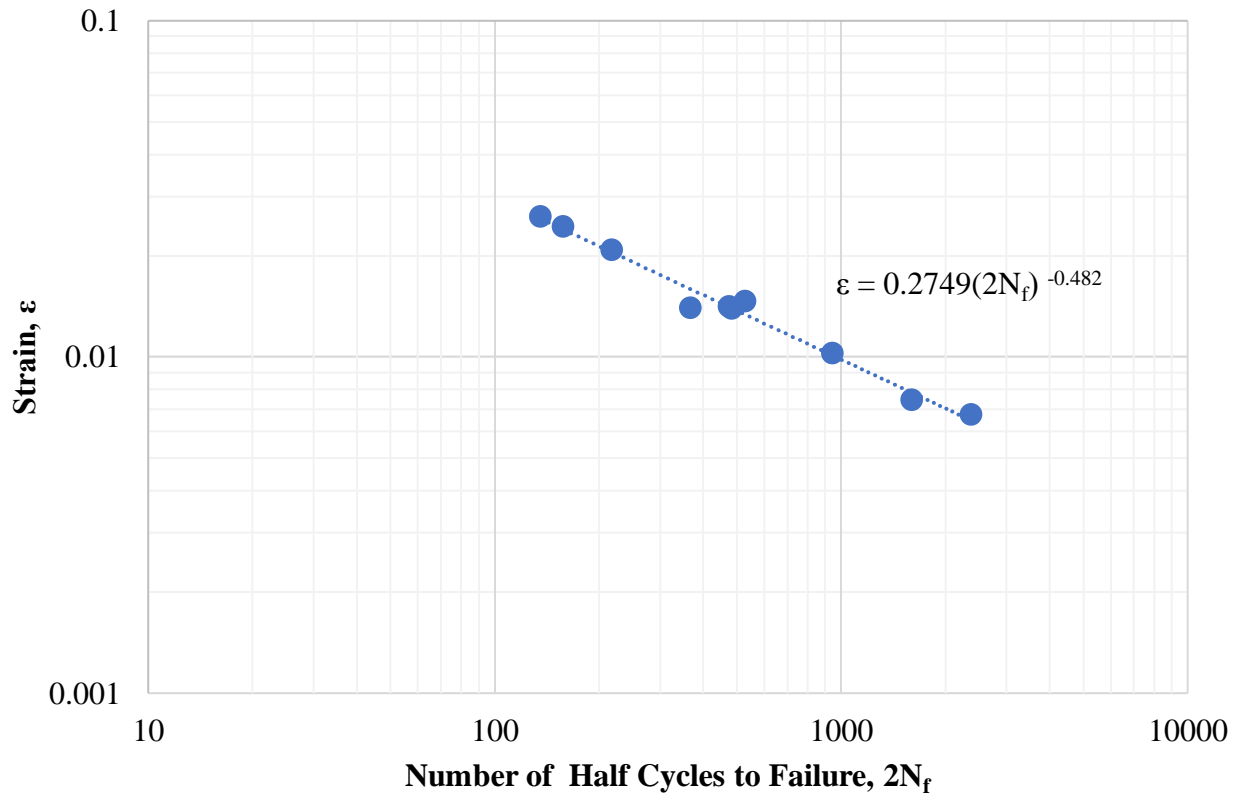


Figure 2.11 Strain vs Number of Half Cycles to Failure for A706 steel (Zhou, 2008)

Hawileh et al. (2009) evaluated the low-cycle fatigue life in #6 sizes ASTM A706 and A615 steel bars, both of Grade 60, and compared these steel bars in hybrid precast frame connections (Hawileh, Rahman, & Tabatabai, 2009). The deformed bars were subjected to cyclic strains ranging from zero to a peak strain that varied between 2 and 8%. Although this study was aimed at evaluating the condition of steel bars in precast hybrid frame connections, the results can equally apply to other similar applications.

The low-cycle fatigue results for A615 and A706 steel bars are shown in Tables 2.5 and 2.6. The graphs showing strain and number of half cycles in log scale are shown in Figures 2.12 and 2.13 for A615 and A706 steel bars respectively.

The number of cycles to failure was comparable between A706 and A615 bars but was generally higher in A615 bars. This is even though A706 bars exhibit higher ductility in monotonic tests.

Figure 2.14 shows the low-cycle fatigue results from Brown & Kunnath (2000), Zhou (2008), and Hawileh (2009) for A615 and A706 steels all in a same graph.

Table 2.5 #6 Specimens: Low-cycle Fatigue Results for A615 steel (Hawileh et al., 2009)

Strain, ϵ	Number of Half Cycles to Failure, $2N_f$
0.02	208
0.02	306
0.04	48
0.04	48
0.06	18
0.06	18
0.08	10
0.08	12

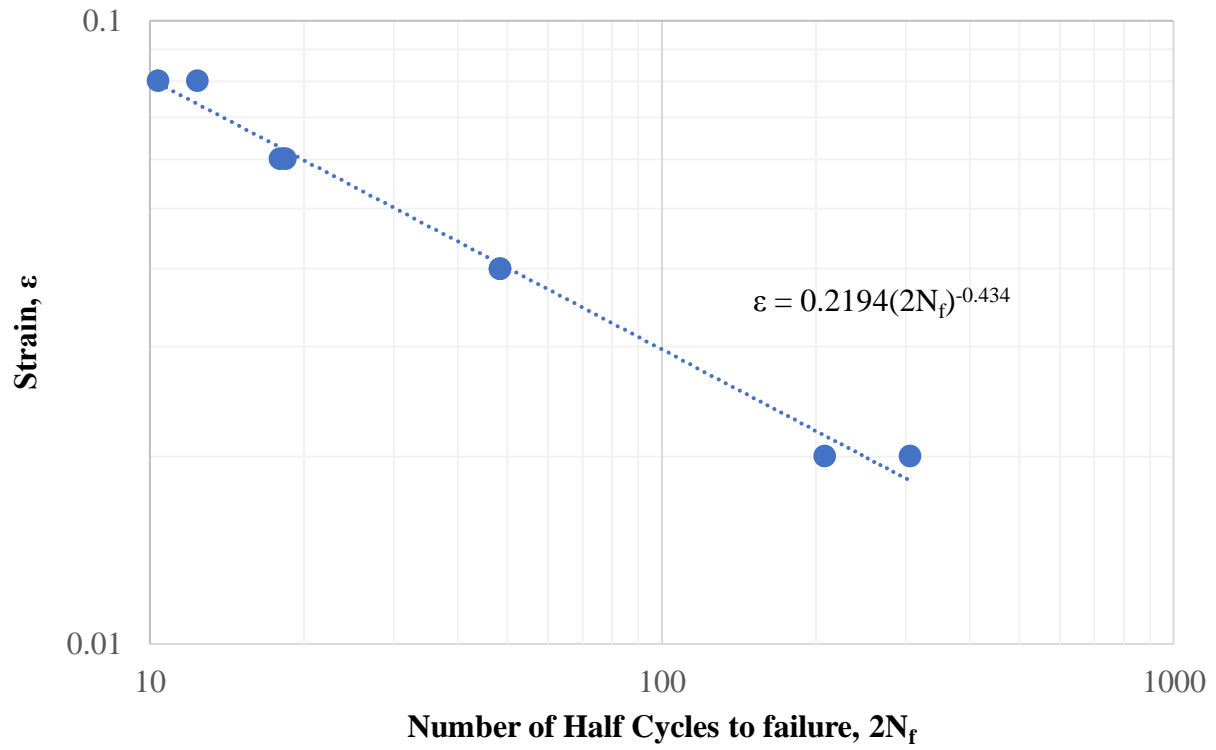


Figure 2.12 Strain vs Number of Half Cycles to Failure for A615 steel (Hawileh et al., 2009)

Table 2.6 #6 Specimens: Low-cycle Fatigue Results for A706 steel (Hawileh et al., 2009)

Strain, ϵ	Number of Half Cycles to Failure, $2N_f$
0.02	248
0.02	206
0.02	224
0.03	74
0.03	82
0.04	36
0.04	36
0.04	39
0.05	18
0.05	22
0.05	24
0.06	14
0.06	14
0.07	10
0.07	10
0.07	10
0.08	8
0.08	8

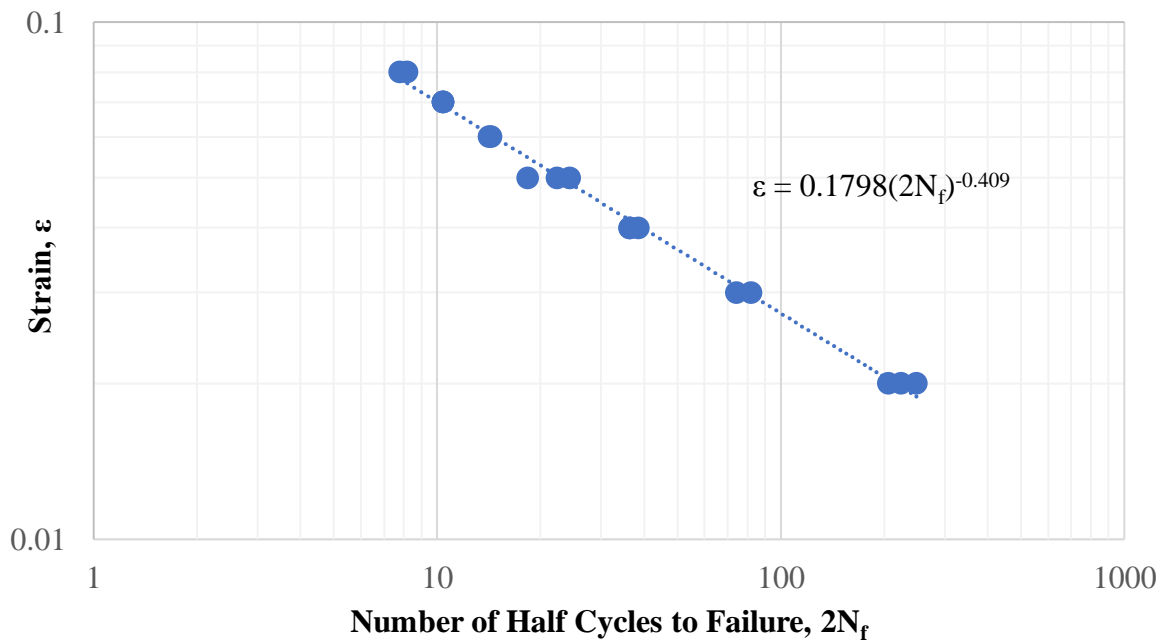


Figure 2.13 Strain vs Number of Half Cycles to Failure for A706 steel (Hawileh et al., 2009)

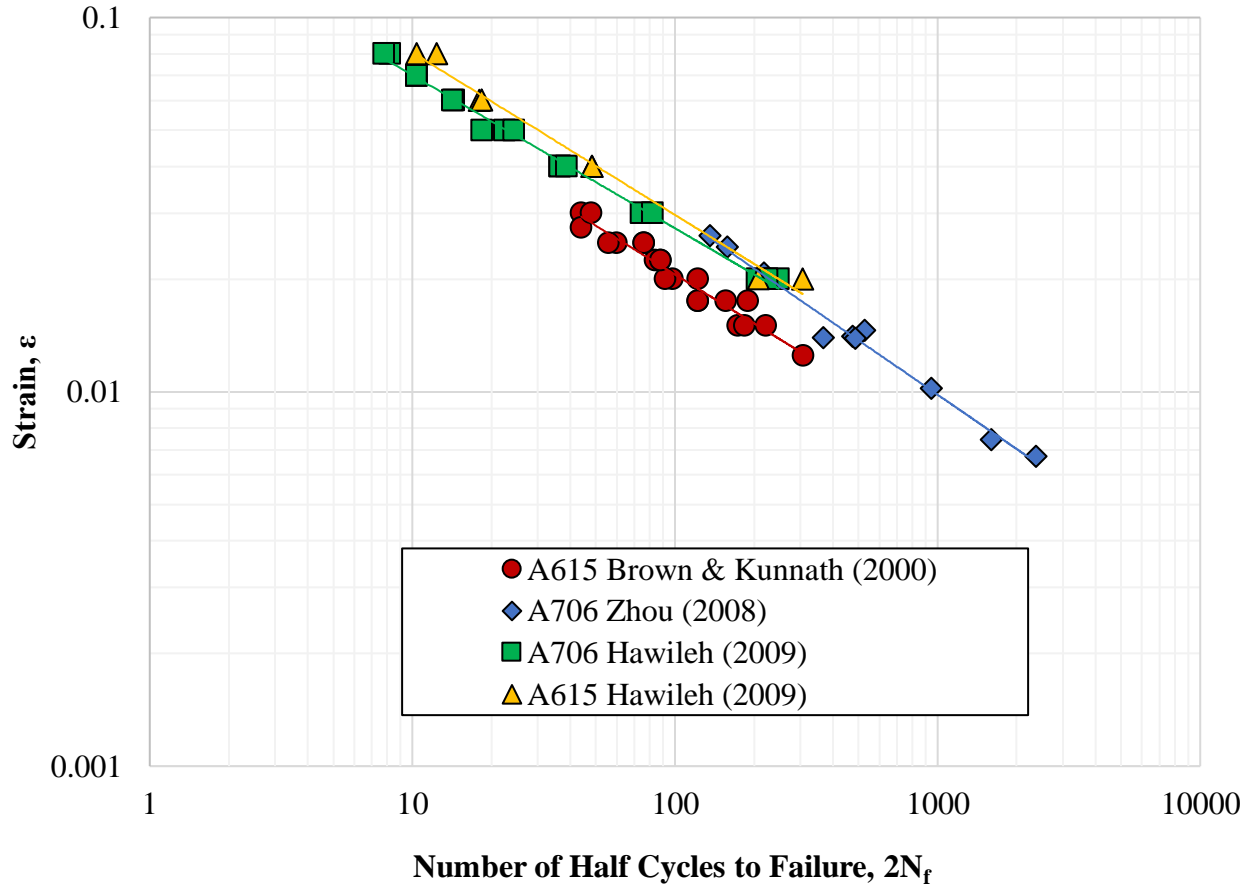


Figure 2.14 Strain vs Number of Half Cycles to Failure for A615 and A706 steels (Brown and Kunnath, 2000) (Zhou, 2008) (Hawileh et al., 2009)

2.3. Comparison of ASTM A615 and ASTM A706 reinforcing steel bars

AASHTO has permitted the use of ASTM A615 Grade 60 or ASTM A706 Grade 60 reinforcing steel bars in bridge columns. Table 2.7 shows the stress properties of ASTM A615 Grade 60 and ASTM A706 Grade 60 rebars (American Association of State Highway and Transportation Officials, 2015). Idaho Transportation Department (ITD) has been using ASTM A615 bars for the bridge columns in Idaho. ASTM A615 rebar is most commonly used in low-stress and less-demanding applications, and makes an economical choice in situations where a

tremendous level of tensile strength is not necessarily needed. Its strength and performance characteristics are grade-dependent, and A615 rebar is available in a full range of standard sizes, including: #3 through #11, #14 and #18. ASTM A706 rebar is a specification given to low-alloy reinforcing bars in either standard lengths or coiled configurations. This rebar grade is processed in open hearths, electric furnaces, or basic oxygen furnaces and is available in numerous grades, including grade 60 and grade 80. A706 steel is especially recommended for capacity-protected structures, and it is commonly used in bent caps, footings, joints, and oversized shafts (Harris Supply Solutions, 2017). While manufacturing A706 steel, the tensile strength shall not be less than 1.25 times the actual yield strength. This specification limits chemical composition and carbon equivalent of the steel to enhance the weldability of the material, and thus A706 steel is known as a weldable rebar (ASTM International, 2017).

Table 2.7 Stress properties of ASTM A706 Grade 60 and ASTM A615 Grade 60 reinforcing steel bars (AASHTO Seismic Guide, 2015).

Property	Notation	Bar Size	ASTM A706 Grade 60	ASTM A615 Grade 60
Specified minimum yield stress (<i>ksi</i>)	f_y	#3-#18	60	60
Expected yield stress (<i>ksi</i>)	f_{ye}	#3-#18	68	68
Expected tensile strength (<i>ksi</i>)	f_{ue}	#3-#18	95	95
Expected yield strain	ϵ_{ye}	#3-#18	0.0023	0.0023
Onset of strain hardening	ϵ_{sh}	#3-#8	0.0150	0.0150
		#9	0.0125	0.0125
		#10 & #11	0.0115	0.0115
		#14	0.0075	0.0075
		#18	0.0050	0.0050
Reduced ultimate tensile strain	ϵ_{su}^R	#4-#10	0.090	0.060
		#11-#18	0.060	0.040
Ultimate tensile strain	ϵ_{su}	#4-#10	0.120	0.090
		#11-#18	0.090	0.060

ASTM A706 steel provides larger values of minimum elongation than those in ASTM A615 steel. A comparison of the requirements for the two specifications is shown in Table 2.8 (Gustafson, 2007).

Table 2.8 Comparison of minimum percent elongation in ASTM A706 and A615 rebars (Gustafson, 2007)

Bar size	Minimum elongation, %	
	A706	A615
#3 to #6	14	9
#7 and #8	12	8
#9 to #11	12	7
#14 and #18	10	7

ASTM A615 rebars are more common and almost all the suppliers carry A615 steel. A706 bars are comparatively newer but, the production and availability has been growing. Considering material cost only, A706 bars cost about \$40 to \$60 *per ton* (1 *ton* = 2000 *lb*) more than A615 bars. The average price (material cost) nationwide for steel reinforcing bars was about \$700 *per ton* in 2007, which was presumed to be the price for A615 bars. The premium for A706 bars translated into a 6 to 9% increase in material cost over A615 bars. To put the premium in perspective, it should be related to the total in-place cost of the reinforcing bars that would include the cost of the material, detailing, fabrication, accessories, transportation, and placing (installing) the bars in the forms. According to the price index issued by the California Department of Transportation, the total in-place cost of reinforcing steel was as high as \$2000 *per ton* in 2007. For the sake of this discussion, let's assume the in-place cost is

\$1500 *per ton*. The premium for using A706 bars instead of A615 bars would be only about 3 to 4% (Gustafson, 2007).

A recent price quote provided by American Construction Supply (ACS), Inc. located in Pocatello, ID presented us with valuable information. According to ACS, the cost for Grade 60 ASTM A615 and A706 steel bars depended upon the bar sizes and their weights. We asked the ACS for price quotes for bar sizes of #9, #10, and #11 with a length of 60 *ft*. The weights for 60 *ft*. rebars of #9, #10, and #11 were 204 *lb.*, 258 *lb.*, and 318 *lb.* respectively. As per ACS, the price for ASTM A706 and ASTM A615 rebars at 60 *ft*. would be \$40.60 *per 100 lb.* (\$0.41/*lb.*) and \$39.98 *per 100 lb.* (\$0.40/*lb.*) respectively. The costs for #9, #10, and #11 rebars at 60 *ft*. are shown in Table 2.9 (American Construction Supply, Inc., 2017).

Table 2.9 Cost comparison for ASTM A706 and ASTM A615 rebars at 60 ft. (American Construction Supply, Inc., 2017)

Bar Sizes	Cost at 60 ft.	
	ASTM A706	ASTM A615
#9	\$82.91	\$81.56
#10	\$104.85	\$103.15
#11	\$129.24	\$127.14

Concrete Construction Supply (CCS) located in Meridian, ID provided us with another valuable information regarding ASTM A615 and A706 rebars. According to them, the weights for #9, #10, and #11 size rebars are 3.4 *lb/ft*, 4.3 *lb/ft*, and 5.3 *lb/ft* respectively. The weights for #9, #10, and #11 at 60 *ft*. would be 204 *lb.*, 258 *lb.*, and 318 *lb.* respectively, which are the same as what the American Construction Supply provided. According to CCS, the price for these rebars would be \$0.80/*lb* and there was no difference in cost between A615 and A706 rebars

(Concrete Construction Supply, 2017). Steel West Inc. located in Chubbuck, ID also gave up some price quotes regarding A615 and A706 rebars. According to them, the prices are the same for both A615 and A706 rebars (about \$0.70/lb) (Steel West Inc., 2017).

2.4. Summary

This chapter presented a review of literature to the study of low-cycle fatigue of steel including reinforcing steel bars. A summary of significant points is presented:

- The cyclic stress-strain curve is represented by a total strain amplitude, which is a combination of elastic and plastic strains.
- When the strain ratio, $R = -1$, the mean stress would be zero.
- Low-cycle fatigue test data for both ASTM A615 and A706 rebars are tabulated and graphed.
- Low-cycle fatigue results for ASTM A615 rebars were collected from studies by Brown & Kunnath (2000) and Hawileh et al. (2009).
- Low-cycle fatigue results for ASTM A706 rebars were collected from studies by Zhou (2008) and Hawileh et al. (2009).
- Comparison of ASTM A615 and ASTM A706 bars was made based on the availability and cost of these reinforcing steel bars.

CHAPTER 3 - METHODOLOGY

This chapter provides the basic methodology for OpenSees modeling of three bridges in Idaho. The bridge modeled in the FHWA “Seismic Design of Bridges Design Example No. 1” document is used as a reference for the modeling of the bridges (Mast, et al., 1996). The use of grouted couplers in the plastic hinge regions of the bridge columns was the agenda for the project of Idaho Transportation Department (ITD) (Ebrahimpour, Earles, Maskey, Tangarife, & Sorensen, 2016). The ITD project employed three models for each of the three ITD bridges selected for the study. These are: (a) bridge with linear-elastic cast-in-place columns, (b) bridge with nonlinear cast-in-place columns (CIP), and (c) bridge with nonlinear precast columns and grouted couplers (GCNP). Since the CIP and the GCNP models did not have much difference in the results, only the former will be included in this chapter along with the linear-elastic model.

3.1. Methods and Assumptions in Modeling the Three Idaho Bridges

The selected bridges were subjected to the ground acceleration of the most seismically active location in Idaho. We found that Montpelier, located in southeast Idaho, is the most seismically active city in Idaho. Site soil classification D (stiff soil) was assumed for all three bridges. Using the USGS seismic design map, this combination of conditions gives a design short duration acceleration of $S_{DS} = 0.907$ and a one-second design acceleration of $S_{D1} = 0.486$ (United States Geological Survey, 2016).

For simplicity, the bridges were assumed to have zero skew. Column bases were assumed to be fixed. For the model with cracked linear-elastic columns, the columns were assumed to extend half the footing depth below the top of the footing (as per FHWA Bridge Design Example 1) (Mast, et al., 1996). For the models with nonlinear materials for columns, the actual length of

the columns was used, but bond-slip elements were added at the bottom and top of the columns. In addition, in the nonlinear models only the columns were assumed to behave in a nonlinear manner; the superstructure was assumed to be linear-elastic.

For the linear-elastic bridge models (i.e., models with cracked linear-elastic columns), the effective column section properties were obtained using a procedure outlined in Section 5.6 of the AASHTO Guide Specifications for LRFD Seismic Bridge Design. For torsional behavior of columns, 20 percent of torsional stiffness of the columns was used. (See Section 5.6.5 of the AASHTO Guide) (American Association of State Highway and Transportation Officials, 2015).

For the nonlinear column's bending and axial behavior, there was no need to use the procedure outlined in Section 5.6 of AASHTO Seismic Design Guide. Nonlinear materials were used for the unconfined concrete, confined concrete, and longitudinal steel bars. In the nonlinear models, the torsional behavior was assumed to be linear-elastic. Similar to the linear model, 20 percent of torsional stiffness of the columns was "aggregated" with (i.e., added to) the nonlinear bending and axial effects.

3.2. Material Properties in Nonlinear Columns

For longitudinal steel reinforcing bars the appropriate material properties for ASTM A706 steel were used as per Table 8.4.2-1 of the LRFD Seismic Bridge Design Guide (American Association of State Highway and Transportation Officials, 2015). OpenSees *ReinforcingSteel* model was used to model steel stress-strain behavior. It should be noted that ITD is currently using ASTM A615 Grade 60 rebars for longitudinal steel reinforcing. The only difference between ASTM A706 and ASTM A615 steel bars is the ultimate strain value. For the bar sizes that we considered for the Idaho bridges, the ultimate strains are 0.09 for A706 steel and 0.06 for

A615 steel. As it will be seen in the later sections, the most stressed bar is in the Parma bridge with a steel strain of approximately 0.01. Using the ASTM A706 steel in our models will allow us to compare the low-cycle fatigue of steel reinforcing bars. We will predict the number of cycles to fracture of the steel bars for both types of steel.

For unconfined concrete, the strength values of cast-in-place concrete as specified in the bridge plans were used. OpenSees *Concrete01* stress-strain model was used for unconfined concrete. As per Sec. 8.4.4 of the LRFD Seismic Bridge Design Guide, a compressive strain of 0.002 at maximum unconfined concrete compressive strength was used (American Association of State Highway and Transportation Officials, 2015).

For the confined concrete, OpenSees *Concrete04* stress-strain model was used. Also, as per Sec. 8.4.4 of the LRFD Seismic Bridge Design Guide, this stress-strain model was used with concrete confined strength and strain values determined by Mander's model (American Association of State Highway and Transportation Officials, 2015) (Mander, Priestley, & Park, Theoretical Stress-Strain Model for Confined Concrete, 1988).

3.3. Method of Seismic Analysis

To keep the analysis simple, the single-mode spectral method was used for all three bridge analyses. In addition, the abutment stiffness values were obtained using the bridge model with cracked linear-elastic columns and the procedure used by ITD shown in Appendix A. The same abutment stiffness values were assumed in the bridge models with nonlinear columns.

To obtain the longitudinal and transverse seismic loads, the bridge model with cracked linear-elastic columns was analyzed. This was done by following the single-mode spectral procedure outlined in the FHWA Seismic Design Example 1 (Mast, et al., 1996). The only

difference was that, as per ITD Technical Advisory Committee recommendation, column bases were assumed to be fixed.

The same longitudinal and transverse seismic loads obtained from the bridge with cracked linear-elastic columns were also used for the bridge models with nonlinear columns (i.e., one with cast-in-place columns, and the other with precast columns and grouted couplers). In accordance with the LRFD Bridge Seismic Reference Manual (2014), the use of the uniform load method or single-mode method is one of the two options in “nonlinear static analysis” (Marsh, Buckle, & Kavazanjian Jr, 2014). Obviously, the procedure in the “nonlinear static analysis” is much less tedious than the “nonlinear dynamic analysis.”

3.4. Bridge on SH-36 over Bear River at Preston

The bridge at Preston is a two-span bridge with a three-column bent. The superstructure is made up of an 8-inch deck thick deck that rests on 5 prestressed bulb tee girders. The substructure is made up of a pier cap, three columns, and their footings all of which are cast-in-place (CIP). Figure 3.1 and 3.2 show the plan and elevation views of the bridge respectively. Columns are octagonal with a distance between two opposite sides of 4 *ft.* with a height of 29.25 *ft.* The column reinforcing is shown in Figure 3.3.

Using the iterative method outlined in Appendix A and the model with cracked linear-elastic columns, the bridge integral abutment stiffness values were estimated in the longitudinal and transverse directions. These stiffness values were used in all three models of the bridge. Appendix B presents the details of bridge seismic load calculations using the single-mode spectral method and the model with cracked linear-elastic columns.

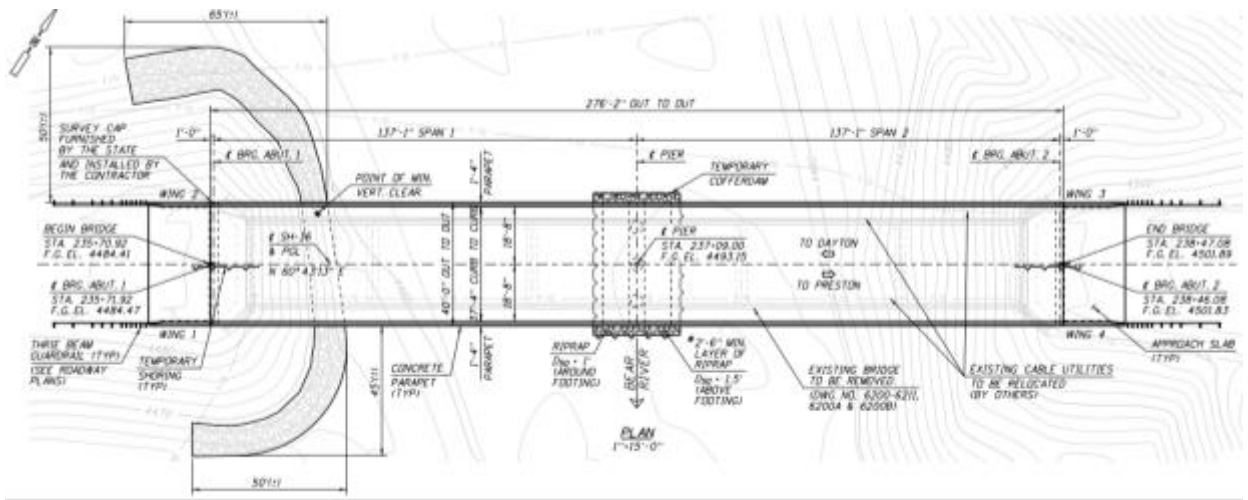


Figure 3.1 Plan View of SH-36 over Bear River Bridge at Preston (NTS)

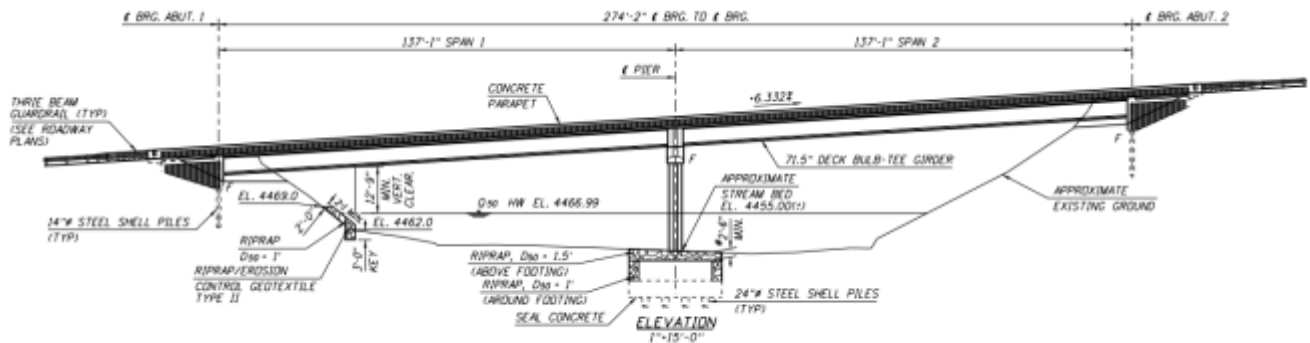


Figure 3.2 Elevation View of SH-36 over Bear River Bridge at Preston (NTS)

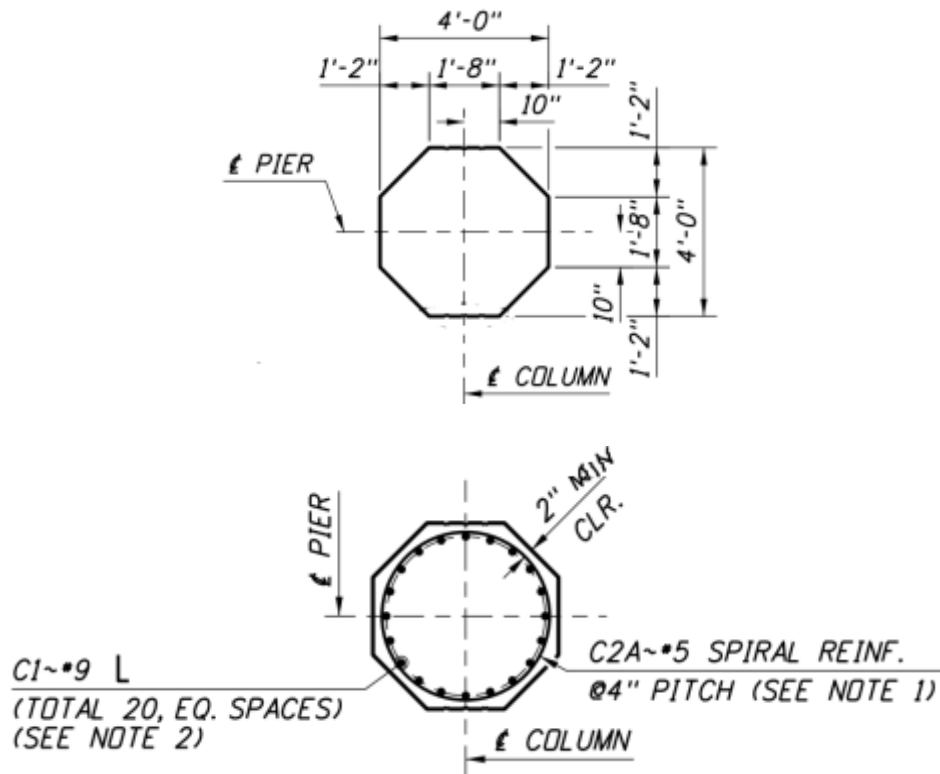


Figure 3.3 Preston Bridge Column Section

3.5. Bridge on US-95 over US-20/26 and UPRR at Parma

The bridge at Parma is a two-span bridge with a three-column bent. The skew in the bridge was removed for ease of modeling. The overall dimensions of the bridge were maintained and the bent and abutment lengths were shortened to match the deck width. The superstructure is made up of an 8-inch-thick deck that rests on 5 prestressed WF66G girders. The substructure is made up of a pier cap, three columns, and their footings all of which are cast-in-place (CIP). Figure 3.4 and 3.5 show the plan and elevation views of the bridge respectively. The bridge has a non-integral superstructure-pier connection. Columns are 3.5 ft. in diameter with a height of 25.6

ft. The column reinforcing is shown in Figure 3.6. The original section with 32 No. 10 steel reinforcing bars were replaced with 16 No. 14 steel bars. This scheme better allows the use of grouted couplers for the bridge with precast columns and grouted couplers.

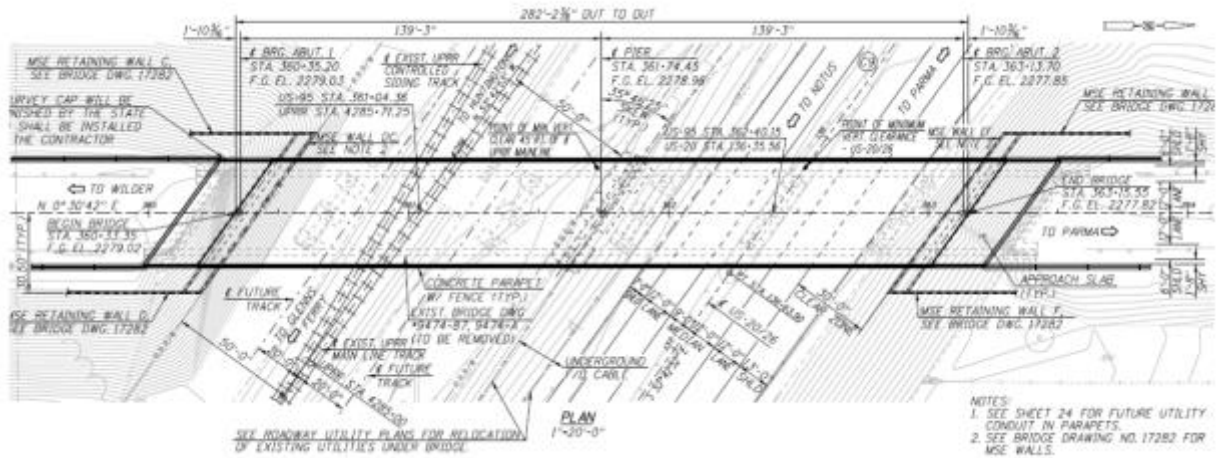


Figure 3.4 Plan View of SH-36 over US-20/26 and UPRR at Parma (NTS)

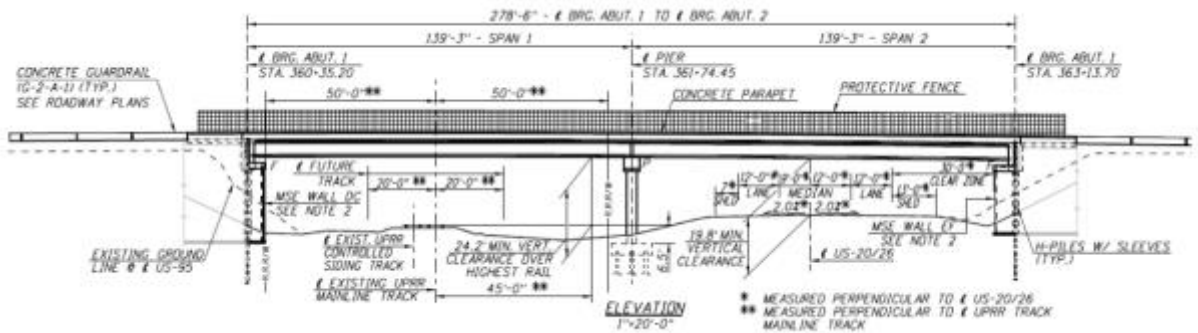


Figure 3.5 Elevation View of SH-36 over US-20/26 and UPRR at Parma (NTS)

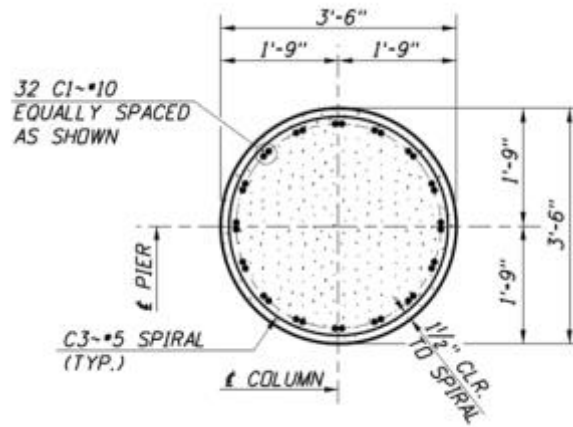


Figure 3.6 Parma Bridge Column Section

3.6. Bridge on SH-22 over I-15 at Dubois

The bridge at Dubois is a two-span bridge with a four-column bent. The superstructure is made up of an 8-inch thick deck that rests on 8 steel girders. The substructure is composed of the pier cap, 4 columns, and half of the footings all being cast in place (CIP). Figure 3.7 and 3.8 show the plan and elevation views of the bridge respectively. This bridge also has a non-integral superstructure-pier connection. The Columns are 3.5 ft. in diameter with a height of 14.05 ft. The column reinforcing is shown in Figure 3.9. The column section has 13 No. 11 steel reinforcing bars.

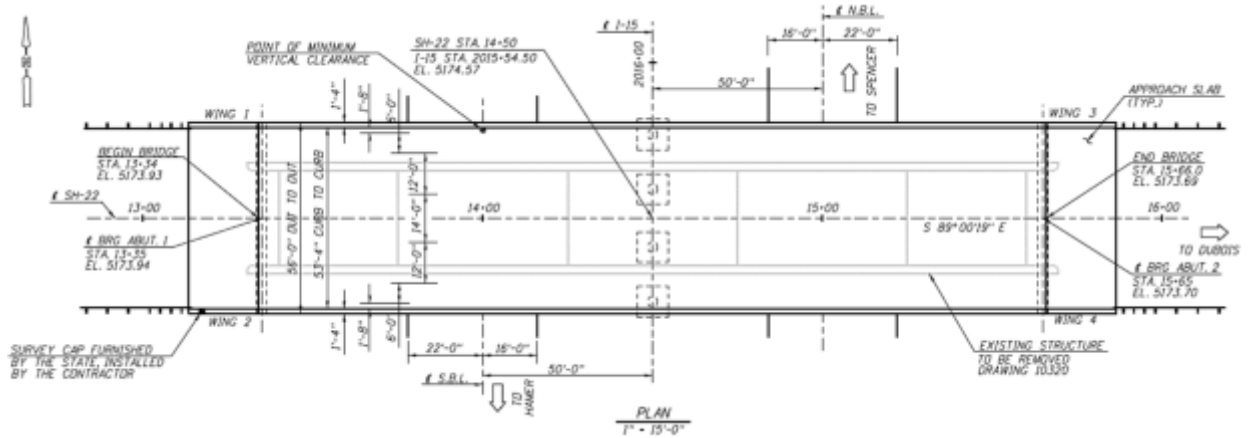


Figure 3.7 Plan View of SH-22 over I-15 Bridge at Dubois (NTS)

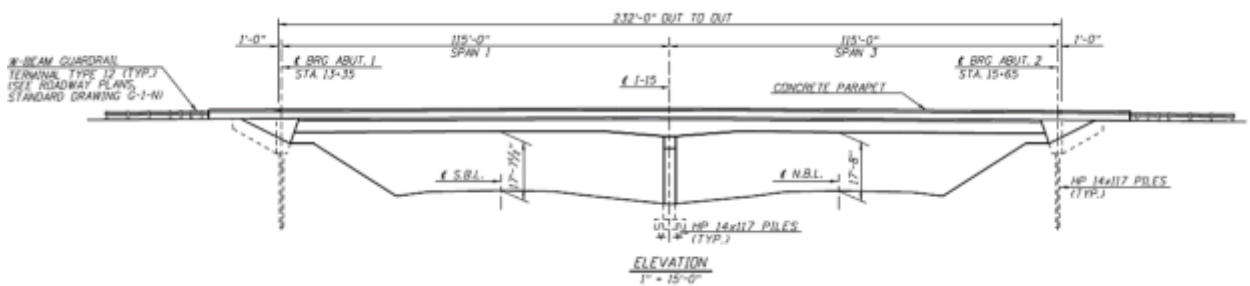


Figure 3.8 Elevation View of SH-22 over I-15 Bridge at Dubois (NTS)

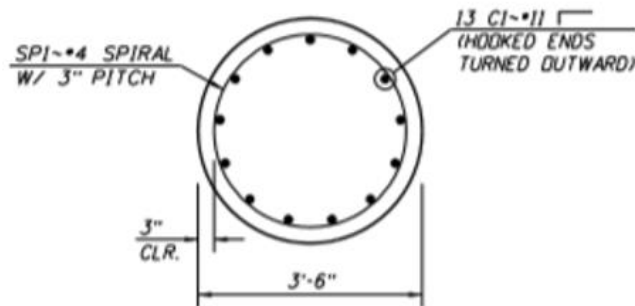


Figure 3.9 Dubois Bridge Column Section

The same process of data analysis used for the bridge at Preston was also used for the Parma and Dubois bridges. The schematics of their computer models and the output displacements, column base reactions, and the top of the column drift values can be found in the Appendix E of the ITD Report (Ebrahimpour, Earles, Maskey, Tangarife, & Sorensen, 2016).

CHAPTER 4 - RESULTS

This chapter presents all the results from the computer analyses for the Preston Bridge and some results for the Parma and Dubois bridges. The graphs for combination of Strain to Number of half cycles to failure for ASTM A615 and ASTM A706 steel bars can also be found in this chapter. The numbers of cycles to failure on various column drifts and strains are estimated with both A615 and A706 bars for the Preston Bridge. Since Parma and Dubois bridges were considered by the ITD Report, all the data analyses are found in that report (Ebrahimpour, Earles, Maskey, Tangarife, & Sorensen, 2016). However, for completeness, the pertinent results from these two bridges are also shown in this chapter.

4.1. Results for Computer Analyses

Using the iterative method outlined in Appendix A and the model with cracked linear-elastic columns, the Preston bridge integral abutment stiffness values were estimated in the longitudinal and transverse directions. These stiffness values were used in all three models of the bridge. Appendix B presents details of bridge seismic load calculations using the single-mode spectral method and the model with cracked linear-elastic columns. As noted above in the section “Method of Seismic Analysis,” the same seismic transverse and longitudinal forces were used with the two bridge models with nonlinear columns. The bond-slip moment-rotation values were obtained similar to the approach used to duplicate University of Nevada, Reno’s bond-slip parameters (Haber, Saiidi, & Sanders, 2013). The bond-slip values for Preston bridge are given in Appendix B. Appendix B also presents the schematics of the Preston bridge computer models, OpenSees input files, and the resulting displacements, column base reactions, and the top of the

column drift values. Table 4.1 shows a summary of the column displacements, drifts, and base reactions at the maximum design load for both transverse and longitudinal loading directions. As it can be seen in Table 4.1, in both linear and non-linear cases, the displacements, drifts, and reactions for the transverse loading controlled. In the longitudinal direction, because of small displacement, cracked linear-elastic model gives smaller reactions and slightly larger displacement. The column drift was obtained by dividing the displacement by the column height.

Table 4.1 Preston Bridge Displacements, Drifts, and Column Base Reactions

	Column Model	
	Cracked Linear-elastic	Nonlinear CIP
Longitudinal		
Top of the Column Displacement, <i>ft</i>	0.099	0.097
Column Drift, %	0.339	0.331
Column Base Shear, <i>k</i>	80.08	94.23
Column Base Moment, <i>k ft</i>	1358	1612
Transverse		
Top of the Column Displacement, <i>ft</i>	0.419	0.561
Column Drift, %	1.434	1.919
Column Base Shear, <i>k</i>	377.41	175.19
Column Base Moment, <i>k ft</i>	6158	2975

Figures 4.1 and 4.2 show the percent of longitudinal and transverse seismic loads versus the top of the column displacement for the linear-elastic and the Nonlinear CIP models considered.

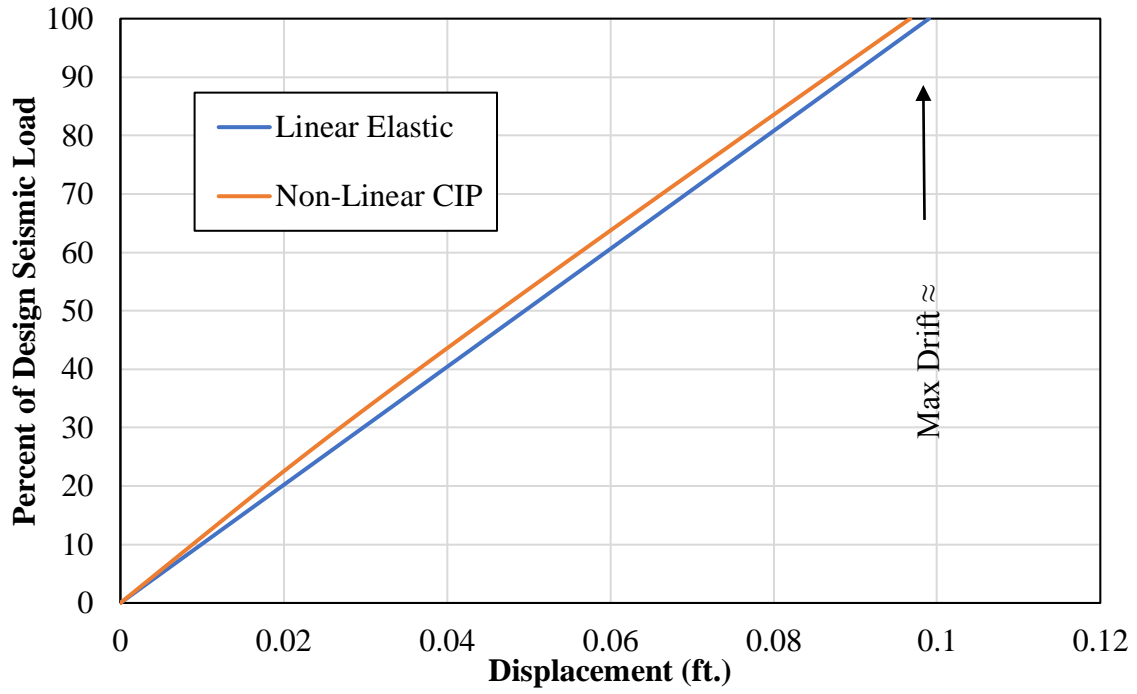


Figure 4.1 Preston Bridge Column Displacements/Drifts under Longitudinal Load

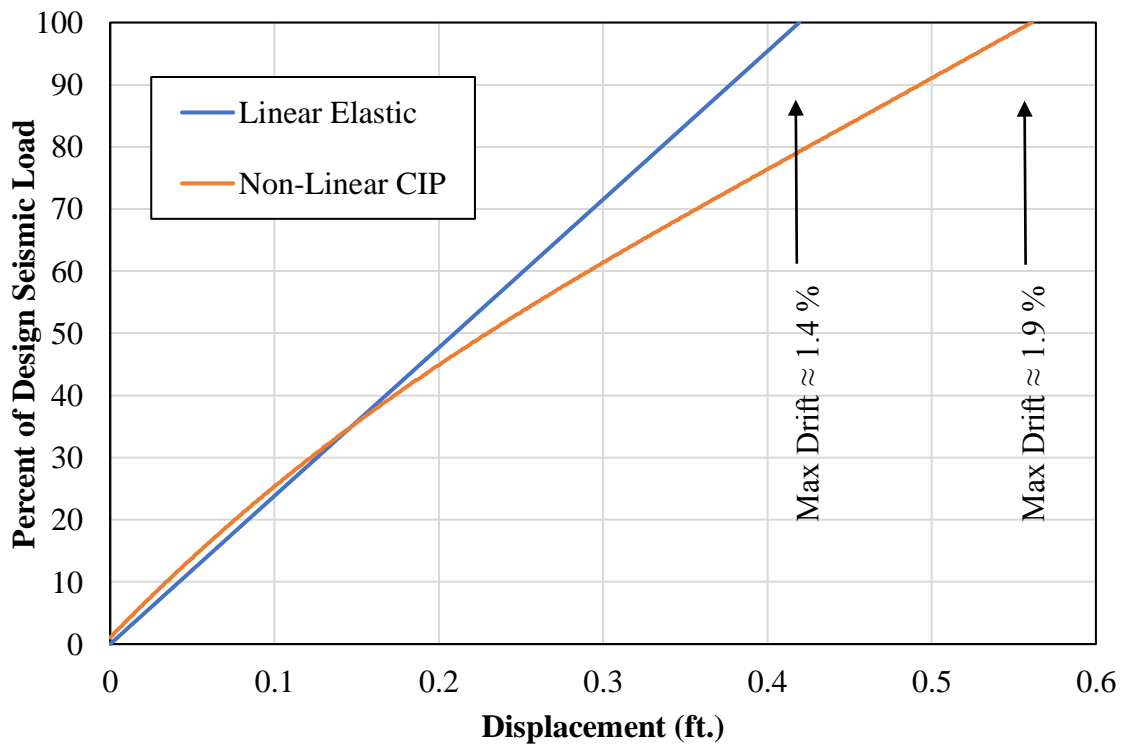


Figure 4.2 Preston Bridge Column Displacements/Drifts under Transverse Load

Figure 4.3 shows the stress-strain values in the most stressed steel bar in the Preston bridge model with precast columns.

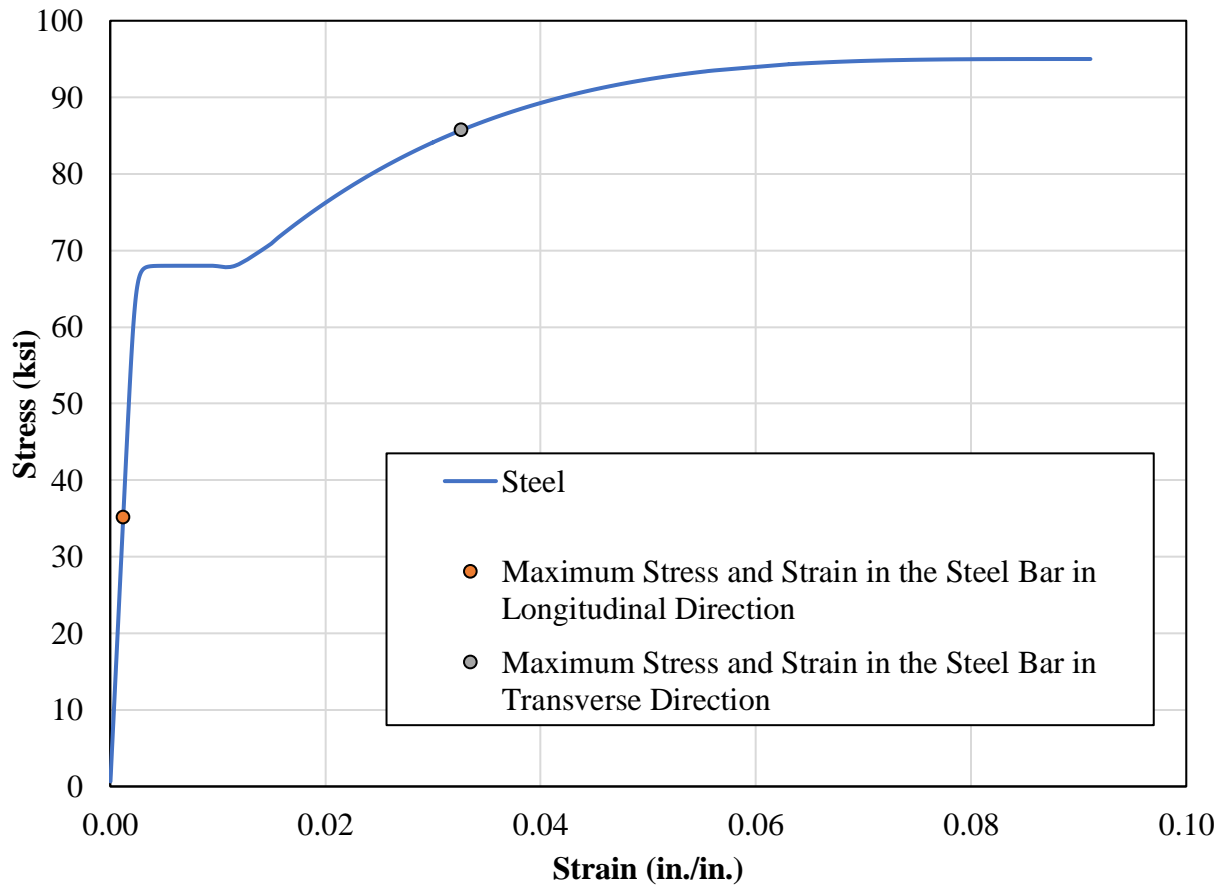


Figure 4.3 Preston Bridge Stress-strain Values in the Most Stressed Steel Bar in the CIP Column

4.2. Comparison of Results with AASHTO Guide Specifications

In this section, we will compare the displacement/drift results with the displacement/drift capacity and demand as per AASHTO Seismic Guide Specifications (American Association of State Highway and Transportation Officials, 2015). The three bridges considered for this study were placed in the most seismically active location in Idaho with soil Site Class D. Using the USGS seismic design map (see Appendix B, Figure B.7), this combination of conditions results in a design short duration acceleration of $S_{DS} = 0.907$ and a design one-second acceleration of $S_{D1} = 0.486$. According to the Seismic Guide Table 3.5-1, S_{D1} of 0.486 (i.e., in the range of $0.30 \leq S_{D1} \leq 0.50$) places the structure in Seismic Design Category (SDC) C.

Using the approximate equation given in Seismic Guide Articles 4.8.1 for Type 1 structure (ductile substructure with essentially elastic superstructure) in SDC C, the displacement capacity, Δ_C , in inches is:

$$\Delta_C = 0.12H_o\{-2.32 \ln(x) - 1.22\} \geq 0.12H_o \quad (4.1)$$

Where, $x = \frac{\Lambda B_o}{H_o}$, H_o = clear column height in *ft*, B_o = column diameter in *ft*, and Λ = end restraint factor ($\Lambda = 2.0$ for fixed top and bottom and $\Lambda = 1.0$ for fixed-free).

The displacement demand may be obtained through elastic analysis and multiplied by displacement magnification factor, R_d , as per Seismic Guide's Article 4.3.3 and used with combination of orthogonal seismic displacements as per Seismic Guide's Article 4.4. Since the transverse displacement is larger in all our bridge models, we need to use the orthogonal combination of the longitudinal displacement. The demand becomes:

$$\Delta_{D,Linear Magnified} = (R_d \Delta_{D,Linear})_T + 0.3(R_d \Delta_{D,Linear})_L \quad (4.2)$$

Where, $\Delta_{D,Linear Magnified}$ = magnified displacement demand through linear-elastic analysis, $(R_d \Delta_{D,Linear})_T$ = magnified transverse displacement demand, and $(R_d \Delta_{D,Linear})_L$ = magnified longitudinal displacement demand. R_d is obtained as follows:

$$R_d = \left(1 - \frac{1}{\mu_D}\right) \frac{T^*}{T} + \frac{1}{\mu_D} \geq 1.0 \text{ for } \frac{T^*}{T} > 1.0 \quad (4.3)$$

$$R_d = 1.0 \text{ for } \frac{T^*}{T} \leq 1.0 \quad (4.4)$$

Where, $T^* = 1.25T_S$, μ_D = maximum local member displacement demand = 3.0 for SDC C, and $T_S = \frac{SD1}{SDS}$.

Alternatively, one may use the transverse and longitudinal displacements obtained through nonlinear analysis. With the combination of orthogonal displacements, the nonlinear demand becomes:

$$\Delta_{D,Nonlinear} = (\Delta_{D,NonLinear})_T + 0.3(\Delta_{D,Nonlinear})_L \quad (4.5)$$

Where, $\Delta_{D,Nonlinear}$ = displacement demand through nonlinear analysis, $(\Delta_{D,NonLinear})_T$ = transverse nonlinear displacement demand, and $(\Delta_{D,Nonlinear})_L$ = longitudinal nonlinear displacement demand.

Following the above steps, Table 4.2 summarizes the displacement demand and capacity of the three bridge columns in this research project.

Table 4.2 Displacement and Drift Capacity versus Demand for Bridge Columns

	Preston	Parma	Dubois
Capacity			
H_o, ft	34.57 ^a	25.6	14.05
B_o, ft	4	3.5	3.5
Δ_c, ft	0.752	0.458	-. ^b
Drift = $\Delta_c/H_o, \%$	2.18	1.79	-. ^b
Demand, Magnified Linear-elastic Analysis			
Transverse R_d	1.177	1.149	1.711
Longitudinal R_d	1.530	1.632	2.077
$\Delta_{D,Linear Magnified}, ft$	0.539	0.402	0.159
Drift = $(\Delta_{D,Linear Magnified})/H_o, \%$	1.56	1.57	1.13
Demand, Nonlinear Analysis			
$\Delta_{D,Nonlinear}, ft$	0.590	0.400	0.128
Drift = $(\Delta_{D,Nonlinear})/H_o, \%$	1.71	1.56	0.91

^a For bridges with bents comprising single or multiple drilled shaft columns in which plastic hinging may occur below such that the clear height dimension would be at the point of fixity in the soil.

^b LRFD Bridge Seismic Guide Article 4.8.1 equations may only be used for clear heights $\geq 15 ft$

As it can be seen from Table 4.2, the drift demand for Preston, Parma, and Dubois bridge columns estimated using the magnified linear-elastic approach are 1.56 percent, 1.57 percent, and 1.13 percent, respectively. The corresponding values obtained through nonlinear approach are 1.71 percent, 1.56 percent, and 0.91 percent, respectively. It should be noted that most departments of transportation use the cracked linear-elastic approach with magnification factors to estimate the nonlinear behavior of the bridge columns.

4.3. Low-cycle fatigue results

In this section, the low cycle fatigue results from Section 2.2 were evaluated and combined to get single strain vs number of half cycles to failure graphs for both ASTM A706 and ASTM A615 steel bars. The plots for ASTM A706 steel from Zhou (2008) in Figure 2.11 and from Hawileh et al. (2009) in Figure 2.13 were found to be very similar. Figure 4.4 shows the combined plot of strain vs number of half cycles to failure for ASTM A706 steel from Zhou (2008) and Hawileh et al. (2009) plots. The equation for the combined strain vs number of half cycles to failure for ASTM A706 plot is shown in Equation (4.6):

$$\varepsilon = 0.1903(2N_f)^{-0.426} \quad (4.6)$$

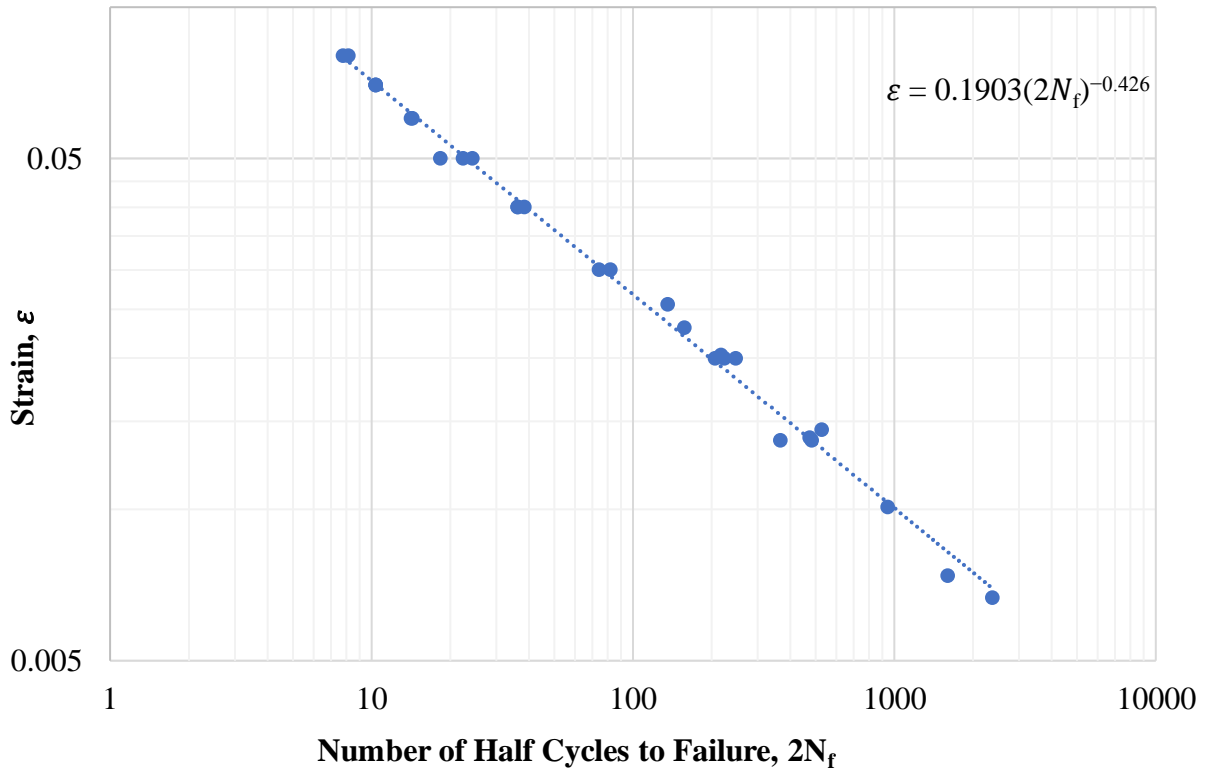


Figure 4.4 Combined Strain vs Number of Half Cycles to Failure plot for ASTM A706 steel from Zhou (2008) and Hawileh et al. (2009)

Unlike the strain vs number of half cycles to failure for ASTM A706 steel plots from Zhou (2008) and Hawileh (2009), the number of half cycles to failure for ASTM A615 steel plots from Brown and Kunnath (2000) in Figure 2.10 and Hawileh (2009) in Figure 2.12 are very dissimilar. Brown and Kunnath's values for number of half cycles to failure are found to be considerably lower than Hawileh's. Therefore, we estimated the number of cycles to failure for ASTM A615 steel in two ways. (i) To be more conservative, Brown and Kunnath's plot for strain vs number of half cycles to failure in Figure 2.10 is used for fatigue behavior of ASTM A615 steel, which is shown in Equation (4.7). (ii) To not disregard Hawileh's research on ASTM A615, the plots from Hawileh (2009) and Brown & Kunnath (2000) are combined as shown in Figure 4.5. The equation for the combined strain vs number of half cycles to failure for ASTM A615 plot is shown in Equation (4.8).

$$\varepsilon = 0.1514(2N_f)^{-0.433} \quad (4.7)$$

$$\varepsilon = 0.2468(2N_f)^{-0.522} \quad (4.8)$$

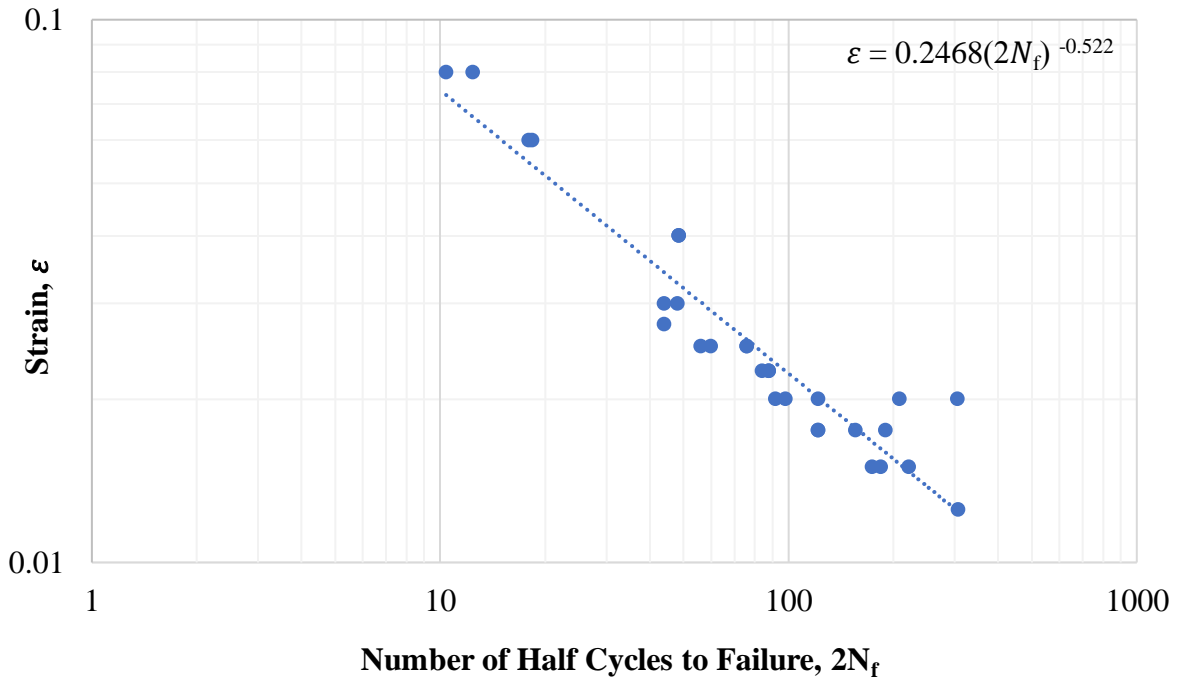


Figure 4.5 Combined Strain vs Number of Half Cycles to Failure plot for ASTM A615 steel from Brown and Kunnath (2000) and Hawileh et al. (2009)

Figure 4.6 shows the combination plots for A615 and A706 steels in the same graph. Equations (4.6), (4.7), and (4.8) are used to find the number of half cycles to failure for various strain values for ASTM A706 and ASTM A615 steel bars respectively. Tables 4.3, 4.4, and 4.5 show the stress and strain values in the most stressed steel bar and the number of half cycles for steel bar fatigue failure for a column in the Preston, Parma, and Dubois bridges respectively. Only steel strain values larger than 0.01 were used to estimate the number of half cycles. Stress and strain values in the most stressed steel bar and the number of half cycles for steel bar fatigue failure for the columns in the Parma and Dubois bridges can also be found in the ITD Report (Ebrahimipour, Earles, Maskey, Tangarife, & Sorensen, 2016).

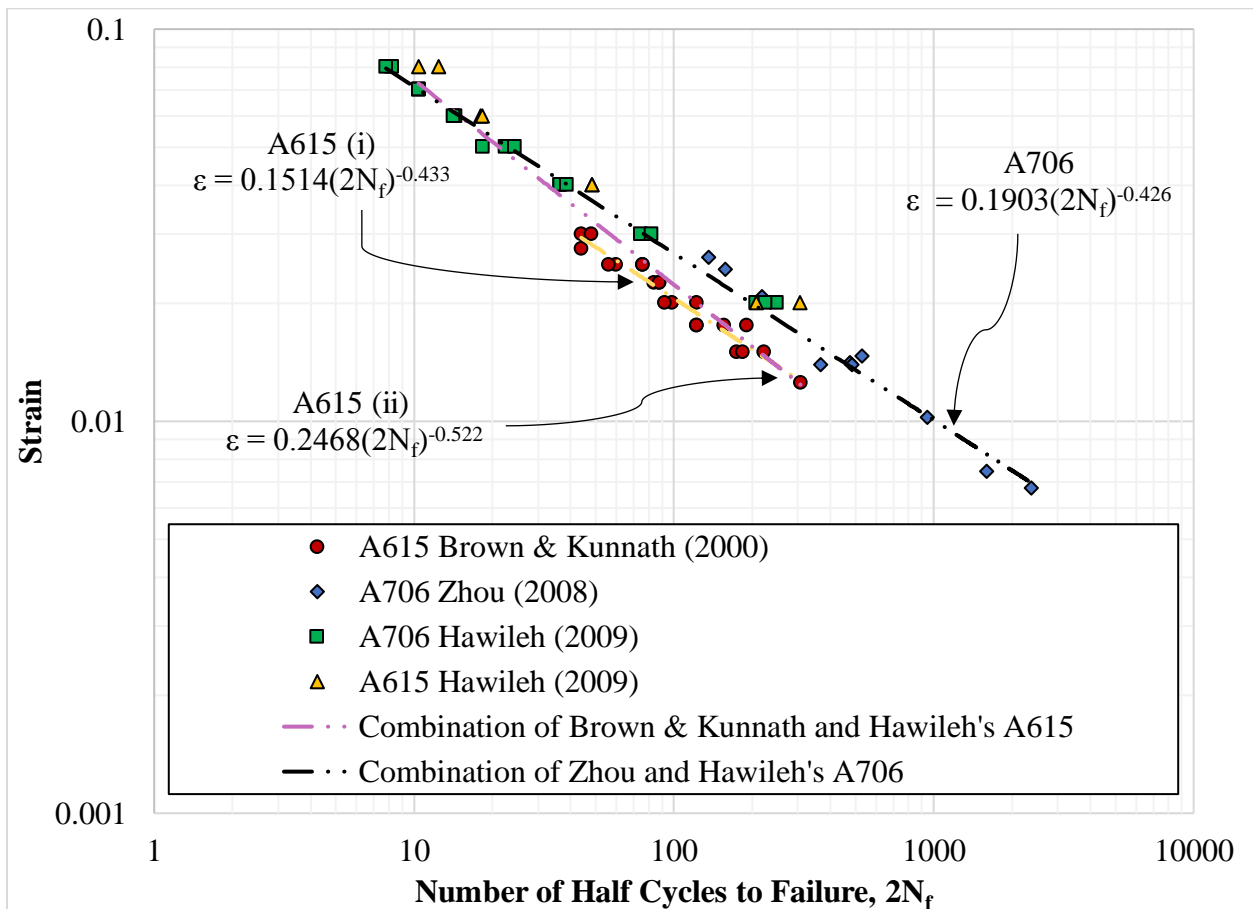


Figure 4.6 Combined Strain vs Number of Half Cycles to Failure plot for ASTM A615 and ASTM A706 steel (Brown and Kunnath, 2000) (Zhou, 2008) (Hawileh et al., 2009)

Table 4.3 Stress and Strain in Steel Bar and Number of Half Cycles for Steel Bar Fatigue Failure for a Preston Bridge Column.

Nonlinear Drift, %	Steel Bar		No. of Half Cycles to Fracture for Grade 60 Steel		
	Stress, ksi	Strain	ASTM A706	ASTM A615	
				(i)	(ii)
0.25	28.55	0.0010	-	-	-
0.5	60.10	0.0021	-	-	-
0.75	67.98	0.0042	-	-	-
1	69.94	0.0139	465	248	247
1.5	84.28	0.0303	75	41	56
2	85.97	0.0331	61	33	47
2.5	87.64	0.0363	49	27	39
3	89.10	0.0396	40	22	33
3.5	90.43	0.0432	33	18	28
4	91.64	0.0471	26	15	24
4.5	92.64	0.0513	22	12	20
5	93.84	0.0630	13	8	14

Table 4.4 Stress and Strain in Steel Bar and Number of Half Cycles for Steel Bar Fatigue Failure for a Parma Bridge Column.

Nonlinear Drift, %	Steel Bar		No. of Half Cycles to Fracture for Grade 60 Steel		
	Stress, ksi	Strain	ASTM A706	ASTM A615	
				(i)	(ii)
0.25	16.32	0.0006	-	-	-
0.5	43.40	0.0015	-	-	-
0.75	65.16	0.0025	-	-	-
1	67.99	0.0045	-	-	-
1.5	73.51	0.0123	619	329	313
2	76.78	0.0156	354	190	198
2.5	80.14	0.0195	210	113	129
3	83.14	0.0236	134	73	90
3.5	86.12	0.0285	86	47	63
4	88.64	0.0338	58	32	45
4.5	90.43	0.0386	42	23	35

Table 4.5 Stress and Strain in Steel Bar and Number of Half Cycles for Steel Bar Fatigue Failure for a Dubois Bridge Column.

Nonlinear Drift, %	Steel Bar		No. of Half Cycles to Fracture for Grade 60 Steel		
	Stress, ksi	Strain	ASTM A706	ASTM A615	
				(i)	(ii)
0.25	33.79	0.0012	-	-	-
0.5	66.25	0.0026	-	-	-
0.75	66.80	0.0028	-	-	-
1	67.24	0.0029	-	-	-
1.5	67.73	0.0032	-	-	-
2	67.92	0.0037	-	-	-
2.5	67.99	0.0044	-	-	-
3	68.00	0.0056	-	-	-
3.5	68.00	0.0088	-	-	-
4	73.59	0.0165	312	168	178
4.5	84.44	0.0294	80	44	59
5	87.92	0.0360	50	28	40

CHAPTER 5 - SUMMARY AND CONCLUSIONS

The objectives of this research were to (a) analyze three bridges from various locations in Idaho under the most severe Idaho seismic conditions; and (b) to compare the fatigue behavior of ASTM A615 and ASTM A706 reinforcing steel bars in these bridge columns.

In the introduction and background section, we discussed the failure of structural components at stress levels much lower than the material yield or ultimate strength. A material subjected to cyclic loading may fail at stress levels much lower than the material yield strength. Most engineering applications that deal with high-cycle fatigue ($10^3 - 10^7$ cycles) and the strain amplitudes rarely exceed 0.01 in the testing. During an earthquake, the strain reversals can have high stress levels and yet still have low number of cycles. The structural components for bridges can undergo large inelastic strains up to 0.06 and fail due to plastic deformations. This type of failure is known as low-cycle fatigue (LCF) failure.

ASTM A615 and ASTM A706 steel bars are used in the columns for most of the bridges in the United States. ASTM A706 bars were initially produced to only one strength level (Grade 60) with a minimum yield strength $f_y = 60,000 \text{ psi}$ (420 MPa), while ASTM A615 can have different grades. However, A706 steel is found in Grades 60 and 80 currently. In broad terms, the production process of ASTM A706 steel is more demanding and includes requirements for controlled tensile properties and restrictions on chemical composition, while ASTM A615 steel does not include comparable requirements. Idaho Transportation Department (ITD) has been using ASTM A615 steel in most of the bridge designs in Idaho. One of the objectives of this research was to consider the possibility of using ASTM A706 bars for Idaho bridge columns, replacing ASTM A615 bars.

In the literature review section, we discussed the fatigue life of a material and low-cycle fatigue for reinforcing steel. Fatemi & Stephens studied the mean stress relaxation and the influence of mean strain/stress on the cyclic stress-strain relationship for a material (Fatemi & Stephens, 1987). However, Koh & Stephens' study concluded that the mean strain doesn't have any positive or negative effect on the fatigue life unless it produces a mean stress (Koh & Stephens, 1991). In this section, we looked at various strain versus number of cycles to fatigue failure plots and how it was modified over the years by different researchers.

Mander's paper initiated the study about low-cycle fatigue behavior in reinforcing steel (Mander, Panthaki, & Kasalanati, Low-Cycle Fatigue Behavior of Reinforcing Steel, 1994). His study is one of the most significant in terms of low-cycle behavior of reinforcing steel and this paper is being referenced in many of the sections in this thesis. This study tested two types of steel which included ASTM A722 type II hot-rolled and proof-stressed alloy-steel bar; and ASTM A615 Grade 40 deformed billet-steel reinforcing bar having a minimum specified yield strength of 276 *MPa*.

We also wrote about various studies conducted for ASTM A615 and ASTM A706 steel bars in the literature review section. Brown and Kunnath tested the ASTM A615 reinforcing steel and estimated the number of half cycles to failure for different strain level in his paper (Brown & Kunnath, 2000). Similarly, Zhou conducted similar research using the ASTM A706 reinforcing steel (Zhou, 2008). Hawileh tested both ASTM A615 and ASTM A706 rebars in his paper and compared the results (Hawileh, Rahman, & Tabatabai, 2009). Low-cycle fatigue results for ASTM A615 and A706 rebars were both tabulated and graphed from all the respective studies.

In the comparison of ASTM A615 and A706 rebars section of the literature review, we looked at the differences in availability and cost for these two types of steel bars. The production and availability of ASTM A706 steel has been increasing. The cost for A706 bars are found to be very close when compared to A615 bars.

As a part of the methodology section, using OpenSees we developed computer models of the cast-in-place (CIP) column used in the experimental project at the University of Nevada, Reno (UNR) and the Idaho Transportation Department (ITD) report (Haber, Saiidi, & Sanders, 2013), (Ebrahimpour, Earles, Maskey, Tangarife, & Sorensen, 2016).

Using computer simulations, we performed seismic analyses of three highway bridges in Idaho by placing them in the most seismically active location in Idaho. In each case, two models were considered; these are: (a) a bridge with cracked linear-elastic columns, (b) a bridge with cast-in-place columns having nonlinear material behavior. Although none of the bridges were designed for the seismic condition considered in this study, using computer simulations, columns from all three bridges performed well. The stresses in the longitudinal reinforcing steel bars were well within the acceptable range. The highest drift experienced was in the transverse direction of the Preston bridge at about 1.71 percent when considering combination of orthogonal displacements. The AASHTO Guide Specifications for LRFD Seismic Bridge Design equations for estimating the magnified linear-elastic drift demand resulted in almost the same values compared to the corresponding drift demand values obtained using nonlinear analysis (American Association of State Highway and Transportation Officials, 2015).

For the strain versus number of half cycles to fatigue failure graphs, we combined Zhou's and Hawileh's graphs for ASTM A706 steel because they were very similar. However, Brown and Kunnath's graphs were more conservative as compared to Hawileh's for ASTM A615 steel.

We estimated number of half cycles to failure for ASTM A615 steel in two ways. The first one was using Brown and Kunnath's plots for ASTM A615 steel. The second one was a combination of Brown and Kunnath and Hawileh's graphs for ASTM A615 steel.

We performed pushover analyses of all three bridges under large drifts to obtain relations between column drift and the low cycle fatigue of the steel reinforcing. The low cycle fatigue life analysis indicates that at higher strains, only a few half cycles is endured by the steel reinforcing before fatigue failure. From Tables 4.3, 4.4, and 4.5, it can be seen that the use of ASTM A706 steel will improve the low cycle fatigue life of the steel reinforcing bars. However, the research by Hawileh (2009) predicted higher number of cycles to failure for ASTM A615 than ASTM A706 steel. Disregarding Hawileh's (2009) data for ASTM A615 steel will result in more conservative fatigue life estimates. When considering a combination for Brown and Kunnath and Hawileh's graphs for ASTM A615, ASTM A706 still performs better in low-cycle fatigue than ASTM A615 for the most part. Given the low-cycle fatigue aspect and the cost of using ASTM A706 steel over ASTM A615 steel is almost the same, it is advisable for ASTM A706 steel to be used in Idaho bridge columns. However, further extensive research is needed in terms of low-cycle fatigue behavior of these steel types to better recommend one over the other.

REFERENCES

- American Association of State Highway and Transportation Officials. (2015). *AASHTO Guide Specification for LRFD Seismic Bridge Design*. Washington, D.C.: American Association of State Highway and Transportation Officials.
- American Construction Supply, Inc. (2017). *American Construction Supply*. Retrieved from American Construction Supply: <http://americanconstructionsupply.com/>
- ASTM International. (2017). *ASTM International*. Retrieved from ASTM International: <https://www.astm.org/Standards/A706.htm>
- Brown, J., & Kunnath, S. K. (2000). *Low-cycle fatigue behavior of longitudinal reinforcement in reinforced concrete bridge columns*.
- Coffin, L. F. (1954). A study of the effects of cyclic thermal stresses on a ductile metal. *trans. ASME* 76, 931-950.
- Concrete Construction Supply. (2017). *Concrete Construction Supply*. Retrieved from Concrete Construction Supply: <http://www.concreteconstructionsupply.com/>
- DeLuca, D. P. (2001). Understanding Fatigue. *Global Gas Turbine News*, 41, 7-10.
- Dodd, L. L., & Restrepo-Posada, J. I. (1995). Model for predicting cyclic behavior of reinforcing steel. *Journal of Structural Engineering*, 121(3), 433-445.
- Ebrahimpour, A., Earles, B. E., Maskey, S., Tangarife, M., & Sorensen, A. D. (2016). *Seismic Performance of Columns with Grouted Couplers in Idaho Accelerated Bridge Construction Applications*. Idaho Transportation Department.
- Fatemi, A., & Stephens, R. I. (1987). Tensile mean stress effects on uniaxial fatigue behavior of 1045 HR steel. *Fatigue'87*, 1, 537-546.
- Gustafson, D. P. (2007). Revisiting low-alloy steel reinforcing bars. *Concrete International*, 29(01), 55-59.

- Haber, Z. B. (2013). *Precast column-footing connections for accelerated bridge construction in seismic zones*. Reno, NV, United States of America: University of Nevada, Reno.
- Haber, Z. B., Saiidi, M. S., & Sanders, a. D. (2013). *Precast Column-Footing Connections for Accelerated Bridge Construction in Seismic Zones*. University of Nevada, Reno, Department of Civil Engineering. Reno: University of Nevada, Reno.
- Harris Supply Solutions. (2017). *Nucor Corporation*. Retrieved 9 2017, from Harris Supply Solutions: <http://www.harrissupplysolutions.com/black-rebar.html>
- Hawileh, R., Rahman, A., & Tabatabai, H. (2009). Evaluation of the Low-Cycle Fatigue Life in ASTM A706 and A615 Grade 60 Steel Reinforcing Bars. *Journal of Materials in Civil Engineering*, 22(1), 65-76.
- Koh, S. K., & Stephens, R. I. (1991). Mean stress effects on low cycle fatigue for a high strength steel. *Fatigue & Fracture of Engineering Materials & Structures*, 14(4), 413-428.
- Mander, J. B., Panthaki, F. D., & Kasalanati, A. (1994). Low-Cycle Fatigue Behavior of Reinforcing Steel. *Journal of Materials in Civil Engineering*, 6(4), 453-468.
- Mander, J. B., Priestley, M. J., & Park, R. (1988, August). Theoretical Stress-Strain Model for Confined Concrete. *Journal of Structural Engineering*, 114(8), 1804-1826.
- Manson, S. S. (1953). *Behavior of materials under conditions of thermal stress*.
- Marsh, M. L., Buckle, I. G., & Kavazanjian Jr, E. (2014). *LRFD Seismic Analysis and Design of Bridges Reference Manual: NHI Course No. 130093 and 130093A*. FHWA-NHI-15-004.
- Mast, R., Marsh, L., Spry, C., Johnson, S., Griebenow, R., Guarre, J., & Wilson, W. (1996). *Seismic Design of Bridges - Design Example No. 1: Two-Span Continuous CIP Concrete Box Bridge*. U.S. Department of Transportation Federal Highway Administration Central Federal Lands Highway Division.
- Morrow, J. (1968). Fatigue design handbook. *Advances in engineering*, 4(3.2), 21-29.

- Nastar, N., Anderson, J. C., Brandow, G. E., & Nigbor, R. L. (2010). Effects of Low-Cycle Fatigue on a Ten-Story Steel Building. *The Structural Design of Tall and Special Buildings*, 19, 95–113.
- Paulay, T., & Priestley, M. N. (1992). *Seismic design of reinforced concrete and masonry buildings*.
- Smith, K. N., Topper, T. H., & Watson, P. (1970). A stress-strain function for the fatigue of metals (Stress-strain function for metal fatigue including mean stress effect). *Journal of materials*, 5, 767-778.
- Steel West Inc. (2017). *Steel West*. Retrieved from Steel West: <http://steelwest.net>
- Stephens, R. I., & Fuchs, H. O. (2001). *Metal Fatigue in Engineering*. John Wiley & Sons, Inc.
- Taylor, A. (2016). The Northridge Earthquake: 20 Years Ago Today. *The Atlantic*. The Atlantic.
- United States Geological Survey. (2016). *U.S. Seismic Design Maps*. Retrieved from U.S. Geological Survey: <http://www.earthquake.usgs.gov/designmaps/us/application.php>
- University of California, Berkeley. (2016). *OpenSees*. Retrieved July 20, 2016, from <http://opensees.berkeley.edu/OpenSees/user/index.php>
- Zhou, Y. (2008). *A pilot experimental study on the low cycle fatigue behavior of stainless steel rebars for earthquake engineering applications*. State University of New York at Buffalo.

APPENDIX A - Procedures for Estimating Integral Abutment Stiffness Values

The procedures for estimating bridge transverse and longitudinal abutment stiffness values are presented in this appendix. These procedures are currently used by the Idaho Transportation Department. For simplicity, in the procedures outlined below, it is assumed that both abutments have: (a) the same pile lateral force-displacement behavior, (b) identical wingwalls (if present), and (c) identical abutment wall area. In the bridge under consideration, some of these assumptions may not apply and procedure may have to be slightly revised. For example, in one of the Idaho bridges considered, the abutments of the bridge had different pile force-displacement behavior. Also, the procedures below assume that the strong direction of H-piles is oriented longitudinally, while weak direction is oriented in transverse direction.

Longitudinal Stiffness

This procedure assumes the same value of longitudinal abutment stiffness for both abutments. This longitudinal stiffness is half of the sum of the longitudinal stiffness values from the two sets of abutment piles and the stiffness of one abutment backfill. As shown in Figure A.1, a linear relation is assumed between the abutment backfill reaction and the corresponding displacement from zero displacement to $0.02H_{aw}$ where, $H_{aw} = \text{height of abutment wall}$. The corresponding maximum force to mobilize the full passive backfill resistance of 7.7 k/ft^2 is $\left(7.7 \frac{\text{k}}{\text{ft}^2}\right) A_{aw}$. Where, A_{aw} is the area of the abutment wall $= H_{aw}L_{aw}$ with L_{aw} being the length of the abutment wall. It is further assumed that the full maximum force remains constant beyond the displacement of $0.02H_{aw}$.

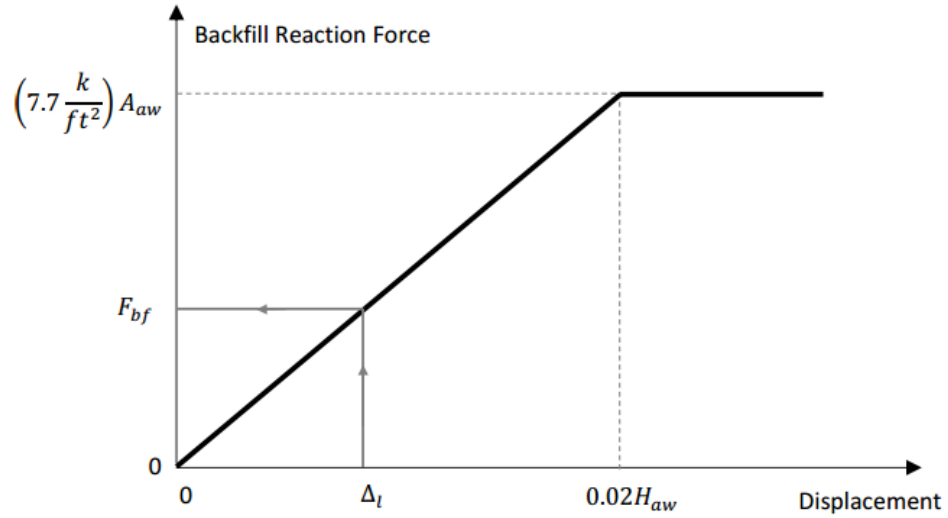


Figure A.1 Abutment Backfill Reaction Force versus Displacement

Figure A.2 shows a typical top of the pile lateral force versus displacement while the pile is bending about the strong axis. In the bridge model, the initial longitudinal pile stiffness is assumed based on $\Delta_0 = 1 \text{ in}$. Here, subscript "0" indicates initial estimates. From the pile force versus displacement in the strong direction, the initial force in the strong direction corresponding to displacement of 1 in is estimated as F_{s0} . The initial pile stiffness in the strong direction is

$$k_{s0} = \frac{F_{s0}}{\Delta_0}$$

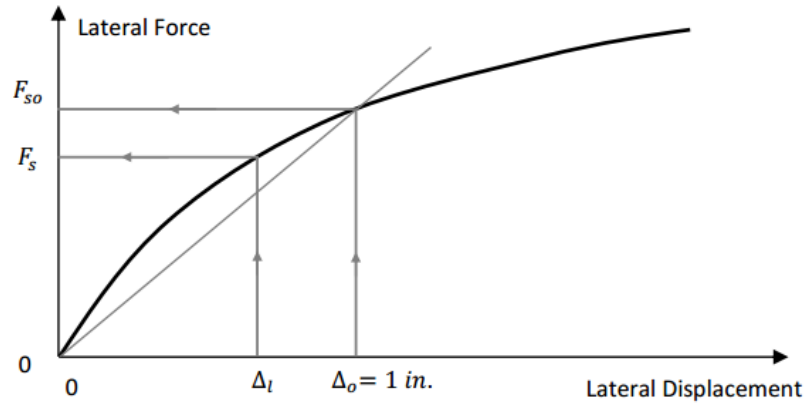


Figure A.2 Top of the Pile Lateral Force versus Displacement, Bending about the Strong Axis

The initial abutment longitudinal stiffness K_{l0} , to be used for both abutments, is estimated as:

$$K_{l0} = \frac{(n_1 + n_2)k_{s0} + \left(\frac{7.7A_{aw}}{d}\right)}{2} \quad (A.1)$$

where, n_1 = the number of piles in Abutment 1, n_2 = the number of piles in Abutment 2, k_{s0} = the initial pile stiffness in the strong direction, A_{aw} = the area of the abutment wall = $H_{aw}L_{aw}$, H_{aw} = height of the abutment wall, L_{aw} = length of the abutment wall, and $d = 0.02H_{aw}$ = deflection needed to mobilize the full passive resistance of 7.7 k/ft².

After loading the bridge linear-elastic model in the longitudinal direction, the average of the bridge longitudinal abutment displacement, Δ_l , is obtained. The average value of longitudinal displacements is used since in this direction the abutment displacements are very close to one another. In addition, determine the longitudinal seismic forces R_{l1} and R_{l2} for Abutments 1 and 2. Let's assume that Δ_l is less than 1 in. As shown in Figures A.1 and A.2, with the new Δ_l value, an abutment backfill reaction force F_{bf} and a revised pile lateral reaction force, F_s is obtained. Check to see if the equilibrium is reached between the sum of longitudinal seismic

forces and abutment backfill resistance, and the lateral pile resistance forces as shown by Equation A.2

$$R_{l1} + R_{l2} \cong (n_1 + n_2)F_s + F_{bf} \quad (A.2)$$

The symbol \cong is used to indicate whether the two sides are approximately equal. If Equation A.2 is not satisfied, change the value of longitudinal abutment stiffness and find the revised average value of longitudinal displacements and abutment seismic forces. With the revised average displacement, find the longitudinal abutment backfill resistance force and the lateral pile resistance forces and see if Equation A.2 is satisfied. This process is repeated a few times until the two sides of Equation A.2 are within 10%. When evaluating a pier, it is recommended to keep the abutment stiffness on the lower side. This would generally result in higher forces and displacements at the pier(s).

Example

Let's assume the initial springs based on 1" displacement result in $\frac{3}{4}$ " displacement and the corresponding force of 600 *kips* at each abutment (1200 *kips* total longitudinal force to be resisted by abutments). Let's also assume we have 10 piles at each abutment and they resist 30 *kips* each at $\frac{3}{4}$ " displacement, so the total pile resistance from both abutments would be $2 * 10 * 30 = 600$ *kips*, leaving $1200 - 600 = 600$ *kips* to be resisted by one abutment backfill. Now we need to check how much backfill resistance we get from $\frac{3}{4}$ " displacement, assuming linear relation from 0" (0 *kips*) to $d = 0.02H$ " ($7.7A_{aw}$). (Any displacement higher than $0.02H$ " will result in a constant backfill resistance of $7.7A_{aw}$). If $\frac{3}{4}$ " displacement results in backfill resistance considerably higher than 600 *kips*, we might increase abutment stiffness, which would give us higher acting seismic force, but smaller displacements. On the other hand,

if $3/4$ " results in backfill resistance quite lower than 600 *kips*, we may need to soften the abutment springs to reduce the acting force, but increase the displacement and associated resistance from piles and backfill. We repeat the process until we get good correlation (within 10%) between abutment acting seismic forces and resulting resistance from piles and backfill based on acting displacement.

Traverse Stiffness

In this procedure abutment forces and displacements are evaluated individually. The wing shear capacity can only be considered effective if it is larger than the difference between acting seismic forces and the piles reaction under given displacement. If otherwise, it is assumed that the wingwall has failed and it does not contribute to the transverse stiffness or resistance. The shear force V_c is calculated using Equation A.3:

$$V_c = 0.0316\beta\sqrt{f'_c}b_vd_v \quad (A.3)$$

Where, $\beta = 2$, f'_c = compressive strength of the concrete, *ksi*, b_v = the height of the wingwall at the interface of wing and abutment, $d_v = \max\left[d_e - \frac{a}{2}, 0.9d_e, 0.72h\right]$, d_e = the effective depth = distance to the center of the back reinforcement from the face of the wingwall = $h - \text{cover} - \text{bar} \frac{\text{diameter}}{2}$, $a = \frac{A_s f_y}{0.85 f'_c b_v}$ = depth of the equivalent compression block; A_s = area of the flexural reinforcement on the backfill side; $f_y = 60 \text{ ksi}$ = yield strength of the flexural reinforcement, and h = the depth of the wingwall (typically 12 *in.*).

Figure A.3 shows a typical top of pile lateral force versus displacement while the pile is bending about the weak axis. Note that here the force values are shown smaller compared to

Figure A.2 (i.e., less force required for a given displacement in the weak direction compared to the strong direction).

In the bridge model, the initial transverse pile stiffness is assumed based on $\Delta_0 = 1 \text{ in.}$ Here, again the subscript “0” indicates initial estimates. From the pile force versus displacement in the weak direction (Figure A.3), the initial force in the weak direction corresponding to displacement of 1 in. is estimated as F_{w0} . The initial pile stiffness in the weak direction is $k_{w0} = \frac{F_{w0}}{\Delta_0}$.

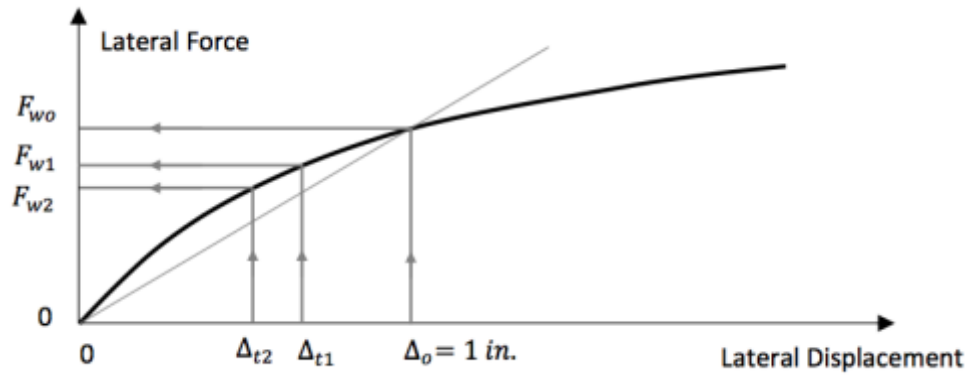


Figure A.3 Top of the Pile Lateral Force versus Displacement, Bending about the Weak Axis

For one of the two abutments, let’s say Abutment 1, the initial value for the transverse stiffness is estimated using Equation A.4. Here, initially the contribution of the wing is not included.

$$K_{t1,0} = n_1 k_{w0} \tag{A.4}$$

Where, n_1 = the number of piles in Abutment 1, and k_{w0} = the initial pile stiffness in the weak direction. Repeat the same process for Abutment 2 to obtain initial value for its transverse stiffness, $K_{t2,0}$:

$$K_{t2,0} = n_2 k_{w0} \quad (A.5)$$

Where, n_2 = the number of piles in Abutment 2.

With the above initial estimates for the abutment transverse stiffness values, load the bridge linear-elastic model in the transverse direction. Determine the transverse displacements and the corresponding seismic forces for Abutments 1 and 2. Note, here unlike the longitudinal direction, the abutment displacements may be significantly different and the use of average value may not be suitable. Let's call the transverse displacements Δ_{t1} and Δ_{t2} and call the transverse forces R_{t1} and R_{t2} . Let's also assume that the displacements are both less than 1 *in.* with the corresponding top of the pile reactions in the weak direction as F_{w1} and F_{w2} as shown in Equation A.3. Now, examine to see if the force equilibrium is maintained as shown by Equations A.6 and A.7.

$$R_{t1} \cong n_1 F_{w1} + F_{wing} \quad (A.6)$$

$$R_{t2} \cong n_2 F_{w2} + F_{wing} \quad (A.7)$$

Where, F_{wing} is the shear force demand on a single wing with a value $F_{wing} \leq V_c$.

If the left-hand sides of Equations A.6 and A.7 are larger than the right-hand side, reduce the transverse spring stiffness values K_{t1} and K_{t2} . This will result in larger transverse displacements and thus lead to larger values for F_{w1} and F_{w2} (see Figure A.3). This process is repeated a few times until the two sides of Equations A.6 and A.7 are within 10%. Again, it is recommended to keep the abutment stiffness values on the lower side. This would generally result in higher forces and displacements at the pier(s). The numerical example below assumes a symmetrical bridge with the same number of piles in each abutment (i.e., $n_1 = n_2$).

Example

Let's assume the initial springs based on 1" displacement result in $\frac{1}{2}$ " movement with 400 *kips* of acting seismic force at each abutment. Assuming that $\frac{1}{2}$ " top of pile movement results in 20 *kips* resistance, we would get $10 * 20 = 200$ *kips* of pile resistance at each abutment, leaving $400 - 200 = 200$ *kips* to be resisted by one wing. If one wing can resist only 100 *kips*, we might try to reduce abutment springs as to reduce the acting seismic force, but increase displacement, which in turn will increase pile reactions and reduce demand on the wing. Assume that softer springs would result in the movement of $\frac{3}{4}$ " and the acting force of 350 *kips* per abutment. Now the resistance from piles may be increased to let's say $10 * 30 \frac{kips}{pile} = 300$ *kips* leaving $350 - 300 = 50$ *kips* to be resisted by a wing, which is ok, since the wing resistance is 100 *kips*. If on other hand we conclude that acting seismic force is higher than combined resistance of piles and one wing (despite the softening of abutment springs) we may assume the wing will be sheared off and we may have to adjust the abutment springs based on piles alone, until we get good convergence again between acting force and pile resistance under given displacement.

APPENDIX B - Bridge Computer Models and Output Data

In this appendix, the details of computer modeling and seismic analyses of the Preston bridge are presented. The computer modeling, analyses, and results about Parma and Dubois bridges can be found in Appendix E of the ITD Report (Ebrahimpour, Earles, Maskey, Tangarife, & Sorensen, 2016).

Bridge on SH-36 over Bear River at Preston, Idaho

The bridge at Preston is a two-span bridge with a three-column bent. The superstructure is made up of an 8-inch deck thick deck that rests on 5 prestressed bulb tee girders. The substructure is made up of a pier cap, three columns, and their footings all of which are cast-in-place.

Soil Spring Stiffness

The abutment walls have 14" ϕ steel shell piles (pipe piles) and the center pier has 24" ϕ steel shell piles. The dimensions of the abutment walls are:

$$H_{aw} = 15 \text{ ft} \quad \text{Height of abutment wall}$$

$$L_{aw} = 40 \text{ ft} \quad \text{Length of abutment wall}$$

The soil spring stiffness for the steel shell piles were derived from the Phase IV Foundation Investigation Report. Figures B.1 and B.2 show force and deflection for a pipe pile. Since spring stiffness equals force divided by deflection ($K = \frac{F}{d}$) the spring stiffness can be estimated by

determining the force at 1 *in* of deflection. The force at 1 in of deflection for both the Northeast and the Southwest Abutments is 66.4 *kips*.

$$k = 66.4 \frac{kips}{in} = 796.8 \frac{kips}{ft}$$

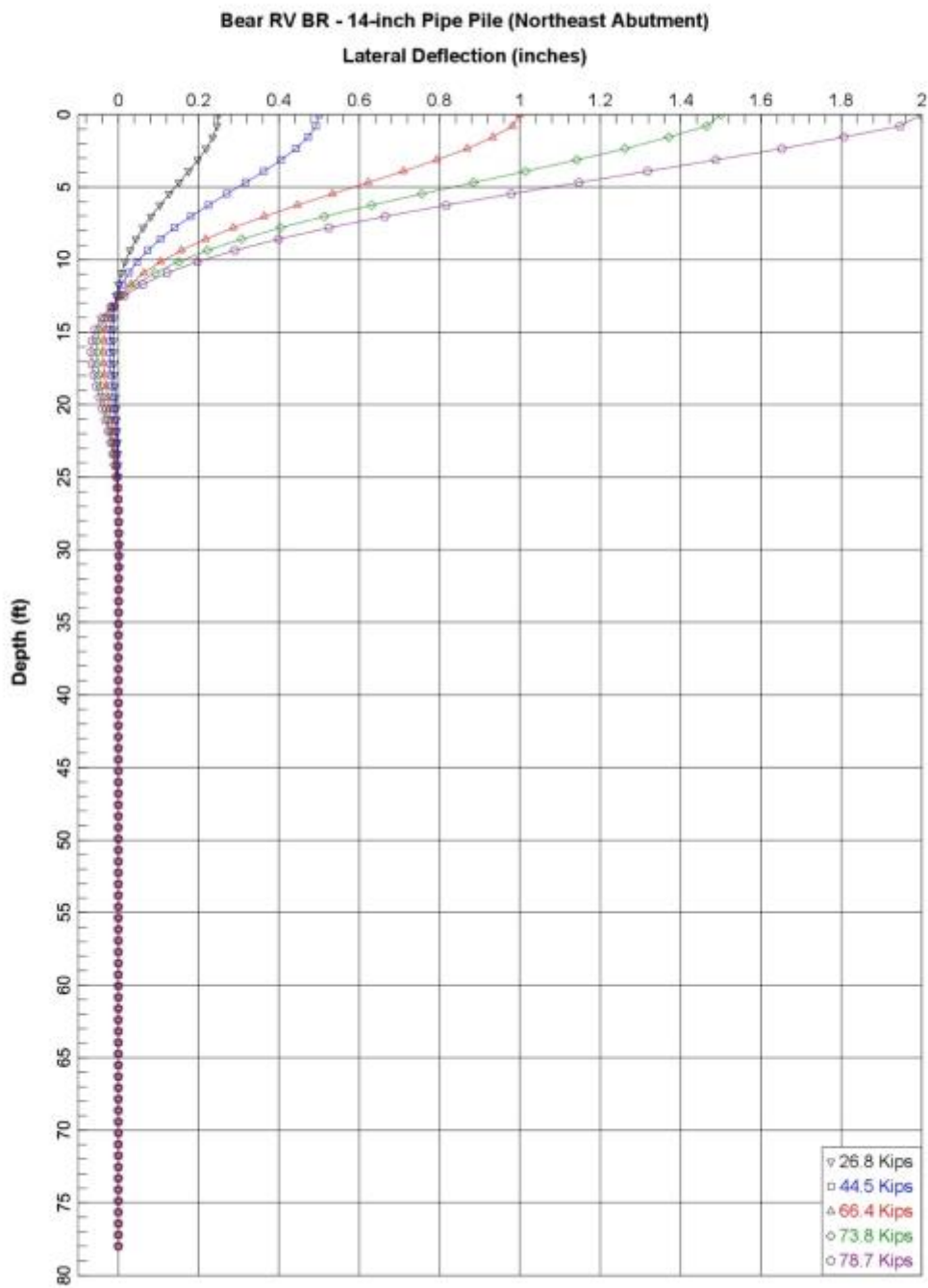


Figure B.1 Preston Bridge Lateral Deflection vs. Depth of a pipe pile (Northeast Abutment)

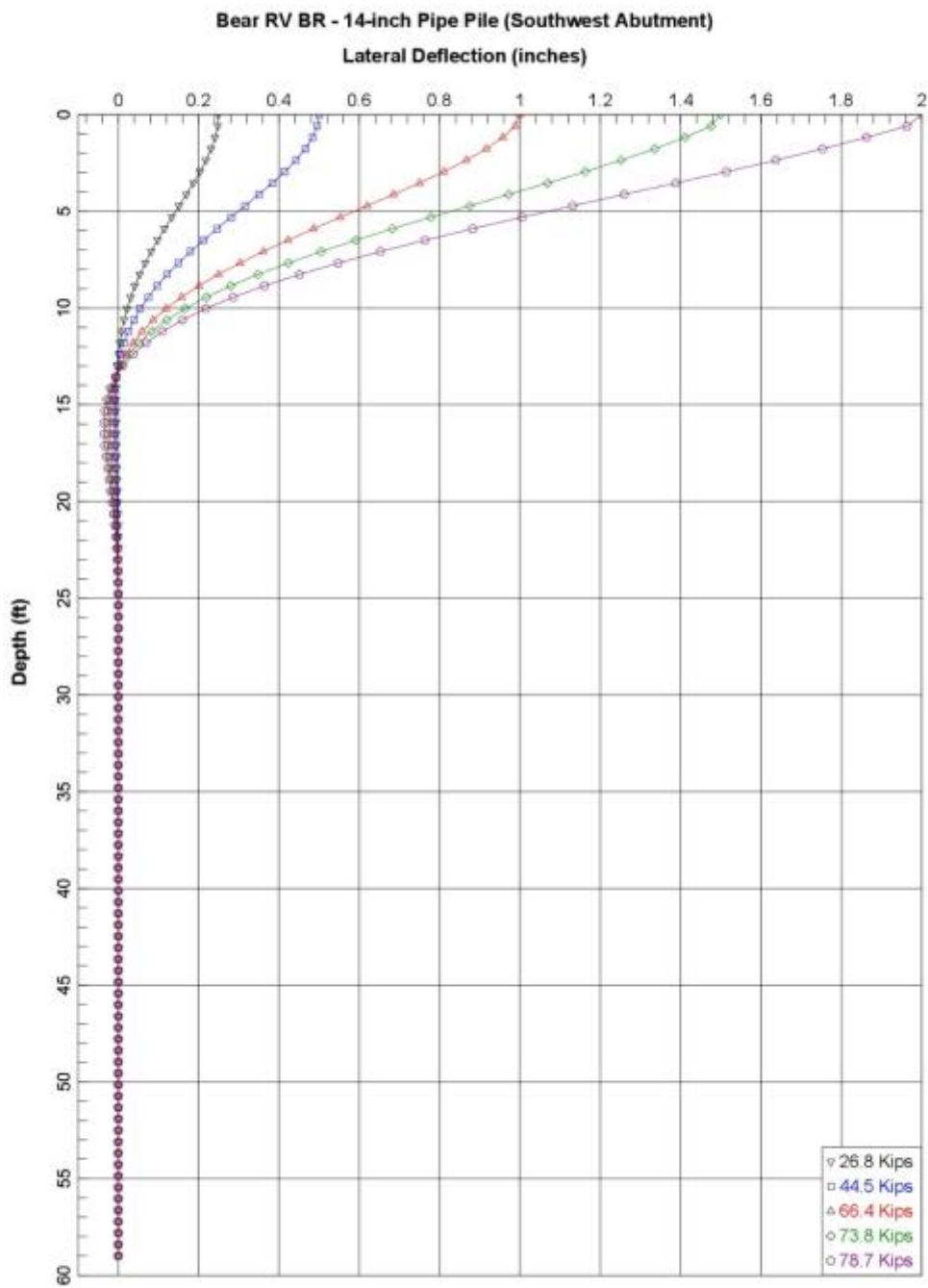


Figure B.2 Preston Bridge Lateral Deflection vs. Depth of a pipe pile (Southwest Abutment)

The initial value due to abutments-spring stiffness in the longitudinal direction is calculated by

$$K_l = \frac{2nk + \left(\frac{7.7A_{aw}}{d}\right)}{2}$$

Where

K_l = The abutments spring stiffness in the longitudinal direction

n = The number of sheet piles in one abutment wall = 8

k = The spring stiffness for one sheet = $796.8 \frac{kips}{ft}$

A_{aw} = The area of the abutment wall = $H_{aw}L_{aw} = 600 ft^2$

d = deflection needed to mobilize full passive resistance = $0.02H_{aw} = 0.3 ft$.

Initial value for the soil spring stiffness in the transverse direction is calculated by

$$K_t = nk$$

Where:

K_t = The spring stiffness in the transverse direction

k = The spring stiffness for one sheet pile = $796.8 \frac{kips}{ft}$

$$K_l = 14,074.4 \frac{kips}{ft}$$

Spring stiffness at abutments the transverse direction

$$K_t = 6,374.4 \frac{kips}{ft}$$

Spring stiffness at abutments the transverse direction

If the reactions at the ends of the bridge are greater than the force needed to displace the sheet piles times the number of piles in a wingwall the excess seismic load will be resisted by the shear capacity of one wingwall, V_c . If the excess seismic force is greater

than V_c it can be assumed that the wingwall has broken off and only the sheet pile capacity resists the seismic force.

A large spring stiffness ($1e12 \text{ kips/ft}$) was used for all other degrees of freedom (DOF's) except the rotation about the centerline (C. L.) of the abutments, which were assigned a value of zero.

$$V_c = \text{shear capacity of one wingwall} = 0.0316\beta(\sqrt{f'_c})b_v d_v$$

Where,

$$\beta = 2.0$$

$$b_v = \text{height of East wingwall} = 9.94 \text{ ft}$$

$$d_v = \text{thickness of wingwall minus distance from backfill face to main flexural reinf.} \\ = 1.5 \text{ ft}$$

$$f'_c = 4 \text{ ksi} = 576 \text{ ksf}$$

$$V_c = 0.0316 * 2 * \sqrt{576} * 9.94 * 1.5 = 22.615 \text{ kips}$$

Superstructure

Properties of the superstructure and its elements are as follows

$L = 274' 2''$	Overall length of the bridge
$A_{sup} = 48.35 \text{ ft}^2$	Cross-sectional area of superstructure without parapets
$A_{gSup} = 53.67 \text{ ft}^2$	Gross cross-sectional area of superstructure including parapets for weight calculations
$f'_{CCIP} = 4.0 \text{ ksi}$	Compressive strength of cast-in-place concrete

$$f'_{cPrestressed} = 8.5 \text{ ksi} \quad \text{Compressive strength of prestressed concrete}$$

$$E_{CIP} = 33000 * 0.145^{1.5} \sqrt{f'_{cCIP}} = 33000(0.145^{1.5})\sqrt{4.0} = 3,644 \text{ ksi}$$

Modulus of elasticity of cast-in-place concrete

$$E_{Prestressed} = 33000(0.14 + 0.001f'_{cPrestressed})^{1.5} \sqrt{f'_c} = 33000(0.14 + (0.001 * 8.5))^{1.5} \sqrt{8.5} = 5505.71 \text{ ksi}$$

Modulus of elasticity of prestressed concrete

$$n = \frac{E_{Prestressed}}{E_{CIP}} = \frac{5505.71}{3644} = 1.511 \quad \text{Modular ratio of elasticity}$$

The moments of inertia of the superstructure were determined by calculating the moments of inertia of the prestressed girders and the transformed moment of inertia of the deck and using the parallel axis theorem,

$$I_s = \sum I_o + Ad^2$$

where:

I_s = the moment of inertia of the superstructure

I_o = the moment of inertia of a section (girder or deck) of the superstructure

A = the area of a section of the superstructure

d = the distance from the centroid of the section to the centroid of the superstructure

$$A_{Girder} = 8.43 \text{ ft}^2 \quad \text{Cross-sectional area one girder}$$

$$I_{yGirder} = 22.09 \text{ ft}^4 \quad \text{Moment of inertia of one girder about the y-axis}$$

$$I_{zGirder} = 34.57 \text{ ft}^4 \quad \text{Moment of inertia of one girder about the z-axis}$$

The transformed moment of inertia and area for the deck was calculated by dividing the value of I_{zDeck} , I_{yDeck} and A_{Deck} by the modular ratio, n . The parapets on the outside edge of the deck were not included in these calculations.

$A_{tDeck} = 17.65 \text{ ft}^2$	Transformed area of deck
$I_{yDeck} = 2353.11 \text{ ft}^4$	Transformed moment of inertia of the deck about the y axis
$I_{zDeck} = 0.6537 \text{ ft}^4$	Transformed moment of inertia of the deck about the z axis
$d_{zGirder} = 1.36 \text{ ft}$	Distance from the centroid of the girder to centroid of superstructure along the y-axis
$d_{zDeck} = 0.73 \text{ ft}$	Distance from the centroid of the deck to centroid of superstructure along the y-axis
$d_{zGirder1,5} = 16.34 \text{ ft}$	Distance from the centroid of the first and fifth girders to the centroid of the superstructure along the z-axis
$d_{zGirder2,4} = 8.17 \text{ ft}$	Distance from the centroid of the second and fourth girders to the centroid of the superstructure along the z-axis
$d_{yGirder3} = 0 \text{ ft}$	Distance from the centroid of the third girder to the centroid of the superstructure along the z-axis
$d_{yGDeck} = 0 \text{ ft}$	Distance from the centroid of the deck to the centroid of superstructure along the z-axis
$I_{ySup} = 2353.11 \text{ ft}^4 + 5(22.09 \text{ ft}^4) + 8.43 \text{ ft}^2[2(16.34 \text{ ft})^2 + 2(8.17 \text{ ft})^2] = 8090.49 \text{ ft}^4$	Transformed moment of inertia of the superstructure about the y-axis

$$I_{zSup} = 0.6537 ft^4 + 17.65 ft^2(0.73 ft)^2 + 5[34.57 ft^4 + 8.43 ft^2(1.36 ft)^2] = 260.87 ft^4$$

Transformed moment of inertia of the superstructure about the z-axis

$$A_{tSup} = A_{tDeck} + \sum A_{Girder} = 17.65 ft^2 + 5(8.43 ft^2) = 59.8 ft^2$$

Transformed area of the superstructure

The modulus of rigidity, G , for the cast-in-place and prestressed concrete are calculated by

$$G = \frac{E}{2(1 + \nu)}$$

where:

ν = Poisson's ratio, typically from 0.15 – 0.2.

$$G_{prestressed} = \frac{5505.71}{2(1+0.2)} = 2,294.05 ksi = 330,343.2 ksf$$

$$G_{CIP} = \frac{3644}{2(1+0.2)} = 1,518.3 ksi = 218,640 ksf$$

Substructure

Properties of the substructure and its elements are as follows

$L_p = 40 ft$	Length of pier cap
$A_{pyz} = 22.5 ft^2$	Cross-sectional area of pier cap in the x-y plane
$L_c = 29' 3''$	Column height
$d_c = 4 ft$	Distance between two sides of the octagonal column

$$A_{cg} = 13.248 \text{ ft}^2$$

Cross-sectional area of one column

$$I_{cg} = 14.08 \text{ ft}^4$$

Gross moment of inertia of one column

Column Reinforcement

The columns are reinforced with 20 #9 bars and a #5 spiral with a 4 in pitch. There is 2 in of cover concrete as shown in Figure B.3.

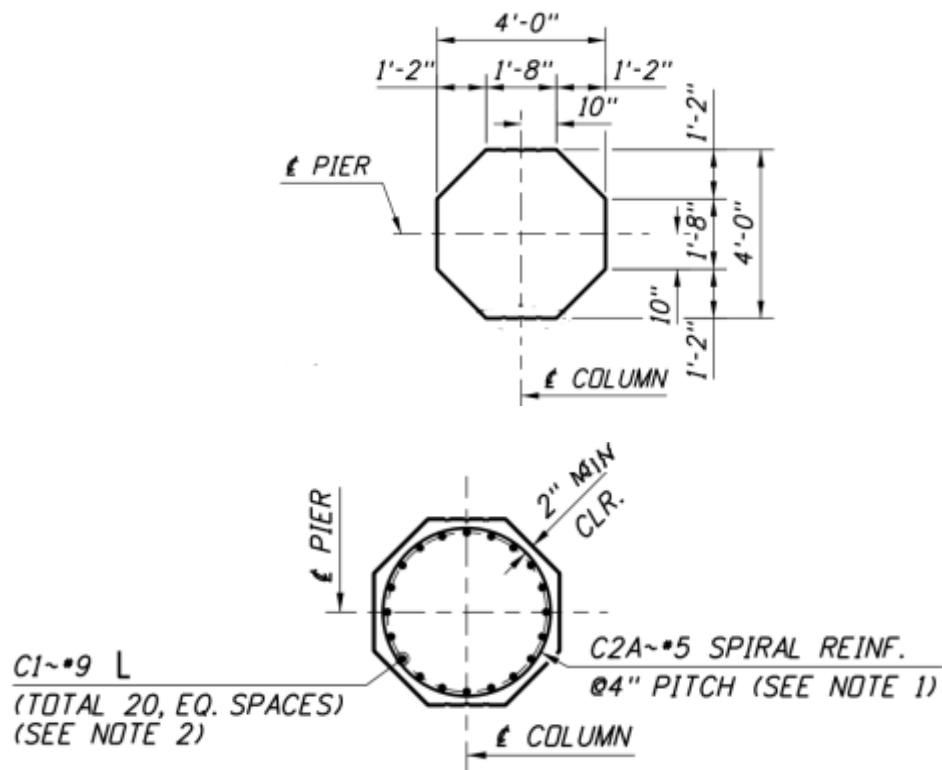


Figure B.3 Preston Bridge Reinforced Column Detail

$A_{r9} = 1 \text{ in}^2$	Cross-sectional area of a #9 bar
$d_s = 0.625''$	Diameter of spiral reinforcing
$A_{st9} = 20A_{r9} = 0.138 \text{ ft}^2$	Total longitudinal steel in one column with #9 bars
$R_9 = 1.74 \text{ ft}$	Distance from the center of the column to the center of the #9 bars

Effective Moment of Inertia and Torsional Moment of Inertia of the Columns

For the effective moment of inertia, the gross moment of inertia is multiplied by the Elastic Stiffness Ratio ($\frac{I_{eff}}{I_{cg}}$). This is obtained from Figure B.4 with the Axial Load Ratio and the ratio of reinforcing steel to concrete.

$$\text{Axial Load Ratio} = \frac{P}{f'_c A_{cg}}$$

Where:

P = The axial load to the column from the self-weight of the bridge = 527.771 kips

The axial load on one column is from half the weight of each span divided by three plus the weight on the node in the pier cap above the column plus half the weight of one column. The dead load to each node is given in Table B.1.

$$\frac{P}{f'_c A_{cg}} = \frac{527.771}{4 * 144 * 13.248} = 0.07$$

$$\frac{A_{st}}{A_{cg}} = \frac{0.138 \text{ ft}^2}{13.248 \text{ ft}^2} = 0.01$$

$$\frac{I_{eff}}{I_{cg}} = 0.34$$

$$I_{ceff} = 0.34 * I_{cg} = 4.787 \text{ ft}^4 \quad \text{Effective moment of inertia of one column}$$

$$J_{gross} = 1.2762 * d_c^4 = 326.707 ft^4 \quad \text{Gross torsional moment of inertia}$$

$$J_{eff} = 0.2J_{gross} = 65.34 ft^4 \quad \text{Effective torsional moment of inertia}$$

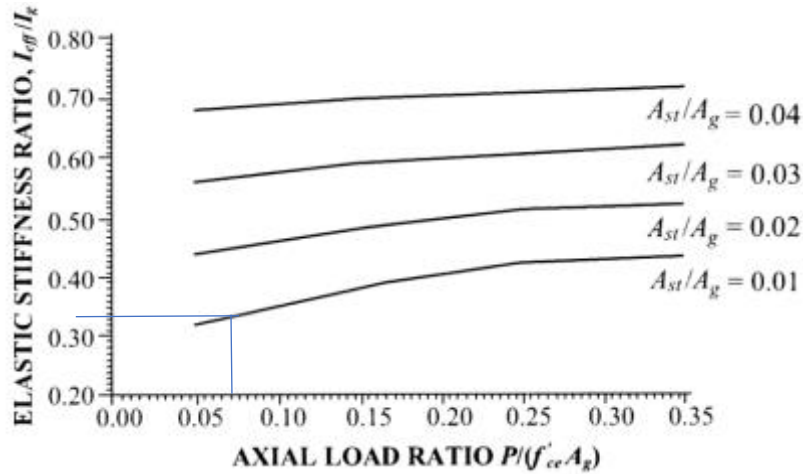


Figure B.4 Preston Bridge Column Elastic Stiffness Ratio (Koh & Stephens, 1991)

Table B.1 Preston Bridge Weight of Structure to Nodes from Deck, Pier Cap, and Top Half of Columns

Section	Cross-sectional area (ft^2)	Length (ft)	Weight of material ($\frac{kips}{ft^3}$)	Overall weight ($kips$)	Weight per foot ($\frac{kips}{ft}$)
Future Wearing Surface					0.028
Deck	26.667	274.167	0.150	1096.68	4.000
Utilities					0.020
Future Utilities					0.020
Girders	21.680	274.167	0.150	891.59	3.252
Parapets	5.330	274.167	0.150	219.20	0.800
Columns	39.744	29.25	0.150	697.51	47.693
Pier Cap	22.500	40	0.150	135.00	3.375

Superstructure	Length (ft)	Materials involved	Weight to node (kips)
Node 1	17.135	Concrete, steel, wearing surface	139.13
Node 2	34.271	Concrete, steel, wearing surface	278.27
Node 3	34.271	Concrete, steel, wearing surface	278.27
Node 4	34.271	Concrete, steel, wearing surface	278.27
Node 5	34.271	Concrete, steel, wearing surface	278.27
Node 6	34.271	Concrete, steel, wearing surface	278.27
Node 7	34.271	Concrete, steel, wearing surface	278.27
Node 8	34.271	Concrete, steel, wearing surface	278.27
Node 9	17.135	Concrete, steel, wearing surface	139.13

Substructure	Length (ft)	Materials involved	Weight to node (kips)	Notes
Node 13	10.000	Concrete	150.001	10.000
Node 17	12.000	Concrete	156.751	12.000
Node 21	10.000	Concrete	150.001	10.000
		TOTAL	2682.866	
		$w(x)$ in $\frac{kip}{ft}$	11.665	

Axial Load to one Interior Column	527.771
--	---------

Linear Elastic Model of the Structure

Each span of the superstructure is modeled as four elements (35.275' each) attached end to end from south to north. A rigid element with a large moment of inertia attaches the superstructure to the pier bent at the midpoint of both. This element starts at the center of gravity of the pier bent and ends at the center of gravity of the superstructure (7.273'). At the top of each column there is another rigid element that starts at the top of the column and ends at the center of gravity of the pier bent (2.25'). The footings of the columns are modeled as an element at the bottom of the columns with the same properties as the columns, except that they are rigid, and are half the depth of the footings in length (2.75'). To model the spring support-condition an extra node and *zeroLength* element is assigned to the abutment ends of the superstructure.

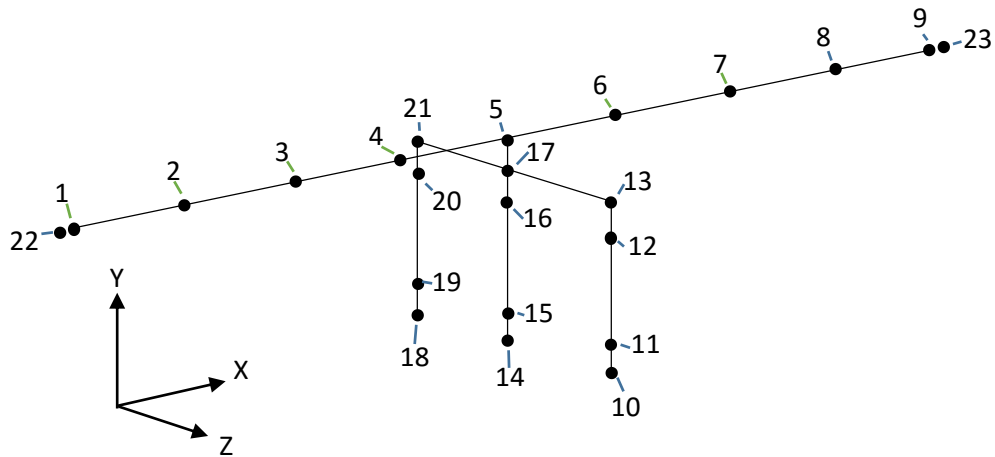


Figure B.5 Preston Bridge Linear Elastic Model with Node Numbers.

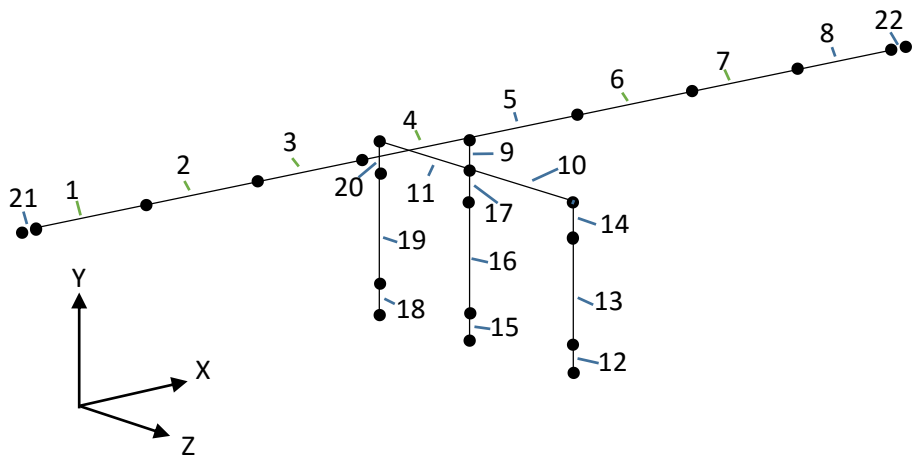


Figure B.6 Preston Bridge Linear Elastic Model with Element Numbers.

Calculation of Seismic Loads

The bridge will be subject to more seismically active conditions than that found near Preston, ID. Montpelier, ID is the most seismically active city in Idaho where there might be a bridge. Figure B.7 shows the Design Maps Summary Report for Montpelier, ID.

Design Maps Summary Report

User-Specified Input

Building Code Reference Document 2009 AASHTO Guide Specifications for LRFD Seismic Bridge Design
(which utilizes USGS hazard data available in 2002)

Site Coordinates 42.32204°N, 111.29481°W

Site Soil Classification Site Class D – “Stiff Soil”



USGS-Provided Output

PGA = 0.322 g	A_s = 0.379 g
S_s = 0.758 g	S_{0.5} = 0.907 g
S₁ = 0.258 g	S_{0.1} = 0.486 g

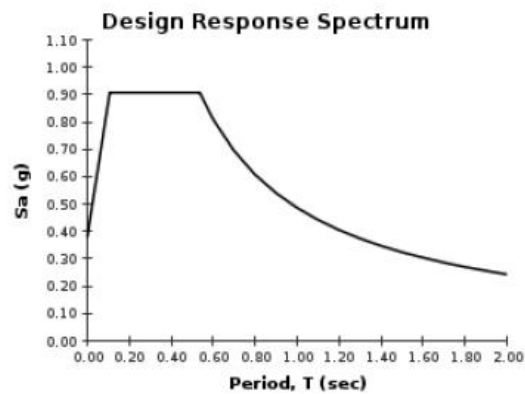


Figure B.7 USGS Design Maps Summary Report

To calculate the seismic loads on the deck of the bridge the displacements at the deck nodes from a uniformly distributed load of 10 kip/ft in the longitudinal and transverse direction are determined and used to calculate the factors α , β , and γ . The factors are used to calculate the loads ($p_e(x)$) at the nodes on the deck. The distributed seismic loads on each element is the average of the loads on the nodes. These loads are shown in column 9 of Tables B.2 and B.3.

$$\alpha = \int_0^L v_s(x) dx$$

$$\beta = \int_0^L w(x)v_s(x)dx$$

$$\gamma = \int_0^L w(x)v_s(x)^2 dx$$

where

$v_x(x)$ = Displacement due to a uniformly distributed load of 10 kips/ft.

$w(x)$ = Weight of the bridge per unit length = 11.665 kip/ft

dx = Tributary length

L = Total length of bridge

$$p_e(x) = \beta C_{sm} w(x) * \frac{v_s(x)}{\gamma}$$

where

$$C_{sm} = S_{DS} = 0.907 \quad \text{for } T_o < T_m < T_s \text{ and}$$

$$C_{sm} = S_{D1}/T_m = 1.303 \quad \text{for } T_m > T_s$$

where

$$T_m = 2\pi \sqrt{\frac{\gamma}{P_0 g \alpha}} = 0.373 \text{ s} \quad \text{for longitudinal loads}$$

$$T_m = 2\pi \sqrt{\frac{\gamma}{P_0 g \alpha}} = 0.529 \text{ s} \quad \text{for transverse loads}$$

$$T_s = S_{D1}/S_{DS} = 0.5358$$

$$T_o = 0.2T_s = 0.1072$$

$$g = 32.2 \frac{ft}{s^2}$$

$$P_0 = 10 \frac{kips}{ft}$$

Table B.2 Preston Bridge Calculation of Seismic Loads in the Longitudinal Direction.

Nodes	x (ft)	dx (ft)	$v_s(x)$ (ft)	$\alpha(x)$ (ft²)	$\beta(x)$ (k ft)	$\gamma(x)$ (k ft²)	$p_e(x)$ $\frac{k}{ft}$	$ave.$ $\frac{k}{ft}$
1	0.00	0.000	0.08985	0.000	0.000	0.000	11.164	
2	34.27	34.27	0.09064	3.093	38.553	3.479	11.262	11.213
3	68.54	34.27	0.09118	3.115	38.838	3.531	11.329	11.296
4	102.81	34.27	0.09148	3.130	39.017	3.563	11.366	11.348
5	137.08	34.27	0.09152	3.136	39.090	3.577	11.372	11.369
6	171.35	34.27	0.09148	3.136	39.090	3.577	11.366	11.369
7	205.62	34.27	0.09118	3.130	39.017	3.563	11.329	11.348
8	239.89	34.27	0.09064	3.115	38.838	3.531	11.262	11.296
9	274.16	34.27	0.08985	3.093	38.553	3.479	11.164	11.213
Totals		274.16		24.947	310.994	28.300		

Table B.3 Preston Bridge Calculation of Seismic Loads in the Transverse Direction.

Nodes	x (ft)	dx (ft)	$v_s(x)$ (ft)	$\alpha(x)$ (ft ²)	$\beta(x)$ (k ft)	$\gamma(x)$ (k ft ²)	$p_e(x)$ $\left(\frac{k}{ft}\right)$	$ave.$ $\left(\frac{k}{ft}\right)$
1	0.00	0.00	-0.17498	0.000	0.000	0.000	10.570	
2	34.27	34.27	-0.17803	-6.049	-75.404	13.309	10.754	10.662
3	68.54	34.27	-0.18361	-6.197	-77.248	13.968	11.091	10.922
4	102.81	34.27	-0.18793	-6.366	-79.361	14.743	11.352	11.221
5	137.08	34.27	-0.18937	-6.465	-80.591	15.203	11.439	11.395
6	171.35	34.27	-0.18793	-6.465	-80.591	15.203	11.352	11.395
7	205.62	34.27	-0.18361	-6.366	-79.361	14.743	11.091	11.221
8	239.89	34.27	-0.17803	-6.197	-77.248	13.968	10.754	10.922
9	274.16	34.27	-0.17498	-6.049	-75.404	13.309	10.570	10.662
Totals		274.16		-50.153	-625.208	114.446	10.997	

Linear Elastic OpenSees Input File for Seismic Load in Transverse Direction

#Two-span Bridge on SH-36 over Bear River at Preston, Idaho

wipe

#Create model with 3 dimensions and 6 DOF

model BasicBuilder -ndm 3 -ndf 6

#Units are kips and feet

#Create 6 DOF nodes

#Superstructure nodes

#	tag	x	y	z
node	1	0.0	39.273	0.0
node	2	34.270	39.273	0.0
node	3	68.540	39.273	0.0
node	4	102.810	39.273	0.0
node	5	137.080	39.273	0.0
node	6	171.350	39.273	0.0
node	7	205.620	39.273	0.0
node	8	239.890	39.273	0.0
node	9	274.160	39.273	0.0

#Substructure nodes

node	10	137.080	0.0	12.000
node	11	137.080	2.75	12.000
node	12	137.080	32.000	12.000
node	13	137.080	34.250	12.000
node	14	137.080	0.0	0.0
node	15	137.080	2.75	0.0
node	16	137.080	32.000	0.0
node	17	137.080	34.250	0.0
node	18	137.080	0.0	-12.000
node	19	137.080	2.75	-12.000
node	20	137.080	32.000	-12.000
node	21	137.080	34.250	-12.000

#Spring support nodes

node	22	0.0	39.273	0.0
node	23	274.160	39.273	0.0

#Specify geometric transformation

geomTransf Linear 1 0 0 1
geomTransf Linear 2 -1 0 0
geomTransf PDelta 3 0 0 1

Fix column bases and abutments in all DOF's

fix 22 1 1 1 1 1 1
fix 23 1 1 1 1 1 1
fix 10 1 1 1 1 1 1
fix 14 1 1 1 1 1 1
fix 18 1 1 1 1 1 1

Create deck elements

element elasticBeamColumn \$eleTag \$iNode \$jNode \$A \$E \$G \$J \$Iy \$Iz \$transfTag

element	elasticBeamColumn	1	1	2	59.80	792822.24	330343.2	1e10	8090.49	260.87	1
element	elasticBeamColumn	2	2	3	59.80	792822.24	330343.2	1e10	8090.49	260.87	1
element	elasticBeamColumn	3	3	4	59.80	792822.24	330343.2	1e10	8090.49	260.87	1
element	elasticBeamColumn	4	4	5	59.80	792822.24	330343.2	1e10	8090.49	260.87	1
element	elasticBeamColumn	5	5	6	59.80	792822.24	330343.2	1e10	8090.49	260.87	1
element	elasticBeamColumn	6	6	7	59.80	792822.24	330343.2	1e10	8090.49	260.87	1
element	elasticBeamColumn	7	7	8	59.80	792822.24	330343.2	1e10	8090.49	260.87	1
element	elasticBeamColumn	8	8	9	59.80	792822.24	330343.2	1e10	8090.49	260.87	1

Create pier bent elements

element	elasticBeamColumn	9	5	17	196.00	524736	218640	1e10	1e10	1e10	3
element	elasticBeamColumn	10	13	17	22.50	524736	218640	1e10	1e10	1e10	2
element	elasticBeamColumn	11	17	21	22.50	524736	218640	1e10	1e10	1e10	2

Create column elements

element	elasticBeamColumn	12	10	11	13.248	524736	218640	1e10	4.787	4.787	3
element	elasticBeamColumn	13	11	12	13.248	524736	218640	65.34	4.787	4.787	3
element	elasticBeamColumn	14	12	13	1e10	524736	218640	1e10	1e10	1e10	3
element	elasticBeamColumn	15	14	15	13.248	524736	218640	1e10	4.787	4.787	3
element	elasticBeamColumn	16	15	16	13.248	524736	218640	65.34	4.787	4.787	3

```

element elasticBeamColumn 17 16 17 1e10 524736 218640 1e10 1e10 1e10 3
element elasticBeamColumn 18 18 19 13.248 524736 218640 1e10 4.787 4.787 3
element elasticBeamColumn 19 19 20 13.248 524736 218640 65.34 4.787 4.787 3
element elasticBeamColumn 20 20 21 1e10 524736 218640 1e10 1e10 1e10 3

# Create spring elements

# Initial abutment stiffnesses to be used with the uniform loads to determine the seismic
loads

#uniaxialMaterial Elastic 1 17.202e3; # Translational stiffness along local x axis of the
abutments, kip/ft
#uniaxialMaterial Elastic 3 5.52e3; # Translational stiffness along local z axis of the
abutments, kip/ft

# Final abutment stiffnesses

uniaxialMaterial Elastic 1 14074.4;# Translational stiffness along local x axis of the
abutments, kip/ft
uniaxialMaterial Elastic 2 1e12; # Translational stiffness along local y axis of the
abutments, kip/ft
uniaxialMaterial Elastic 3 2300; # Translational stiffness along local z axis of the
abutments, kip/ft
uniaxialMaterial Elastic 4 1e12; # Rotational stiffness about local x axes of the abutments,
kip.ft/radian
uniaxialMaterial Elastic 5 1e12; # Rotational stiffness about local y axis of the abutments,
kip.ft/radian
uniaxialMaterial Elastic 6 0; # Rotational stiffness about the local z axis of the
abutment, kip.ft/radian

# Spring elements using above stiffness values
# element zeroLength $eleTag $iNode $jNode -mat $matTag1 $matTag2 ... -dir $dir1 $dir2 ...

element zeroLength 21 22 1 -mat 1 2 3 4 5 6 -dir 1 2 3 4 5 6
element zeroLength 22 9 23 -mat 1 2 3 4 5 6 -dir 1 2 3 4 5 6

# Create recorder files

#recorder Node -file Nodes1-9DispLong_BR_elastic.out -time -nodeRange 1 9 -dof 1 disp
recorder Node -file Nodes1-9DispTrans_BR_elastic.out -time -nodeRange 1 9 -dof 3 disp
#recorder Node -file Long_BR_Column_Displacement_Long.out -time -node 12 16 20 -dof 1 disp
#recorder Node -file Long_BR_Column_Reactions_Long.out -time -node 10 14 18 -dof 1 2 6
reaction
recorder Node -file Long_BR_Column_Displacement_Trans.out -time -node 12 16 20 -dof 3 disp
recorder Node -file Long_BR_Column_Reactions_Trans.out -time -node 10 14 18 -dof 3 2 4
reaction
recorder Node -file Node22_Reaction_Trans_BR_elastic.out -time -node 22 -dof 3 reaction
recorder Node -file Node23_Reaction_Trans_BR_elastic.out -time -node 23 -dof 3 reaction

# Assign gravity loads

pattern Plain 1 Constant {
# tag FX FY FZ MX MY MZ
load 1 0.0 -139.130 0.0 0.0 0.0 0.0
load 2 0.0 -278.270 0.0 0.0 0.0 0.0
load 3 0.0 -278.270 0.0 0.0 0.0 0.0
load 4 0.0 -278.270 0.0 0.0 0.0 0.0
load 5 0.0 -278.270 0.0 0.0 0.0 0.0
load 6 0.0 -278.270 0.0 0.0 0.0 0.0
load 7 0.0 -278.270 0.0 0.0 0.0 0.0

```

```

load 8      0.0    -278.270  0.0  0.0  0.0  0.0
load 9      0.0    -139.130  0.0  0.0  0.0  0.0
load 13     0.0    -150.001  0.0  0.0  0.0  0.0
load 17     0.0    -156.751  0.0  0.0  0.0  0.0
load 21     0.0    -150.001  0.0  0.0  0.0  0.0
}

constraints Plain

numberer Plain

system BandGeneral

test NormDispIncr 1.0e-8 6

algorithm Newton

integrator LoadControl 1

analysis Static

analyze 1

#Reset time to perform pushover analysis

loadConst -time 0.0

# Create load pattern for horizontal loading
#The 10 kip/ft load should be activated when placing a uniform load of 10 kip/ft in the
longitudinal or transverse direction
#These loads should be used with the initial abutment stiffnesses

#pattern Plain 2 Linear {
#eleLoad -ele $eleTag1 <$eleTag2 ....> -type -beamUniform $Wy $Wz <$Wx>
#eleLoad -ele 1 2 3 4 5 6 7 8 -type beamUniform 0 0 10
#}

#pattern Plain 3 Linear {
# eleLoad -ele $eleTag1 <$eleTag2 ....> -type -beamUniform $Wy $Wz <$Wx>
#eleLoad -ele 1 2 3 4 5 6 7 8 -type beamUniform 0 -10 0
#}

#Transverse seismic loads

pattern Plain 4 Linear {
eleLoad -ele 1 -type beamUniform 0 10.662 0
}

pattern Plain 5 Linear {
eleLoad -ele 2 -type beamUniform 0 10.922 0
}

pattern Plain 6 Linear {
eleLoad -ele 3 -type beamUniform 0 11.221 0
}

pattern Plain 7 Linear {
eleLoad -ele 4 -type beamUniform 0 11.395 0
}

```

```
pattern Plain 8 Linear {
eleLoad -ele 5 -type beamUniform 0 11.395 0
}
```

```
pattern Plain 9 Linear {
eleLoad -ele 6 -type beamUniform 0 11.221 0
}
```

```
pattern Plain 10 Linear {
eleLoad -ele 7 -type beamUniform 0 10.922 0
}
```

```
pattern Plain 11 Linear {
eleLoad -ele 8 -type beamUniform 0 10.662 0
}
```

The following eight loading patterns should be activated instead of the previous eight, when loading in the longitudinal direction

```
#pattern Plain 12 Linear {
#eleLoad -ele 1 -type beamUniform 0 0 10.000
#}
```

```
#pattern Plain 13 Linear {
#eleLoad -ele 2 -type beamUniform 0 0 10.000
#}
```

```
#pattern Plain 14 Linear {
#eleLoad -ele 3 -type beamUniform 0 0 10.000
#}
```

```
#pattern Plain 15 Linear {
#eleLoad -ele 4 -type beamUniform 0 0 10.000
#}
```

```
#pattern Plain 16 Linear {
#eleLoad -ele 5 -type beamUniform 0 0 10.000
#}
```

```
#pattern Plain 17 Linear {
#eleLoad -ele 6 -type beamUniform 0 0 10.000
#}
```

```
#pattern Plain 18 Linear {
#eleLoad -ele 7 -type beamUniform 0 0 10.000
#}
```

```
#pattern Plain 19 Linear {
#eleLoad -ele 8 -type beamUniform 0 0 10.000
#}
```

```
constraints Plain
```

```
numberer Plain
```

```
system BandGeneral
```

```
test NormDispIncr 1.0e-8 6
```

```
algorithm Newton
```

integrator LoadControl 0.01

analysis Static

analyze 100

Determination of Final Soil Spring Stiffness

The final estimations of the bridge transverse and longitudinal abutment stiffness values are accomplished with an iterative process. In the longitudinal direction, the backfill behind the abutment wall as well as the embedded piles resist the seismic forces at the ends of the deck. The following procedure is used to achieve a correlation between these.

1. Determine the displacements and OpenSees reactions at the end nodes of the deck.
2. Add the OpenSees reactions from both abutments. This sum is the total longitudinal demand force on an abutment.
3. Determine the force that each pile resists based on the displacements and multiply it by the total number of piles from both abutments.
4. Determine the abutment wall force by subtracting the pile resistance from the total demand on the abutment.
5. Compare the displacement at the end nodes to $0.02H_{aw}$.
 - a. If it is greater – the wall force is $7.7A_{aw}$.
 - b. If it is smaller – the wall force is calculated by a linear interpolation

$$F = \Delta \left(\frac{7.7A_{aw}}{0.02H_{aw}} \right)$$

- i. F = the wall capacity,
- ii. Δ = the displacement of the end node.

6. Compare the abutment demand to the abutment capacity (i.e., sum of the forces of the piles and the backfill force).
 - a. If it is greater, increase abutment stiffness.
 - b. If it is smaller, decrease abutment stiffness.
7. Repeat process until the combined backfill force and pile force is within 10% of the value of the longitudinal demand force.

Longitudinal Direction:

The reactions at the abutments, Node 22 and 23 = $R_1 = R_2 = 1429.77 \text{ kips}$

The deflections at the abutments, Node 1 and 9 = 0.101587 ft

From Figures:

$$F_{NE} = 70 \text{ k and } F_{SW} = 70 \text{ k}$$

$$\text{So, Demand Force} = R_1 + R_2 = 2859.54 \text{ kips}$$

$$\text{Now, } (F_{NE} + F_{SW}) * 8 \text{ piles} = 1120 \text{ kips}$$

Comparing deflections at abutments to $0.02H_{aw}$:

$$0.101587 \text{ ft} < 0.02H_{aw}$$

$$\text{Backfill Wall force, } F_{bf} = \frac{\Delta(7.7A_{aw})}{0.02H_{aw}} = \frac{0.101587 * 7.7 * 15 * 40}{0.02 * 15} = 1564.44 \text{ kips}$$

$$\text{Capacity} = 1120 + 1564.44 = 2684.44 \text{ kips}$$

Table B.4 Preston Bridge Final Abutment Stiffness Calculation for Longitudinal Direction

Iteration	Longitudinal Displacement (ft)		Total Demand (kips)	Total Capacity (kips)	$K \left(\frac{kips}{ft} \right)$	Correlation (%)
	node 1	node 10				
1	0.101587	0.101587	2859.54	2684.44	14074.4	6.123

The transverse abutment stiffness values depend only on the resistance of the piles in one abutment wall. The procedure is simple because the abutments are similar and there are no wingwalls.

1. Determine the displacements and OpenSees reactions at the end nodes of the deck. The OpenSees reactions are the demand forces on each abutment.
2. Based on the displacements determine the force that one pile resists.
3. Multiply the force that one pile resists by the number of piles in each abutment.
4. Compare the total force that the piles from one abutment resist to the demand.
 - a. If it is greater, increase abutment stiffness.
 - b. If it is smaller, decrease abutment stiffness.
5. Repeat procedure until the pile resistance is within 10% of the abutment demand.

Transverse Direction:

The reactions at the one abutment = $Demand = R = 1115.36 k$

Displacement at the one abutment = $0.174976 ft$.

From Figure:

$$F = 78.7 k$$

Now, $Capacity = 8 * F = 8(78.7 k) = 629.6 k$

Since, $Demand - Capacity = 485.76 > V_c$, the wingwall breaks and the wingwall capacity cannot be added

Table B.5 Preston Bridge Final Abutment Stiffness Calculation for Transverse Direction

Iteration	Transverse Displacement (ft)		Total Demand (kips)	Total Capacity (kips)	$K \left(\frac{kips}{ft} \right)$	Correlation (%)
	node 1	node 10				
1	0.174976	0.174976	1115.360	629.60	6374.40	43.5519
2	0.277215	0.277215	1120.060	759.88	4000.00	32.1572
3	0.3299	0.3299	1055.680	822.35	3200.00	22.1027
4	0.362159	0.362159	1014.040	860.80	2800.00	15.1118
5	0.450205	0.450205	900.410	964.16	2000.00	7.0801
6	0.41259	0.41259	948.957	919.88	2300.00	3.0641

The final estimation for the abutment stiffness values are

$K_l = 14,074.4 kips/ft$ Longitudinal abutment stiffness

$K_t = 2,300 kips/ft$ Transverse abutment stiffness

As a check, the final abutment stiffness values were used in the OpenSees program with the uniformly distributed load used for calculating the seismic loads to see how the new stiffness values would affect the calculation of the seismic loads. The results are shown in the Tables B.7 and B.8. The longitudinal stiffness values didn't change and the difference in the transverse values was less than 5%. The final transverse stiffness values were softer than the initial values and this produced less of a difference in the seismic forces from the end of the deck to the center so that the characteristic trapezoidal shape of the seismic forces was flatter than before.

Table B.6 Preston Bridge Comparison of Updated and Original Transverse Design Loads

Updated Design Loads ($\frac{kips}{ft}$)	Original Design Loads ($\frac{kips}{ft}$)
10.970	10.662
11.036	10.922
11.099	11.221
11.123	11.395
11.123	11.395
11.099	11.221
11.036	10.922
10.970	10.662

Table B.7 Preston Bridge Linear Elastic Displacements and Column Base Reactions for Seismic Loads in the Longitudinal Direction

Nodes	Displacement (<i>ft.</i>)	Columns	Shear (<i>k</i>)	Axial (<i>k</i>)	Moment (<i>k ft</i>)
Deck		1	-80.080	609.786	1357.590
1	0.10159	2	-80.080	609.786	1357.590
2	0.10248	3	-80.080	609.786	1357.590
3	0.10310				
4	0.10343				
5	0.10349				
6	0.10343				
7	0.10310				
8	0.10248				
9	0.10159				
Top of the Columns					
12	0.09903				
16	0.09903				
20	0.09903				

Table B.8 Preston Bridge Linear Elastic Displacements and Column Base Reactions for Seismic Loads in the Transverse Direction

Nodes	Displacement (ft.)	Columns	Shear (k)	Axial (k)	Moment (k ft)
Deck		1	-377.069	609.812	-6152.560
1	0.41259	2	-377.414	609.776	-6158.190
2	0.41455	3	-377.069	609.812	-6152.560
3	0.41760				
4	0.41927				
5	0.41944				
6	0.41927				
7	0.41760				
8	0.41455				
9	0.41259				
Top of the Columns					
12	0.41906				
16	0.41944				
20	0.41906				

The column height is 29.25 *ft* and the drift in the longitudinal and transverse directions for top of the columns are shown in Table B.9.

Table B.9 Preston Bridge Linear Elastic Calculated Drift for Top of the Columns

Node	12	16	20
Long. drift (%)	0.3386	0.3386	0.3386
Trans. drift (%)	1.4327	1.4340	1.4327

Nonlinear CIP Model of the Structure

The non-linear model of the bridge superstructure and the column bent is the same as that of the linear elastic model. The columns are modeled with a *nonlinearBeamColumn* and a fiber section which describes the dimensions and properties of the reinforcing steel in the column. Additionally, a *zeroLength* element is placed at the top and bottom of the columns to model bond-slip at the column- footing and column-bent interfaces and the footing is removed from the model.

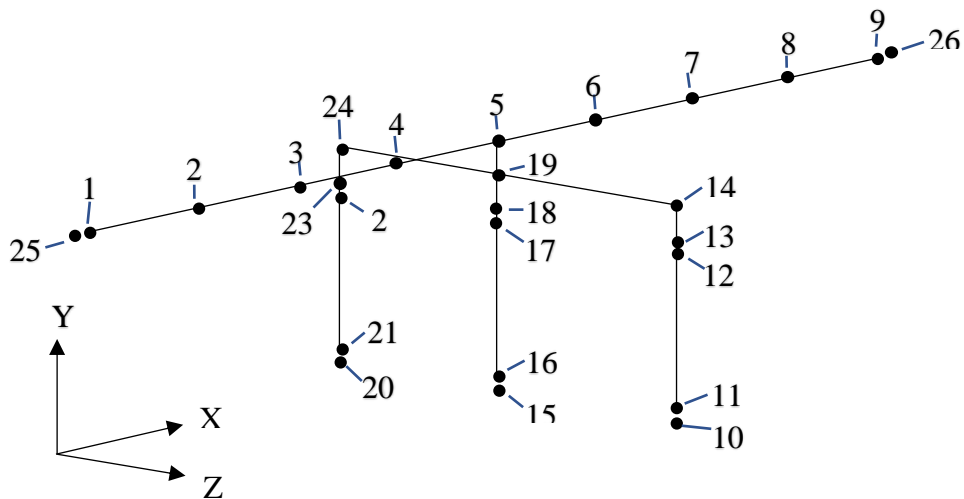


Figure B.8 Preston Bridge Nonlinear Cast-in-place Model with Node Numbers

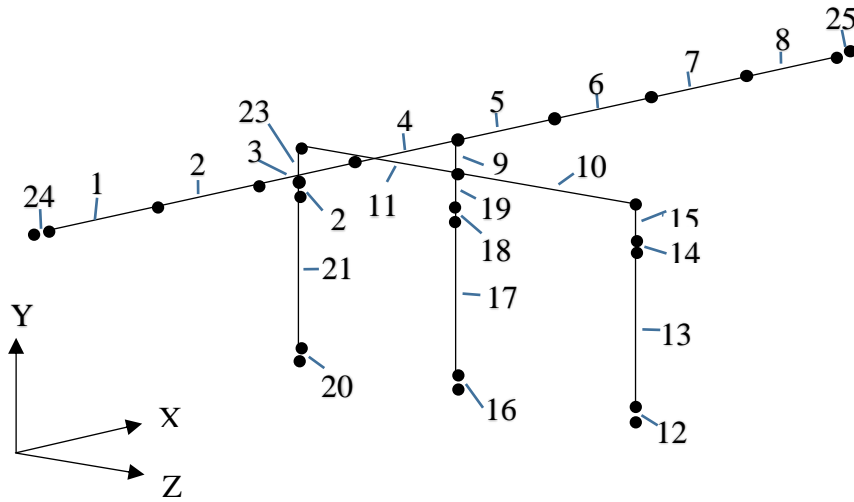


Figure B.9 Preston Bridge Nonlinear Cast-in-place Model with Element Numbers

The following dimensions are required for modeling the fiber section.

$d_{r9} = 1.128 \text{ in}$ Diameter of a #9 reinforcing bar

$d_s = 0.625''$ Diameter of spiral reinforcing

$R_9 = 1.74 \text{ ft}$ Distance from the center of the column to the center of the #9 bars

Material Properties

Unconfined Concrete

As previously determined the modulus of elasticity, E , and the modulus of rigidity, G , for cast-in-place concrete are:

$E_{CIP} = 3,644 \text{ ksi} = 524,736 \text{ ksf}$ Modulus of elasticity of cast-in-place concrete

$G_{CIP} = 218,640 \text{ ksf}$ Modulus of rigidity of cast-in-place concrete

Peak strain for 4000 *psi* concrete is 0.002 and ultimate strain is 0.005.

Reinforcing Steel

The grade of the steel is specified in the plans. For the Preston Bridge the steel is Grade 60. The following properties are found in Table 8.4.2-1 in the AASHTO Guide Specifications for LRFD Seismic Bridge Design, 2011, Sec. 8-4.

$$f_y = 68 \text{ ksi} = 9,792 \text{ ksf}$$

$$f_u = 95 \text{ ksi} = 13,680 \text{ ksf}$$

The strain for a #9 bar at strain hardening is

$$e_{sh} = 0.0125$$

The ultimate strain is

$$e_u = 0.09$$

The modulus of elasticity for steel is

$$E = 29,000 \text{ ksi} = 4,176,000 \text{ ksf}$$

The slope of the line at strain hardening is

$$E_{sh} = 1,247 \text{ ksi} = 179,568 \text{ ksf}$$

Confined Concrete Strength Using Theoretical Stress-Strain Model Developed by Mander et al.

AASHTO Guide Specifications for LRFD Seismic Bridge Design, 2011, Sec. 8.4.4, Concrete Modeling, specifies that confined concrete should be modeled based on Mander's stress-strain model. Following the procedure outlined by Mander et al., we obtained the following properties for the confined concrete (Mander, Priestley, & Park, Theoretical Stress-Strain Model for Confined Concrete, 1988).

$f'_{cc} = 5.604 \text{ ksi} = 806.976 \text{ ksf}$	Confined concrete compressive strength
$\varepsilon_{cc} = 0.006$	Confined concrete strain at maximum strength
$\varepsilon_{cu} = 0.016$	Confined concrete ultimate strain

Modeling Bond-slip

To model the bond-slip of the reinforcing steel at the interfaces between the footing and column and the bent and the column a *zeroLength* element with hysteretic material properties is used.

The *uniaxialMaterial Hysteretic* command in OpenSees requires values from a moment-curvature analysis of the cross-section of the column. A *zeroLength* element with the same cross-section as that of the reinforced column was created in a separate tcl file to analyze the material's behavior. An axial load equal to the average axial load seen by the columns and a moment of 1 kip in was applied to the element. The stresses and strains in the reinforcing steel on the tension and compression side of the section as well as the concrete at the same location were recorded. The reaction was also recorded. The slip can be calculated using equations from Section 8.2.3.1 in the Haber report (Haber Z. B., 2013).

$$\delta_{slip} = \begin{cases} \frac{\varepsilon_s L_1}{2} & \text{if } \varepsilon_s \leq \varepsilon_y \\ \frac{\varepsilon_y L_1}{2} + \frac{(\varepsilon_s - \varepsilon_y) L_2}{2} & \text{if } \varepsilon_s > \varepsilon_y \end{cases}$$

Where:

ε_s = strain in the reinforcing steel on the tension side of the column

ε_y = yield strain of the reinforcing steel

L_1 and L_2 can be determined by

$$L_1 = \frac{f_s d_b}{4u}$$

$$L_2 = \frac{(f_s - f_y) d_b}{4u}$$

Where:

f_s = stress in the reinforcing steel on the tension side of the column

f_y = maximum stress of the reinforcing steel

d_b = diameter of one reinforcing bar

u can be calculated by

$$u = \frac{9.5\sqrt{f'_c}}{d_b} \leq 800 \text{ psi}$$

Where:

f'_c = the compressive strength of concrete

Once the slip is found the rotation of the column that corresponds to each moment is calculated

by

$$\theta_{slip} = \tan^{-1} \left(\frac{\delta_{slip}}{c - d} \right)$$

Where:

c = neutral axis location determined from moment-curvature analysis

d = column diameter

A graph of the moment vs. rotation with an idealized bilinear curve for the Preston Bridge is shown in Figure B.10.

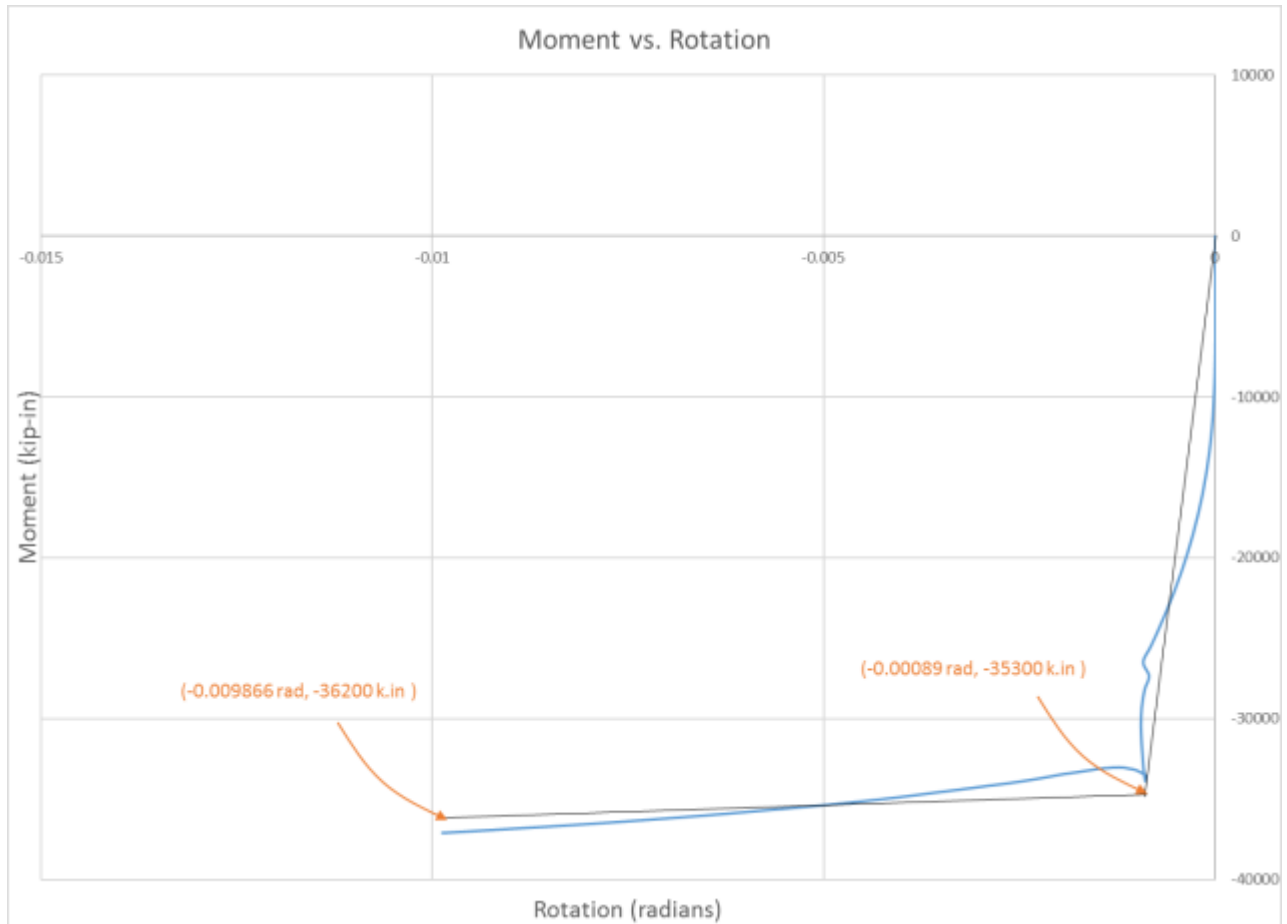


Figure B.10 Preston Bridge Moment vs Rotation

The *uniaxialMaterial Hysteretic* command in OpenSees requires the stress and strain at the first point of inflection and the ultimate stress and strain on the bilinear approximation of the moment-rotation curve. These values are

$s1p = 35,300 \text{ k in} = 2,941.67 \text{ k ft}$ Moment at the first point of the envelope in the positive direction

$e1p = 0.00089$ Angle at the first point of the envelope in the positive direction

$s2p = 36,200 \text{ k in} = 3,016.67 \text{ k ft}$ Moment at the second point of the envelope in the positive direction

$e2p = 0.009866$

Angle at the second point of the envelope in the positive
direction

Because of the symmetry of the column the moments and rotations in the negative direction are the same as those in the positive direction.

Moment-curvature OpenSees Input File

```
#Clear cached data existing in the program
wipe

#Values in kips and feet

#Create Model with 2 dimensions and 3 degrees of freedom
model BasicBuilder -ndm 2 -ndf 3

#Create 3 DOF nodes
#      tag    x    y
node   1     0.0  0.0
node   2     0.0  0.0

#Fix node 1 in all DOF and node 2 in the y direction
fix 1 1 1 1 1
fix 2 0 1 0

#Create uniaxial materials for Concrete and Steel
# uniaxialMaterial Concrete01 $matTag $fpc $epsc0 $fpcu $epsU
uniaxialMaterial Concrete01 1 -4.0 -0.002 0 -0.005
# uniaxialMaterial Concrete04 $matTag $fc $ec $ecu $Ec <$ft $et> <$beta>
uniaxialMaterial Concrete04 2 -5.604 -0.006 -0.016 3644
# uniaxialMaterial ReinforcingSteel $matTag $fy $fu $Es $Esh $esh $eult
uniaxialMaterial ReinforcingSteel 3 68 95 29000 1247 0.0125 0.09

#Create fiber section with Defined Concrete and Rebar
section Fiber 1 {
#patch circ $matTag $numSubdivCirc $numSubdivRad $yCenter $zCenter $intRad $extRad <$startAng
endAng>
patch circ 2 44 10 0 0 0 20.88 0 360
patch circ 1 44 2 0 0 20.88 24.64 0 360
```

```

#layer circ $matTag $numBar $areaBar $yCenter $zCenter $radius <$startAng $endAng>
layer circ 3 20 1 0 0 20.88 0 360
}

#Create zero length element between nodes 1 and 2

element zeroLengthSection 1 1 2 1

#Set up time series

timeSeries Linear 1

#Create recorder files: displacements and reactions

recorder Node -file MomentSection-BR.out -node 1 -dof 3 reaction
recorder Element -file TensionStrain_steel-BR.out -ele 1 section fiber -20.88 0 3
stressStrain
recorder Element -file TensionStrain_concrete-BR.out -ele 1 section fiber -20.88 0 2
stressStrain
recorder Element -file CompressiveStrain-steel-BR.out -ele 1 section fiber 20.88 0 3
stressStrain
recorder Element -file CompressiveStrain-concrete-BR.out -ele 1 section fiber 20.88 0 2
stressStrain

pattern Plain 1 Constant {
load 2 -622 0 0
}

integrator LoadControl 0.0
system SparseGeneral -piv
test NormUnbalance 1.0e-9 10
numberer Plain
constraints Plain
algorithm Newton
analysis Static
analyze 1

pattern Plain 2 Linear {
load 2 0.0 0.0 -1.0
}

integrator DisplacementControl 2 3 0.000005
analyze 500

```

Non-Linear Cast-in-Place OpenSees Input File for Seismic Load in Transverse Direction

#Two-span Bridge on SH-36 over Bear River at Preston, Idaho

wipe

#Create model with 3 dimensions and 6 DOF

model BasicBuilder -ndm 3 -ndf 6

#Units are kips and feet

#Create 6 DOF nodes

#Superstructure nodes

#	tag	x	y	z
node	1	0.0	39.273	0.0
node	2	34.270	39.273	0.0
node	3	68.540	39.273	0.0
node	4	102.810	39.273	0.0
node	5	137.080	39.273	0.0
node	6	171.350	39.273	0.0
node	7	205.620	39.273	0.0
node	8	239.890	39.273	0.0
node	9	274.160	39.273	0.0

#Substructure nodes

node	10	137.080	0.0	12.000
node	11	137.080	0.0	12.000
node	12	137.080	32.000	12.000
node	13	137.080	32.000	12.000
node	14	137.080	34.250	12.000
node	15	137.080	0.0	0.0
node	16	137.080	0.0	0.0
node	17	137.080	32.000	0.0
node	18	137.080	32.000	0.0
node	19	137.080	34.250	0.0
node	20	137.080	0.0	-12.000
node	21	137.080	0.0	-12.000
node	22	137.080	32.000	-12.000
node	23	137.080	32.000	-12.000
node	24	137.080	34.250	-12.000

#Spring support nodes

node	25	0.0	39.273	0.0
node	26	274.160	39.273	0.0

#Specify geometric transformation

```
geomTransf Linear 1 0 0 1
geomTransf Linear 2 -1 0 0
geomTransf PDelta 3 0 0 1
```

Fix column bases and abutments in all DOF's

```
fix 25 1 1 1 1 1 1
fix 26 1 1 1 1 1 1
```

```

fix 10 1 1 1 1 1 1
fix 15 1 1 1 1 1 1
fix 20 1 1 1 1 1 1

#Create uniaxial materials for concrete and steel

# uniaxialMaterial Concrete01 $matTag $fpc $epsc0 $fpcu $epsU
uniaxialMaterial Concrete01 1 -576.0 -0.002 0 -0.005

# uniaxialMaterial Concrete04 $matTag $fc $ec $ecu $Ec <$ft $et> <$beta>
uniaxialMaterial Concrete04 2 -806.976 -0.006 -0.016 524736

# uniaxialMaterial ReinforcingSteel $matTag $fy $fu $Es $Esh $esh $eult
uniaxialMaterial ReinforcingSteel 3 9792 13680 4176000 179568 0.0125 0.09

#Create hysteretic uniaxial material to model bond-slip

# uniaxialMaterial Hysteretic $matTag $s1p $e1p $s2p $e2p $s1n $e1n $s2n $e2n $pinchX $pinchY
$damage1 $damage2 <$beta>
uniaxialMaterial Hysteretic 4 2941.67 0.00089 3016.67 0.009866 -2941.67 -0.00089 -
3016.67 -0.009866 1 1 0 0 0.35

uniaxialMaterial Elastic 5 1e12

#Create fiber section with Defined Concrete and Rebar

section Fiber 1 {
#patch circ $matTag $numSubdivCirc $numSubdivRad $yCenter $zCenter $intRad $extRad <$startAng
endAng>
patch circ 2 44 10 0 0 0 1.74 0 360
patch circ 1 44 2 0 0 1.74 2.05 0 360
#layer circ $matTag $numBar $areaBar $yCenter $zCenter $radius <$startAng $endAng>
layer circ 3 20 6.9444e-3 0 0 1.74 0 360
}

# Define shear stiffness (GJ) elastic material

set Gc 218640
set Jc 326.7
set GJ [expr $Gc*$Jc]
uniaxialMaterial Elastic 6 $GJ

section Aggregator 2 6 T -section 1

# Create deck elements

# element elasticBeamColumn $eleTag $iNode $jNode $A $E $G $J $Iy $Iz $transfTag
element elasticBeamColumn 1 1 2 59.80 792822.24 330343.2 1e10 8090.49 260.87 1
element elasticBeamColumn 2 2 3 59.80 792822.24 330343.2 1e10 8090.49 260.87 1
element elasticBeamColumn 3 3 4 59.80 792822.24 330343.2 1e10 8090.49 260.87 1
element elasticBeamColumn 4 4 5 59.80 792822.24 330343.2 1e10 8090.49 260.87 1
element elasticBeamColumn 5 5 6 59.80 792822.24 330343.2 1e10 8090.49 260.87 1
element elasticBeamColumn 6 6 7 59.80 792822.24 330343.2 1e10 8090.49 260.87 1
element elasticBeamColumn 7 7 8 59.80 792822.24 330343.2 1e10 8090.49 260.87 1
element elasticBeamColumn 8 8 9 59.80 792822.24 330343.2 1e10 8090.49 260.87 1

```

```

# Create pier bent elements

element elasticBeamColumn 9 5 19 1e10 524736 218640 1e10 1e10 1e10 3
element elasticBeamColumn 10 14 19 25.23 524736 218640 1e10 1e10 1e10 2
element elasticBeamColumn 11 19 24 25.23 524736 218640 1e10 1e10 1e10 2

# Create column elements

# element nonlinearBeamColumn $eleTag $iNode $jNode $numIntgrPts $secTag $transfTag
# element zeroLength $eleTag $iNode $jNode -mat $matTag1 $matTag2 ... -dir $dir1 $dir2 ...

element zeroLength 12 10 11 -mat 5 5 5 4 4 4 -dir 1 2 3 4 5 6
element nonlinearBeamColumn 13 11 12 9 2 3
element zeroLength 14 12 13 -mat 5 5 5 4 4 4 -dir 1 2 3 4 5 6
element elasticBeamColumn 15 13 14 1e10 524736 218640 1e10 1e10 1e10 3
element zeroLength 16 15 16 -mat 5 5 5 4 4 4 -dir 1 2 3 4 5 6
element nonlinearBeamColumn 17 16 17 9 2 3
element zeroLength 18 17 18 -mat 5 5 5 4 4 4 -dir 1 2 3 4 5 6
element elasticBeamColumn 19 18 19 1e10 524736 218640 1e10 1e10 1e10 3
element zeroLength 20 20 21 -mat 5 5 5 4 4 4 -dir 1 2 3 4 5 6
element nonlinearBeamColumn 21 21 22 9 2 3
element zeroLength 22 22 23 -mat 5 5 5 4 4 4 -dir 1 2 3 4 5 6
element elasticBeamColumn 23 23 24 1e10 524736 218640 1e10 1e10 1e10 3

# Create spring elements

uniaxialMaterial Elastic 7 14074.4; # Translational stiffness along X axis of the abutments,
kip/ft
uniaxialMaterial Elastic 8 1e12; # Translational stiffness along Y axis of the abutments,
kip/ft
uniaxialMaterial Elastic 9 2300; # Translational stiffness along Z axis of the abutments,
kip/ft
uniaxialMaterial Elastic 10 1e12; # Rotational stiffness about X axes of the abutments,
kip.ft/radian
uniaxialMaterial Elastic 11 1e12; # Rotational stiffness about Y axis of the abutments,
kip.ft/radian
uniaxialMaterial Elastic 12 0; # Rotational stiffness about the Z axis of the abutment,
kip.ft/radian

# Spring elements using above stiffness values
# element zeroLength $eleTag $iNode $jNode -mat $matTag1 $matTag2 ... -dir $dir1 $dir2 ...

element zeroLength 24 25 1 -mat 7 8 9 10 11 12 -dir 1 2 3 4 5 6
element zeroLength 25 9 26 -mat 7 8 9 10 11 12 -dir 1 2 3 4 5 6

# Create recorder files

#recorder Node -file Nodes1-9_NonLin_Displacement_Long_BR.out -time -nodeRange 1 9 -dof 1 disp
recorder Node -file Nodes1-9_NonLin_Displacement_Trans_BR.out -time -nodeRange 1 9 -dof 3 disp
#recorder Node -file Column_Reactions_Long_BR.out -time -node 10 15 20 -dof 1 2 6 reaction
#recorder Node -file Column_Displacement_Long_BR.out -time -node 12 17 22 -dof 1 disp
recorder Node -file Column_Reactions_Trans_BR.out -time -node 10 15 20 -dof 3 2 4 reaction
recorder Node -file Column_Displacement_Trans_BR.out -time -node 12 17 22 -dof 3 disp
recorder Element -file Stress-Strain_Steel_Tension_Long.out -time -ele 17 section 1 fiber 1.74
0 3 stressStrain
recorder Element -file Stress-Strain_Steel_Compression_Long.out -time -ele 17 section 1 fiber
-1.74 0 3 stressStrain
recorder Element -file Stress-Strain_Concrete_Compression_Long.out -time -ele 17 section 1
fiber -1.74 0 2 stressStrain

```

```

# Assign gravity loads

pattern Plain 1 Constant {
#   tag    FX      FY      FZ    MX    MY    MZ
load 1    0.0    -139.130  0.0  0.0  0.0  0.0
load 2    0.0    -278.270  0.0  0.0  0.0  0.0
load 3    0.0    -278.270  0.0  0.0  0.0  0.0
load 4    0.0    -278.270  0.0  0.0  0.0  0.0
load 5    0.0    -278.270  0.0  0.0  0.0  0.0
load 6    0.0    -278.270  0.0  0.0  0.0  0.0
load 7    0.0    -278.270  0.0  0.0  0.0  0.0
load 8    0.0    -278.270  0.0  0.0  0.0  0.0
load 9    0.0    -139.130  0.0  0.0  0.0  0.0
load 14   0.0    -150.001  0.0  0.0  0.0  0.0
load 19   0.0    -156.751  0.0  0.0  0.0  0.0
load 24   0.0    -150.001  0.0  0.0  0.0  0.0
}

constraints Plain

numberer Plain

system BandGeneral

test NormDispIncr 1.0e-8 6

algorithm Newton

integrator LoadControl 1

analysis Static

analyze 1

#Reset time to perform pushover analysis

loadConst -time 0.0

# Create horizontal load patterns
#Transverse seismic loads

pattern Plain 4 Linear {
eleLoad -ele 1 -type beamUniform 0 10.662 0
}

pattern Plain 5 Linear {
eleLoad -ele 2 -type beamUniform 0 10.922 0
}

pattern Plain 6 Linear {
eleLoad -ele 3 -type beamUniform 0 11.221 0
}

pattern Plain 7 Linear {
eleLoad -ele 4 -type beamUniform 0 11.395 0
}

pattern Plain 8 Linear {
eleLoad -ele 5 -type beamUniform 0 11.395 0
}

```

```
pattern Plain 9 Linear {
eleLoad -ele 6 -type beamUniform 0 11.221 0
}
```

```
pattern Plain 10 Linear {
eleLoad -ele 7 -type beamUniform 0 10.922 0
}
```

```
pattern Plain 11 Linear {
eleLoad -ele 8 -type beamUniform 0 10.662 0
}
```

The following eight loading patterns should be activated instead of the previous eight, when loading in the longitudinal direction

```
#pattern Plain 12 Linear {
#eleLoad -ele 1 -type beamUniform 0 0 10.000
#}
```

```
#pattern Plain 13 Linear {
#eleLoad -ele 2 -type beamUniform 0 0 10.000
#}
```

```
#pattern Plain 14 Linear {
#eleLoad -ele 3 -type beamUniform 0 0 10.000
#}
```

```
#pattern Plain 15 Linear {
#eleLoad -ele 4 -type beamUniform 0 0 10.000
#}
```

```
#pattern Plain 16 Linear {
#eleLoad -ele 5 -type beamUniform 0 0 10.000
#}
```

```
#pattern Plain 17 Linear {
#eleLoad -ele 6 -type beamUniform 0 0 10.000
#}
```

```
#pattern Plain 18 Linear {
#eleLoad -ele 7 -type beamUniform 0 0 10.000
#}
```

```
#pattern Plain 19 Linear {
#eleLoad -ele 8 -type beamUniform 0 0 10.000
#}
```

constraints Plain

numberer RCM

system BandSPD

algorithm Linear

integrator LoadControl 0.01

analysis Static

analyze 100

Nonlinear CIP Model Analysis Results

Tables B.10 and B.11 show the displacements and column base reactions for the longitudinal and transverse directions, respectively.

Table B.10 Preston Bridge Nonlinear CIP Displacements and Column Base Reactions for Seismic Loads in the Longitudinal Direction

Nodes	Displacement (ft.)	Columns	Shear (k)	Axial (k)	Moment (k ft)
Deck		1	-94.230	610.280	1612.030
1	0.10008	2	-94.230	610.280	1612.030
2	0.10096	3	-94.230	610.280	1612.030
3	0.10156				
4	0.10188				
5	0.10192				
6	0.10188				
7	0.10156				
8	0.10096				
9	0.10008				
Top of the Columns					
12	0.09673				
17	0.09673				
22	0.09673				

Table B.11 Preston Bridge Nonlinear CIP Displacements and Column Base Reactions for Seismic Loads in the Transverse Direction

Nodes	Displacement (ft.)	Columns	Shear (k)	Axial (k)	Moment (k ft)
Deck		1	-175.192	613.812	-2975.300
1	0.54432	2	-175.191	613.837	-2975.340
2	0.54787	3	-175.192	613.812	-2975.300
3	0.55441				
4	0.55956				
5	0.56131				
6	0.55956				
7	0.55441				
8	0.54787				
9	0.54432				
Top of the Columns					
12	0.56116				
17	0.56131				
22	0.56116				

The column height is 29.25 ft and the drift in the longitudinal and transverse directions for top of the columns are in Table B.12.

Table B.12 Preston Bridge Nonlinear CIP Calculated Drift for Top of the Columns

Node	12	17	22
Long. drift (%)	0.3307	0.3307	0.3307
Trans. drift (%)	1.9185	1.9190	1.9185